

Editorial Board

Dr. Mohammad I. Malkawi

Associate Professor, Department of Software Engineering

Jordan

Dr. Kaveh Ostad-Ali-Askari

Assistant Professor, Department of Civil Engineering, Isfahan (Khorasgan) Branch,

Iran

Dr. Mohammed A. Akour

Associate Professor in the Department of Software Engineering,

Jordan

Dr. Mohammad mehdi hassani

Faculty of Computer Engineering

Iran

Prof.Ratnakaram Venkata Nadh (Ph.D)

Professor & Head - Chemistry Department, Dy. Director - Admissions

India

Dr. SIDDIKOV ILKHOMJON KHAKIMOVICH

Head of the Department of "Power Supply Systems",

Uzbekistan

Dr.S.DHANASEKARAN

Associate Professor in the Department of Computer Science and Engineering,

India

Younes El Kacimi, Ph. D.

Science Faculty, Department of Chemistry Kénitra

Morocco

Denis Chemezov

Lecturer, Vladimir Industrial College, Vladimir

Russia

RICHARD O. AFOLABI, Ph.D.

Department of Petroleum Engineering,

Nigeria

Volume 2 ISSUE 6

November-December 2018

The influence of the Calcium Silicate panel on Soil-paper walls in low income houses in Indonesia

Vincentius Totok Noerwasito

Contributions on Knowledge Management in Mechanical Engineering

Ghelase Daniela || Daschievici Luiza

Cutting Process Control

Daschievici Luiza || Ghelase Daniela

The Influence Study of The Mole Ratio Reactant in Ceftriaxone Sodium Synthesis Against The Yield of The Production

Rohimmahtunnessa Azhar || Alfani Danny Arbianto || Agus Supriyono, Firdayani

MHD Newtonian and non-Newtonian Nano Fluid Flow Passing On A Magnetic Sphere with Mixed Convection Effect

Basuki Widodo || Yolanda Norasia || Dieky Adzkiya

Parameters calculation of turbulent fluid flow in a pipe of a circular cross section

Denis Chemezov || Svetlana Tyurina || Irina Medvedeva || Lyudmila Smirnova || Elena Bogomolova || Margarita Bakhmeteva || Alexandra Strunina ||

Nina Melenteva

HIGGSBOSON RADIUS of ACTION

Antonio Puccini

Modeling and Simulation of a Water Gas Shift Reactor operating at a low pressure

Wail El Bazi || Abderrahim El-Abidi || Moulay Saddik Kadiri || Said Yadir

Properties of Geopolymer Bricks Exposed To High Temperatures

Ghada D. Abdel-Hameed

In vitro Evaluation of the Antimicrobial and Antioxidant activities of juniperus oxycedrus essential oil (Cade oil)

Fatiha Abdellah || Boukraa Laid || Si Mohamed Hammoudi || Rachida Benaraba

Combining of Cryptography and Steganography for Improving of Security

Muharrem Tuncay Gençoglu || Sarhad Baez Hasan

Physico-Chemical Analysis of River Benue within Makurdi Reach for Irrigational Use

Aho M.I || Ajayi, S.D || Lagasi, J.E.

The influence of the Calcium Silicate panel on Soil-paper walls in low income houses in Indonesia

Vincentius Totok Noerwasito

*Department Architecture Institut Teknologi Sepuluh Nopember Surabaya
Indonesia*

ABSTRACT

Building materials used for the walls of simple houses in lower-middle-class areas in Indonesia are currently dominated by brick. This study proposes that soil-paper blocks coated with calcium silicate board may be a suitable alternative, with high embodied energy and density. The research aims to obtain an optimal wall thickness to provide protection against cooling and embodied energy in low income houses, as well as against the temperature conditions in these buildings in highland and lowland areas. Determination of wall thickness is performed by simulation of a 9 m² building model with thick variables. Cooling calculations involved the use of Archipak software. Temperature measurements were carried out using a data logger on a sample of soil-paper blocks. The results indicate that the optimal wall thickness for protection against cooling and embodied energy is 8 cm. Soil-paper block has a lower density than brick. The use of calcium silicate boards does not affect the internal temperature of a low income house, but they can be used as protection against rainwater and as a substitute for wall plastering.

Keywords—low income houses; soil-paper; calcium silicate board; wall thickness; sample blocks.

I. INTRODUCTION

Building materials for simple housed walls for the lower-middle class in Indonesia are currently dominated by red bricks. Such bricks have high embodied energy equivalent to 3677 MJ / m² [2], due to their use of combustion energy. It is therefore necessary to find a replacement material that does not require such a burning process. One such material is soil block. The disadvantage of this material is that is relatively heavy, with a density reaching 1700–1800 kg/m³ [9]. Currently, in urban areas there is a significant amount of paper waste, which has potential to be processed into wall building materials. Soil block when mixed with paper material will decrease its density. The combination of these materials is referred to as soil-paper block.

This study discusses the building of walls using paper and soil. The raw material of this wall material is paper mixed with soil and cement, which provides additional wall strength [4][5]. The production process of this material involves not burning but rather compaction and drying in a natural way, similar to the production of compressed earth blocks [9]. The limitation of walls using paper materials is that they are not resistant to rainwater [6]. To solve this problem, the outer and inner walls are coated with calcium silicate panels. Another function of the panel is replacing the cement plaster on the wall.

This research aims to obtain the ideal wall thickness. It targets the main issue of how to obtain optimal wall thickness and indoor temperature. There are two category energy in buildings Embodied energy and Operational energy [7]. In this study cooling as part of operational energy. The wall thickness in this case is optimal in terms of cooling and embodied energy. Cooling is energy produced by materials to cool buildings, while the energy for building material production processes from basic materials used for construction is termed embodied energy [8]. The value of these two energies is obtained by calculating the amount of cooling and embodied energy in the building; this value is

calculated using a building simulation, while temperature measurements are taken from value thicknesses of the ideal wall according to the simulation results. The building model used for the simulation is a building of length 3 m, width 3 m and height 3 m. The wall thickness used in the building simulation varies. Production of block soil-paper samples is carried out on selected wall thicknesses, and the composition used is adjusted to the desired block density (1000kg/m^3).

II. RESEARCH METHODS

This study analyses wall-building material comprising soil-paper blocks coated with calcium silicate board. Cement is added as a binder between soil and paper, a process which improves hardness and density. Activities undertaken included producing a building design simulation model using a wall of soil-paper block coated with a calcium silicate board (Fig. 1).

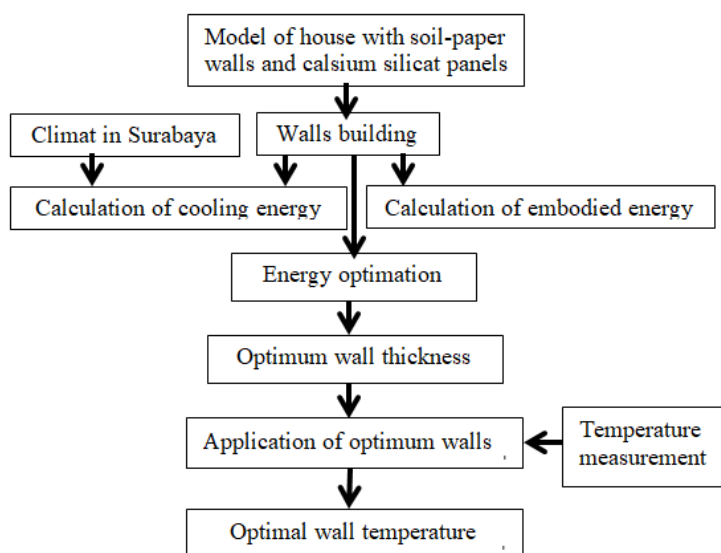


Figure 1 Flow of research approach

The dimensions of the building model were determined according to the size of the dwelling. In this case, the type of space chosen is a bedroom. Hence, the model dimension is a simulated building of size 3 x 3 m (Fig. 2). An alternative wall design is produced to obtain optimal results in terms of cooling and embodied energy conditions in the building. This aim was achieved using different wall thicknesses, which was one variable used in this research. The wall condition can be seen in Figure 3, while wall variables are shown in Table 1.

Table 1 Variables of papercrete wall with calcium silicate panels

| wall thickness (cm) | code |
|---------------------|------|
| 8 | W1 |
| 10 | W2 |
| 12 | W3 |
| 15 | W4 |

The simulation of cooling calculation is performed using the wall thickness variable. Results are expressed as cooling per years and temperature inside the building. A good wall thickness alternative is walls that are minimally cooling. The local climate (Surabaya, Indonesia) was a primary driver of this study. Simulation of cooling calculation used Archipak software. The calculation of embodied energy is supported by standard data of embodied energy per unit from each material. In this case, the material used the same wall variables, and hence the embodied energy from the wall variables will be the same and the wall volume becomes more important.

Energy optimization was performed on alternative buildings with different wall thicknesses. Regarding cooling and wall volume, a good building is one that has optimum levels of these factors. Further temperature measurements on soil-paper block wall samples with calcium silicate boards and without calcium silicate panels were performed on selected wall thicknesses. Temperature measurements involved use of a data logger.

III. DISCUSSION AND RESULTS

The research was conducted by taking the case of the Surabaya area of Indonesia. Surabaya is located at position 7.20 LS. Mean temperatures are 23.6–33.8 ° C and humidity levels average between 50–92%. Observing local climatic conditions is important in terms of energy saving in buildings to obtain more comfortable conditions inside them.

Factors studied include the extent to which the wall can reduce cooling in the building. The efficient use of building materials also received attention. Therefore, in this study the calculation of cooling and embodied energy was performed for energy saving in the building. A simulation model involving a building of width 3 m, length 3 m and height 3 m was used (Fig. 2). The building has recycled paper walls coated with calcium silicate panels. The roof is tiled, with the floor being plastered.

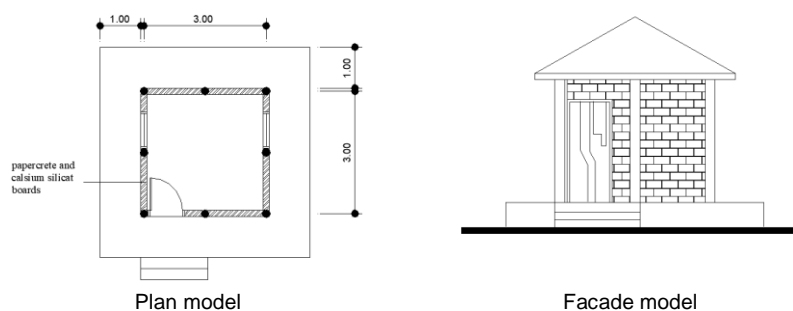


Figure 2 Plan and facade of building model

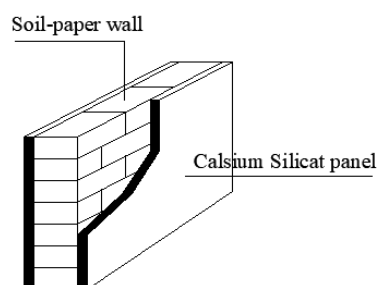
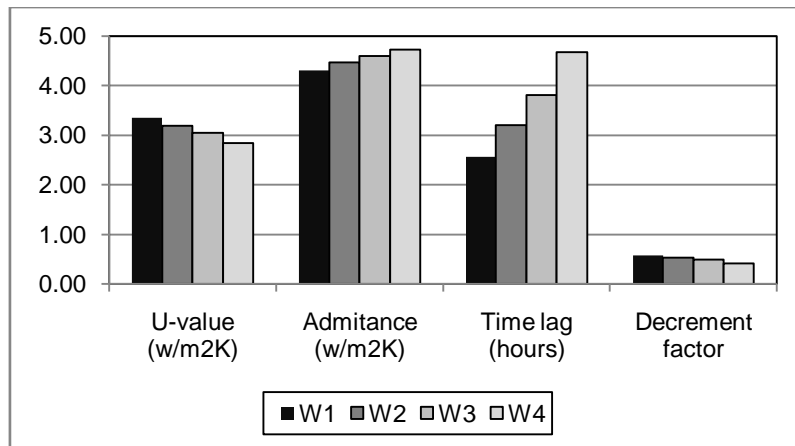


Figure 3 Wall details

III.1. Cooling energy

Materials have thermal characteristics which respond to the climate, hence the warm humid conditions in Indonesia significantly influence the material types selected. The decrease of energy in this research is enabled by using a soil-paper wall building with calcium silicate boards. Cooling involves those temperatures which are above thermal comfort inside buildings. The cooling calculations were performed by simulating the building model using Archipak software. The important factors required to obtain cooling in buildings comprise the thermal properties of the walls and the climatic conditions of Surabaya.

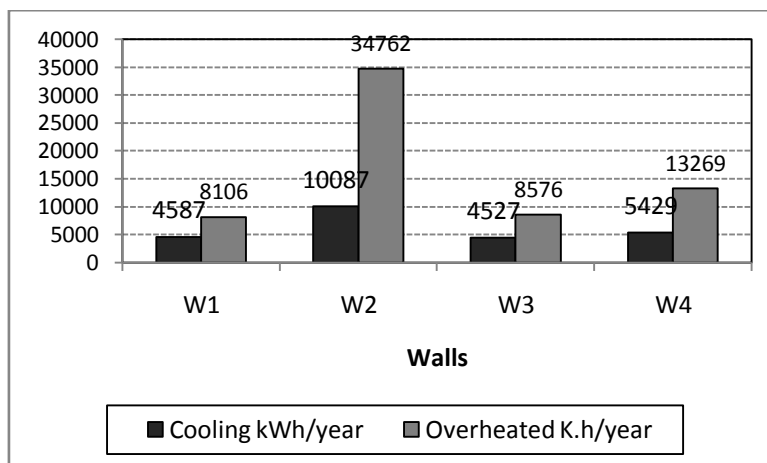
The research variables included building wall thickness. The number of variables that form the building model amounted to four pieces with different wall thicknesses. In this study, the code for the building model is 'W' and is characterized by '1, 2, 3, 4', which indicate the model types with different wall characteristics. The thermal properties of each wall of the thickness of the building model can be observed in Figure 4.



Source: calculation by Archipak5.

Figure 4 Thermal properties of soil-paper walls and calcium silicate panels

This figure illustrates that the wall thickness affects its thermal properties. The U value and decrement factor decrease for walls of increased thickness, as observed in the W4 model. Admittance and time lag increased in buildings with larger wall thicknesses. Based on the thermal properties of wall materials, cooling in buildings can be calculated. The value of cooling is determined for a year because it is more evenly distributed over that time period (Fig. 5).



Source: calculation by Archipak5.

Figure 5 Cooling energy per year for wall soil-paper and calcium silicate panels

Figure 5 illustrates that the highest cooling load is in the W2 building model, which is a building with a wall thickness of 10 cm, while the lowest cooling load was observed for the W3 building model, with a wall of thickness 12 cm. Differences between the cooling load for buildings in W1 and W3 were not significant (1.3%). The comparison between low and high cooling loads in all four buildings was 5560 Kwh/year or 123%. The condition of cooling in buildings without use of calcium silicate boards is also required (Table 2).

Table 2 Cooling energy types of Soil-paper wall without panels (WP)

| code | cooling kWh/year | overhotedK.h/year |
|------|------------------|-------------------|
| W1WP | 4595 | 7588 |
| W2WP | 4557 | 8052 |
| W3WP | 5058 | 8788 |
| W4WP | 5007 | 8917 |

Table 2 shows the increase in cooling of the building model. In buildings with increased wall thickness, the value of cooling of the wall without panels differs in each building. This result indicates that the effect of calcium silicate board use is different for each building. For example, for walls of 8 cm thickness, the use of a panel has little effect, while for 10 cm thick walls, such panels were highly influential.

III.2 Embodied Energy

The energy required to produce a final product from raw materials is termed embodied energy. One of the characteristics of green products is that they have low embodied energy [1]. Transportation and product delivery is one way to reduce the embodied energy value [11]. Each material has a different embodied energy. Materials used for the building model with their embodied energy per unit provided can be seen in Table 3.

Table 3 Embodied energy per unit material

| materials | embodied energy/unit |
|-----------------------|-------------------------|
| Soil-paper wall | 4,81 MJ/kg |
| Panel calsium silicat | 13550 MJ/m ³ |
| Roof tile | 251 MJ/m ² |
| floor | 5250 MJ/m ³ |
| Wooden door/window | 388 MJ/m ² |

In this building model, the most influential material is the embodied energy of the paper composition and calcium silicate boards, due to the weight and volume of both materials. Embodied energy calculation results from each building are illustrated in Figure 7. Figure 6 shows the increase in embodied energy due to the increase in wall thickness. In the building model, an 8 cm thick wall (W1) has the lowest embodied energy, while the 15 cm thick wall (W4) has the highest of such energy. This result demonstrates that large material volumes will also produce high embodied energy per m2. Therefore, in this case, the wall volume becomes important.

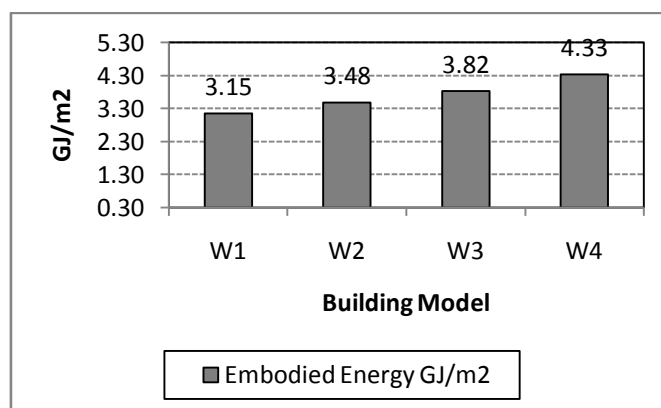


Figure 6 Embodied energy graph of each building model

III.3 Optimization

The condition of each building model has a different energy rating value between cooling energy with embodied energy. Some building models have low embodied energy but have high cooling energy, while there are also models of high embodied energy but low cooling energy. It is therefore necessary to optimize the two energies of each building model. To perform the energy optimization, data is required for annual cooling energy and embodied energy per year. The values of cooling energy and embodied energy are provided in Table 4.

Table 4 Cooling energy and embodied energy for each building model

| no | code | wall thickness (cm) | cooling energy (Kwh/years) | embodied energy (GJ/m ²) |
|----|------|---------------------|----------------------------|--------------------------------------|
| 1 | W1 | 8 | 4587 | 3,15 |
| 2 | W2 | 10 | 10087 | 3,48 |
| 3 | W3 | 12 | 4527 | 3,82 |
| 4 | W4 | 15 | 5429 | 4,33 |

Optimization is carried out by examining the energy position of cooling energy and embodied energy value of the building model. The optimization process uses graphs (Fig. 7). On the graph there are four zones. The best and worst zones are 1 and 4, respectively. Because the main consideration criterion for the appropriate assessment of the building model is the low cooling energy value, the embodied energy value must also be relatively low, based on consideration of good zone scale criteria, starting from zones 1 through 4.

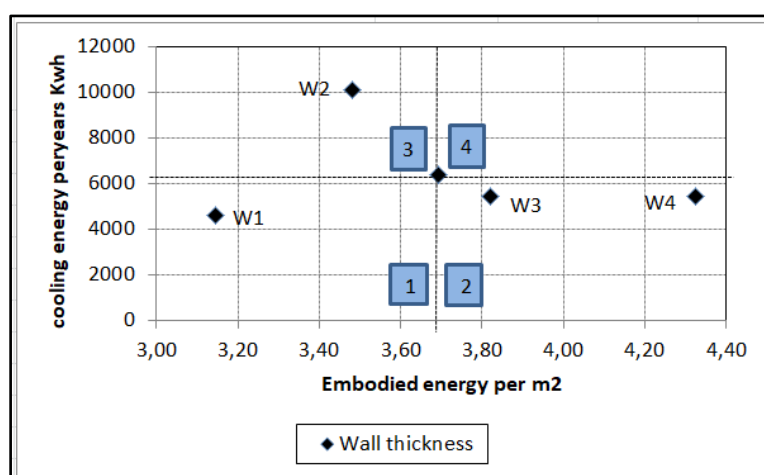


Figure 7 Position chart of each model of building in terms of cooling energy and embodied energy

In Figure 7, the position of the building model in zone 1 is model W1. The building model located on zone 2 is W3 and W4. W2 is located in zone 4. The W1 model has an cooling energy higher than W3, but the difference is relatively low (5.8%). The annual embodied energy value of W1 is lower than for W3 (21.3%). The W1 building model has a lower cooling energy value compared to W2 (201%), while the embodied energy value of W1 is lower than that for W2 (10%), based on the position of the W1 model with respect to both W2 and W3 building models. Hence, W1 is the optimal building model. The building has an annual cooling energy of 8106 K.h and an embodied energy value per year of 3.15 GJ /m².

The effect of using calcium silicate boards on the optimal building must be determined. Therefore, wall conditions without calcium silicate boards require values of cooling energy and embodied energy from the model to be determined. Figure 8 show the difference in cooling energy load (6.3%) and embodied energy (5%) of a building model with 8 cm wall thickness. The value of the difference is relatively small and insignificant. This result indicates that the presence of the calcium silicate panel has little effect on building energy.

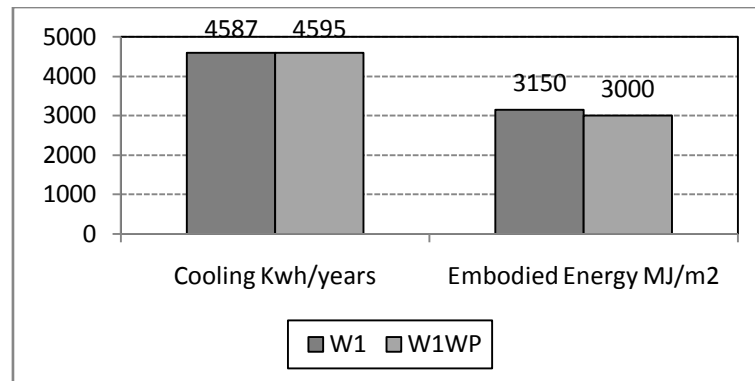


Figure 8 Position graph of optimal energy building model (W1) with or without panels (W1WP)

III.4 Application block

Walls of 8 cm thickness were found to be optimal. For that, we need to make a sample block that has a thickness of 8 cm. The resulting block has a soil weight composition of 50% by weight of paper while the cement composition is 20% of the total weight. Soil used in accordance for a soil block should contain 45% sand [10]. The shape of the block is made with a thickness of 8 cm width of 30 cm and length of 50 cm, with a weight of 10–12 kg. The resulting block density is 850–1000 kg / m³. Both outer and inner sides of the block are coated with 2 mm thick calcium silicate boards. As a comparison, red brick has a density of 1700 kg/m³, while soil block’s density is 2050 kg/m³. A typical soil-paper block can be seen in Figures 9 and 10.



Figure 9 Soil-paper block with calcium silicate panels



Figure 10 Soil-paper blocks without calcium silicate panels (WP)

Sample temperature measurements were made by constructing a room model of the block arrangement as high as 30 cm. The data logger analysed pairs of outside and indoor models. Field measurements of temperatures inside and outside the model are given in Figure 11. In the morning,

inside temperatures are generally higher than those outside while during the day, indoor temperatures tend to be lower. Temperatures at night are higher than those outside. The ideal temperature conditions are during the day, so that the walls can reduce heat. But in the afternoon, the room temperature is higher than the outside temperature. The wall is therefore more optimal during the day. Indoor temperature models without Calcium Silicat panels in the noon and afternoon are lower than the models with Calcium Silicat panels. This shows that the Calcium Silicat model without panels is better than the model with the Calcium Silicat panels.

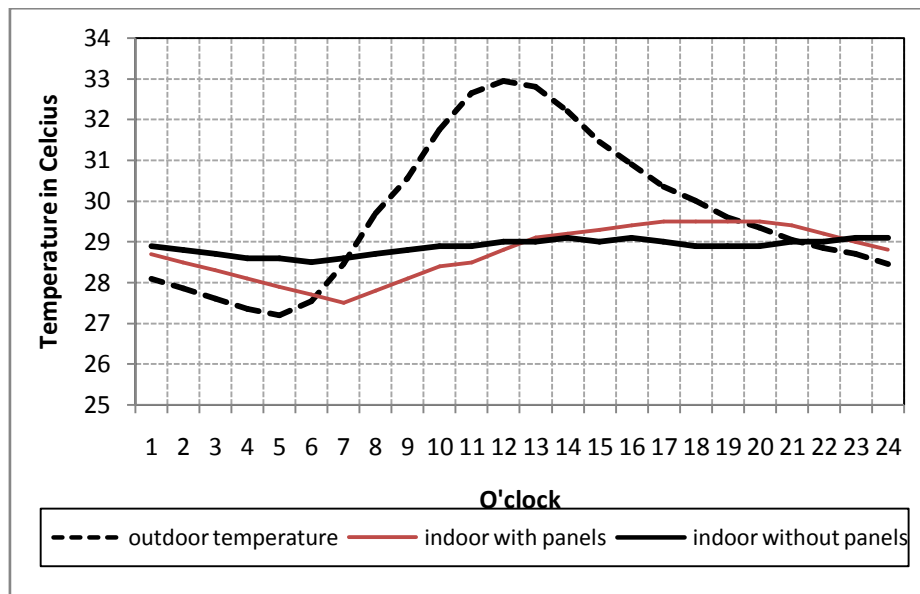


Figure 11 outdoor and Indoor temperature condition models

CONCLUSIONS

Soil-paper block walls with calcium silicate board with an cooling energy and embodied energy are optimal when they are of 8 cm thickness. Soil-paper block samples are lighter than compressed earth block (CEB) and red bricks because the former have lower densities than CEB and red bricks.

The use of 8 cm calcium silicate boards for a simple house leads to indoor temperatures at night being warmer than without such boards. This result shows that the use of calcium silicate boards is not necessary and they are probably more suitable as protection from rainwater or as a substitute for wall plastering. But on thicker walls, calcium silicate boards have an effect on the indoor temperature of the building.

The disadvantage of using a calcium silicate board on soil-paper wall in a low income house is that it interferes with the aesthetic appearance of soil-paper walls. The use of such boards on walls also causes an increase in the embodied energy of the walls.

In this study, the process of drying soil-paper blocks was found to require a relatively long time due to the characteristics of the pulp paper, which takes a long time to dry. Hence, the determination of soil-paper block length and width must also be considered.

ACKNOWLEDGEMENT

We thank LPPM-Institut Teknologi Sepuluh Nopember Surabaya for the financial support for this research

REFERENCES

[1] Amatruda, John. Green product. National Institute of Building Sciences.2004

- [2] Arman Hashemi, Heather Cruickshank. Embodied Energy of Fired Bricks: The Case of Uganda and Tanzania. paper presented at 14th International Conference on Sustainable Energy Technologies – SET, Nottingham, UK. 2015.
- [3] Bashar S. Mohammed. European Journal of Scientific Research, *EuroJournals Publishing*, ISSN 1450-216X Vol.34 No.4, pp.455-462. 2009.
- [4] Garret Mcelroy et al. Make It Complete With Papercrete, *Engineering 215 Intro to Design*. Haiti,. 2010
- [5] Jil Tushar, Saransh Joshi. Paper Crete: A Sustainable Building Material. *Strategic Technologies of Complex Environmental Issues-A Sustainable Approach*, Pp85-90, 2015.
- [6] Myriam Marie Delcasse et al. A Papercrete brick consists of recycled material and therefore cost is low compared to conventional bricks, *Int. Journal of Engineering Research and Application*, www.ijera.com ISSN : 2248-9622, Vol. 7, Issue 3, (Part -6) March, pp.09-14. 2017.
- [7] Nand Kishore Gupta, Anil Kumar Sharma, Anupama Sharma. *Open Journal of Energy Efficiency*, 2, pp171-175. 2013.
- [8] Petrosian Baris Der, Erik Johansson. Construction and Environment improving energy efficiency, *Building issues* No.2 vol 10. LCHS Lund University, Lund Sweden. 2000.
- [9] Rigasi Vincent Blocs de terre comprime. Vol 1 Manuel de Production. CRA-Terre EAG. Grenoble, France. 1995.
- [10] Sattary A, Thorpe, D. Optimizing embodied energy of building construction through bioclimatic principles. paper presented at Smith, S.D (Ed) Procs 28th Annual ARCOM Conference, 3-5 September, Edinburgh, UK, Association of Researchers in Construction Management, 2012,

Contributions on Knowledge Management in Mechanical Engineering

Ghelase Daniela, Daschievici Luiza

*“Dunarea de Jos” University of Galati
Galati, Romania*

ABSTRACT

Knowledge management (KM) has become an effective way of managing organization's intellectual capital or, in other words, organization's full experience, skills and knowledge that is relevant for more effective performance in future. The paper proposes a knowledge management to achieve a competitive control of the machining systems. Then an application of Knowledge Management in engineering has been attempted to explain. The model can be used by the manager for the choosing of competitive orders.

Keywords—*knowledge management, mechanical engineering, information technology, machining system, marketing knowledge, competitive management*

I. Introduction

The market dynamics is further passed to the mode of operation and management. In a knowledge-based society and economy, operations such as determining the relevant information and aggregating them into pieces of knowledge must be automated, because in such a complex and unpredictable environment, they are indispensable tools for creating, searching and structuring knowledge.

The interaction between the economic environment and the manufacturing system is a major source of knowledge about the economic environment and the manufacturing system themselves [5]. Consequently, it is necessary to exist a knowledge management system to avoid increased costs, waste of time and increased errors.

The recognition of the Knowledge Management (KM) imperative will provide an impetus for enterprise to understand and nurture their knowledge resources and activities.

KM has assumed a broad range of meanings from its inception; however, most of the published material remains ambiguous and provides little empirical evidence to support a specific definition for the knowledge management concept. KM has been acknowledged as being important to competitive advantage and organizational progress.

Thus, a clear understanding and agreement about KM should prove to be of great value for enterprises. As enterprises strive to create a competitive advantage with their products and services, they continue to contemplate the KM concept and the impact on organizational success.

In a effort to define KM, enterprises must determine which corporate knowledge should be harvested, organized managed and shared. A general definition has been 'getting the right information to the right people at the right time' in order for them to make better decisions.

Knowledge management implementation is an advantage for the enterprise from viewpoint of the competitiveness. The new knowledge will be used both in the enterprise management and to develop new products and new services or make important changes in the business decisions.

By means of learning, the enterprise which uses the knowledge able to adapt and respond continuously to the changes of the business environment.

An important goal of KM is seen to be the sharing of best practice. So, by the improving the flow of knowledge through the enterprise can be obtained the following benefits: the sharing of the best practice around business processes; the ability to respond more effectively to customer demands.

Due to technology facilitates the rapid exchange of information, the pace of acquisition is growing exponentially in both large and small enterprises. The vast amounts of knowledge possessed by the enterprises are spread across countless structured and unstructured sources.

To improve processes and bring new products to the market faster and more cheaply, the enterprises have to identify, make available and apply this knowledge. Thus, information must be understood, organized and transformed for problems solving. Consequently, information transformed in product is knowledge and coordination of this kind of knowledge is made by means of knowledge management.

As shown above, the manufacturing industry faces the challenge of responding quickly to the ever-changing requirements of customers. It is necessary that in these high competitive environments, enterprises to control production system dynamics of such as:

- change in the product types and variants;
- change in the production quantities.

Enterprises have to develop and implement more responsive and flexible manufacturing systems based on knowledge. By this way, they can respond to outgoing and difficult to predict change in production requirements and make products with high quality, low cost and fast delivery.

II. Related Literature

The paper is related to several strands of literature.

To be competitive organizations should react adequately, interpret non-standardized information for problem solving and decision making, as well as change their infrastructure and management strategies [8]. Usually there are a lot of information and knowledge within organizations, but at the same time many of them (service organizations, in particular) are “information rich and knowledge poor.” The information and knowledge assets, often called an “intellectual capital,” i.e., knowledge that can be converted into value, make a great potential for organizations if utilized well [1].

Knowledge management (KM) has become an effective way of managing organization's intellectual capital or, in other words, organization's full experience, skills and knowledge that is relevant for more effective performance in future.

Studies in KM mainly focus on organizational knowledge captured in corporate and/or organizational memories [2], and on the development of knowledge management systems (KMS). However these initiatives in organizations have often run into difficulties mainly because the expansion of individual's personal tacit knowledge to knowledge of organization as a whole causes implementation problems.

The paper [6] is concerned with a application of knowledge management on the mechatronic system. The Internet –based CNC machining center has been considered and its knowledge management model has been prepared. The model prepared has been analyzed for machining performance of the manufacturing system. The architecture of KM model of internet – based mechatronic system is presented in the Fig.1.

The system presented in this paper consists of KM model (PC), mechatronic system (CNC machining center), user unit (PC, SMS) and data, information converter unit. KM model consists of knowledge bank compare, internet and network connection, commentary and management units. Operations of CNC Machining Center which is the main production unit of the system can be controlled both by the machine tool control panel and by e-mail, network from distant places. Also, the machine tool equipped with a lot of sensors so that the machine tool performance can be monitored and unexpected conditions can be controlled.

Motivated by the literature discussed above, this paper presents a knowledge management structure of the machining system to provide competitiveness of the enterprise.

III. Knowledge Management in Engineering

Knowledge-based engineering is an engineering methodology in which knowledge about the product, the techniques used in design, analysis, and manufacturing, is stored in a special product model [23].

Knowledge discovery in databases (KDD) is the non-trivial process of identifying valid, novel, potentially useful, and ultimately understandable patterns in data. It can acquire implicit and useful knowledge in large scale datasets, and involves an integration of multiple disciplines such as statistics, artificial intelligence, machine learning, pattern recognition, etc. KDD has had great success in commercial areas, and has begun to be used in knowledge acquisition of engineering disciplines. The overall KDD process includes data selection, data preprocessing, data transformation, data mining, interpretation, and evaluation, as shown in Fig. 2 [21].

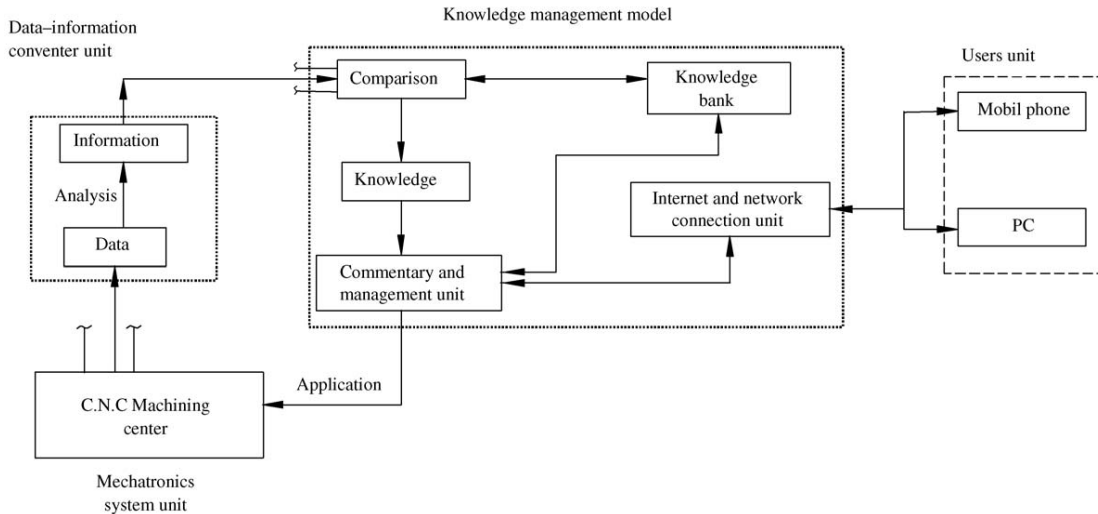


Fig.1 System diagram of KM of internet – based mechatronic system

Defining data, information and knowledge is difficult. It is possible to distinguish between data, information and knowledge on base of external means or from the perspectives of the user.

In [6] it is shown that, data are considered as raw facts, information is regarded as an organized set of data, and knowledge is perceived as meaningful information.

Data consists of symbols that represent objects, events, and their properties. Information is data that has been made useful. Information answers who, what, where, when, and how many questions. Information is helpful in deciding what to do, not how to do it.

Knowledge consists of instructions and know-how. Knowledge answers how questions. Knowledge is more than information. Information is data organized into meaningful patterns. Information is transformed into knowledge when a person or an intelligence system reads, understands, interprets and applies the information to a specific work function.

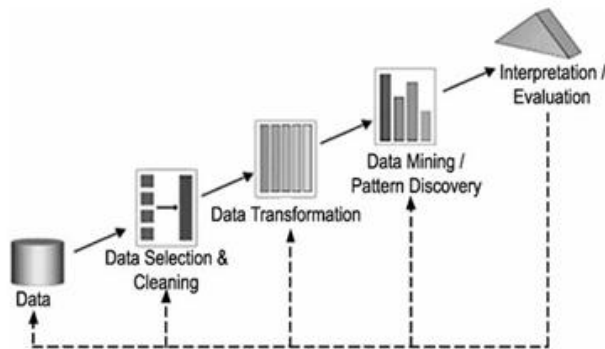


Fig. 2 The process of knowledge discovery

One person's or one intelligence system's knowledge can be another person's or intelligence system's information. If the information can not be applied to anything, it remains just information.

However, a person can take that same information, understand it and interpret it in the context of previous experience, and apply to anything, it is transformed to knowledge.

Information is becoming ever more important in engineering. It is not suitable to use data, information and knowledge conventionally. That is there is conceptual confusion. Also, today's technological products need interaction between different disciplines. So the confusion increases more. At the multidisciplinary engineering system, any discipline contains some information peculiar to system. However, most of the information mean essentially same even if they are expressed in different terms in different disciplines. Therefore, the available information must be evaluated, simplified and transformed into usable form that is knowledge.

Next, the knowledge is coordinated and connected with the system. So, a kind of know-how is acquired for the technological product. This case is generally based on a model, while it has special characteristics. An example of machining system has been analyzed in the following section. The model produced by technical

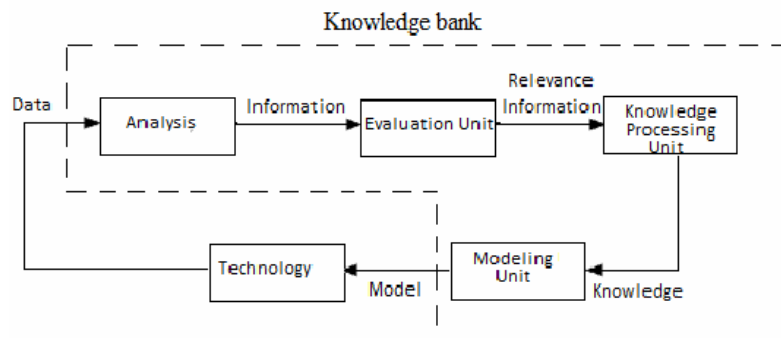


Fig. 3 KM model

knowledge which is acquired by the interaction of data, information and knowledge, by the coordination and the application of them on engineering system. KM model is presented in Fig. 3. KM is a comprehensive process of knowledge creation, knowledge validation, knowledge presentation, knowledge distribution and knowledge application. When KM model is applied by the enterprise into its production process it is obtained increasing competitiveness of the product in the market. That is KM model can be used for every stage of the engineering works such us design, manufacture, maintenance and repair.

IV. Conclusion

Today, information has become more important. Even data, information and knowledge are often used as if they have same meaning. This problem raises difficulties in engineering. It is necessary to exist a knowledge management system to avoid increased costs, waste of time and increased errors.

Knowledge-based engineering is an engineering methodology in which knowledge about the product, the techniques used in design, analysis, and manufacturing, is stored in a special product model.

In this paper the model of the knowledge management of the mechanical engineering was proposed.

Using and comparing marketing knowledge with stored and updated ones the machining model is carried out, analyzed and on its basis are generated instructions regarding the progress of the machining process in order to obtain maximum competitiveness.

By modeling and simulations, the manager can decide if the order is accepted and control the machining system to satisfy the customer demands.

To achieve these objectives, the competitive management uses the reinforcement learning to get to know the market and the unsupervised on-line learning technique to get to know the machining system.

Note that we propose to give managers a knowledge management model, so that they can interact with the economic environment (market).

This knowledge management model represents a technical-economic model that can be used for competitive management of the manufacturing process without requesting experiments and based on the extraction of the knowledge from the previous experience.

References

- 1) D. Apshvalka, & J. Grundspenkis “Making organizations to act more intelligently in the framework of the organizational knowledge management system”, Scientific proceedings of Riga Technical University, 5th series computer science, applied computer systems, Vol. 17, Riga: RTU Publishing, 2003, p. 72–82.
- 2) A. Brooking, “Corporate memory: Strategies for knowledge management”, London: International Thomson Business Press, 1999.
- 3) T. Chen, “Evaluating the mid-term competitiveness of a product in a semiconductor fabrication factory with a systematic procedure”, Computers & Industrial Engineering, Volume 53, Issue 3, October 2007, p. 499-513.

- 4) J.H. Dyer, K. Nobeoka, “Creating and managing a high-performance knowledge-sharing network: The Toyota case”, *Strategic Management Journal*, Chichester, 21-2000-3, p. 345-367.
- 5) Y. Koren, G. Ulsoy, „Reconfigurable manufacturing system having a production capacity method for designing and method for changing its production capacity”, in United States Patent, US 6, 349, 237 B1, 2002
- 6) D. Karayel, S. Ozkan, R. Keles, „General framework for distributed knowledge management in mechatronic systems”, *Journal of Intelligent Manufacturing*, 15, 2004, p. 511-515.

Cutting Process Control

Daschievici Luiza, Ghelase Daniela

“Dunarea de Jos” University of Galati
Galati, Romania

ABSTRACT

Adaptive-optimal control involves re-identification of the machining process and the model obtained is used to calculate the optimal process parameters.

Optimal control characterizes the addition of the technical and economic indicators to process parameters. Characteristic for performance technical indicators is that their dependence to parameter values of process has a limitative, what leads to one of the following conclusions, appropriately or inappropriately, and therefore can serve as restrictions in optimization problem.

Economic indicators have a continuous dependence of process parameters and therefore they are used as objective functions.

Keywords— manufacturing system, adaptive-optimal control, cutting process

I. Introduction

In the course of cutting process the monitored sizes are the following:

Cutting regime parameters; Processing error ; Position of the tool subassembly at a time (CNC machine); The actual size of the processed surface; Surface roughness; Static and dynamic stability of the cutting process; Cutting force; Temperature of the cutting area; Cutting power.

For monitoring parameters or the performance indicators of the manufacturing process the following techniques are used: For position of the cutting-tool subassembly is used the transducers system of CNC machine; For measurement the processing error are used dimensional inspection tools; For the cutting force are used transducers attached at the subassembly of the tool or piece; For temperature measurement are used the natural thermocouple (tool-piece) or thermal radiation of the machined surface.

Monitoring is at large intervals. In cases where monitoring is done online, the interpretation of monitoring results is the same as for offline monitoring. Even when both the measurement and interpretation of results is on-line (continuous), the result is used to maintain constant parameters of the process and not to recalculate its optimum value.

II. Characteristics of Conventional Control

It is characterized in that the model of the process remains unchanged and the result of the management represents necessary values of the process parameters. Values of the process parameters are set before and held constant during the development of process. For example: is constant: cutting regime, geometry of the cutting tool, processing material and features of the technological system.

Sometimes instead of the parameters: v , s , t of the regime of cutting are maintained constant values of cutting speed, force and feed rate of cutting and another time are maintained constant the speed, power and depth of cutting. So, from the process parameters are selected an independent set of parameters whose values are held constant during the process. Selected values of process parameters (which are held constant) is calculated on the basis of general mathematical models that are used in the management of any process. Eg speed cutting is determined depending on the tool durability, feed rate of cutting is determined depending the roughness of required surface, depth of cutting is determined depending on the size of the perform and achieved size, the geometry of the tool is determined depending on the geometrical features of processed surface. Dimensional control in conventional regime is characterized by:

- Off-line measurement of surface dimensions processed;

- The change the position of the tool relative to the materials just after the surface has been generated completely;
- Even when measuring of dimension is done online, change of the position of the tool relative to the material is made after the surface has been generated completely.

III. Optimal Control of Cutting Process

Basically, it is found that processing system evolves in time and space, making as a model, valid at a time and in a certain place, not to be suitable at another time and in another place. Other disadvantages would be:

- Does not take into account the characteristics of each specimen processed;
- Does not take into account errors of the technological system;
- There is no forecast on the evolution of the system in time and space.

Optimal control in conventional regime is characterized in that:

- Determining the optimal parameter values is based on general mathematical models applied in all particular cases encountered;
- The optimization criterion is the cost or productivity;
- The restrictions from the problem of the optimization are given by the limitations imposed technical indicators of performance of the process, such as speed minimum and maximum of the principal axle of the machine-tool, the minimum and maximum value of the feed rate, the maximum power of the motor drive, the maximum roughness of the surface ;
- The geometry of the tool is determined on the basis of general qualitative indications;
- Overcoming restrictions initially considered is ascertained after what the processing is occurred;
- It is not done the monitoring of the performance indicators of the process, but just only of the inputs in the process.

The objective of the optimal control is not getting imposed values of performance indicators, but getting the most favorable values of them. The parameter values corresponding to the most favorable performance indicator values are called optimal values.

Adaptive-optimal control involves re-identification of the machining process and the model obtained is used to calculate the optimal process parameters.

Optimal control characterizes the addition of the technical and economic indicators to process parameters. Characteristic for performance technical indicators is that their dependence to parameter values of process has a limitative, what leads to one of the following conclusions, appropriately or inappropriately, and therefore can serve as restrictions in optimization problem.

Economic indicators have a continuous dependence of process parameters and therefore they are used as objective functions.

IV. Strategies for Optimal Management of Cutting Process

To achieve various optimization criteria and, sometimes, to achieve concomitant such criteria it use different strategies. So,

A) To obtain a high productivity are used the following strategies:

- a) - feed rate strategy adapted to the cutting path - in which the processing time is reduced by a cutting operation along the cutting direction with minimum force and a reduced error and maximizing the speed of advance;
- b) selection of process parameters (feed rate, cutting depth, cutting speed) can have significant influence on system performance on productivity;
- c) Another work [1] analyzes productivity and problem of the preventive control maintenance for a manufacturing system on a machine-tool that processes multiple tracks simultaneously. The objective of such a study is to determine productivity and ensure a continuous supply of the machine-tool so that the total costs to be minimal. In the work [5] in which the author refers to the fact that adjusting the cutting forces lead to significant economic benefits by increasing productivity and improving quality operations. This is a challenge since the variation of the forces vary significantly in cutting normal conditions. The controllers can not guarantee system performance and stability since the force varies and substantial research effort was conducted to develop an adaptive controller. Consequently, in industry this technology it is applied reduced

B): To get a surface with a good quality it is used:

- a) - the surface control strategy of the in which processing errors are minimized by using an offset control of the surface, based on a prediction of the processing error ;
- b) - [1] presents an optimization model in terms of selection parameters of the machine tools that lead to a certain amount of material removed for a certain quality of surface and a certain durability of the cutting tools. The interpretation is based on the models presented by [2] to predict the surface roughness, cutting the maximum

temperature, distribution of the residual stress on the processing surface and using of the parameters of the machine-tool and of the cutting conditions. The numerical results demonstrate that the procedure can be considered as an advantage used to specify variations of the machine-tool for developing of the data base of the variables of the machine. This unified model is proposed for to represent the strategy for a adaptive control system of the machine-tool process. In conclusion, this computerized procedure is presented to illustrate the potential of planning of the car by determining the optimum parameters that maximize material removal rate to achieve the desired parameters of the surface. The procedure takes into account the limits and plastic deformations of the tool. An interesting result of this study is that, the increasing of the compressive residual stress limits desired reduce the optimum value of the cutting speed and obviously the rate of the reduction of material removed. This, because the cutting speed generates fractional heat and residual gradient produces residual stresses in the surface of the part [6]. This work describes a unified optimization model that takes into account the integrity of the surface and stability of the tool and it was based on physical relations of the processes of the machine. Model and simulated results can be applied in the development of the decision basic data for adaptive control of the machining process.

c) Another approach in terms of optimization is done in [1]. In this paper it is studied an algorithm based on optimizing stimulated and Hooke-Jeeves search model is developed to optimize cutting operations in multiple passes. Machine parameters are determined to optimize conditions and minimization of cost per unit of product, taking into account certain limitations. The results of experiments demonstrate that the optimization algorithm for limitations nonlinear, called SA / PS is effective for solving complex optimization problems.

The algorithm SA / PS can be inserted into a CAPP system for generating optimum parameters of the machine-tool. In this paper it was presented a cutting operation with multiple passes and a hybrid procedure based on simulation algorithm of the normalization and SA / PS for search was applied to the problem of optimizing machine tool. The algorithm SA / PS can achieve a non-linear solution in a spatial solution extremely rare compared with the notion of time. The effectiveness of this algorithm was demonstrated by a base experiment.

C) To achieve two goals simultaneously:

a) proposed strategies to improve productivity when conditions generated by cutting force and certain dimensional limitations. This strategy proposes a new processing aid, namely drawing a map of the maximum feed rates. In this map, the maximum permitted feed rate, depending on the required limitations, every checkpoint along the direction of processing are determined using a generating model of the surface. With this help, a part of the program is able to select a optimum cutting direction and a feed rate to reduce processing time. The strategy consists of three modules: 1 - selection of the control point; 2 - map of maximum feed speed; 3 - feed rate. So:

- Checkpoints are selected on the control surfaces. Number of points is selected depending of the imposed accuracy and density can vary. For each geometric point, cutting force and error of the processing are evaluated in sub-modules;

- The main goal is getting of the feed rate map for control of surfaces;

- The map reflects important information for choosing and selecting cutting speed. So, the processing time can be significantly reduced when surface processing, cutting forces and dimensional accuracy can be controlled using the proposed strategy.

b) A system type map is proposed in [3] too. This article proposes an algorithm for designing a control system of maps which consists of several separate maps, each of them is used to monitor the stage of a critical process from processing of a product. The algorithm consists of all maps integrated into an integrated system. Thus, the performance characteristics of a system as a whole can be significantly improved and product quality can be increased. One such improvement is achieved without additional costs or too much effort. Furthermore, operators can easily analyze, depending on the maps that are displayed on the display, the current situation at some point.

D) To maximize profits:

a) The strategy is a optimization function from point of view of geometrical quality, of productivity of system and cost. Geometric quality of the product is modeled as a set of functions based on the general propagation of the model variation, the productivity being a function of the processing and the cost, represents the sum of cost of production and the quality cost. Solving optimization problem leads to the determination of the best parameters of price and tolerance. The researchers followed a specific target for optimal demonstration character of the processing. It may list a number of ways of determining:

- By monitoring the durability of cutting and cutting tool;

- By monitoring of the cutting process and the durability of tool cutting;

The determination of an optimal algorithm for evaluation of process parameters;

- By looking for certain types of cutting tools;

- By monitoring tool wear;

- The determination of the parameters of the machine-tool.

The differences come from the definition of optimization criteria, character online and off-line of the process, of the adaptive character or not of the algorithm.

Regarding optimization of cutting in multiple passes, which imposed certain restrictions, [5] considers that, the operation in one pass is not always the most economical and productive in terms of restrictions and demonstrates that cutting process in two or three passes may be cheaper or shorter in terms of time spent.

Optimization is determined by the combination of the geometric and linear programming. The operation in one pass is optimum if it is limited only to reach the highest speed possible - which is not a general requirement. Most common are the situations where restrictions are related to cutting force, a some roughness of surface, a durability of cutting tool and cutting speed.

In the latter case, two passes or three passes may be more economical and can be performed in a shorter time than the processing operation.

c) In the work [6] is studied the optimal control of material removal rate to achieve a optimal rate of cutting of a cutting tool so, to be able to achieve maximum profit. This paper focuses not only on the rate of material what is removed in manufacturing process, integrated in mathematical formulas as objective functions, but it and implements the calculation of the variables to control the cutting rate.

E). Ensuring of a longer durability of the cutting tool

a) In [7] is presented a statistical model that uses the idea from the rehabilitation theory and statistical control of quality. The model is based on Taylor's equation so that information can be used relative to the existing relations between the cutting data and cutting tool durability.

b) Another study which is based on the cutting parameters optimization is studied for increase of durability tool. Improving sustainability is essential in order to reduce production costs as much as possible. The tools have a limited durability, which is why we need to find ways to increase the sustainability and critical process parameters cutting. Cutting tools deteriorates either through gradually wear of the cutting edge or due to plastic deformation at which they are subject. Usually, criteria of establishing sustainability are established as predetermined values. Obviously, any development will lead to an increase in durability.

The paper [4] shows the influence of the variation of speed on the durability when cutting. The paper [2] propose a new equation for durability.

d) Another study is achieved by [5] which shows that in the series production it uses the same cutting tool for cutting of the different parts having different cutting parameters. In such a case, the optim moments are those when tools need to be changed when it reaches the minimum production cost and a maximum rate of productivity. This paper analyzes the status of the processed surface and material waste from cutting tool using an algorithm of processing / analyzing and micro-optical images.

F) Minimize production costs

Such a strategy is presented in [5] which proposed a model of cutting in multiple passes. Using Lagrange method, cutting optimal time for each cutting tool is stored and the cost due Lagrange multiplier is multiplied.

V. Conclusions

Analyzing the current solutions of optimal or adaptive control of machining processes, the following conclusions are:

- Optimization of cutting is done by calculating the optimal parameters in its design stage of the technological process, following that they will be set and maintained at a constant value throughout the process of processing.
- Changing the parameter values is achieved to long periods and does not lead to the desired performance indicators;
- When monitoring is done online, the information obtained is used to delay and not for process optimization but keeping constant or limiting of values of some parameters.
- The mathematical models used to calculate the optimal parameters are generated and not resulted from the identification of real machining process or of the technological system used to achieve processing;
- The optimization algorithm of the technological process does not take into account the market success of the product and neither actual characteristics of each processed piece.
- Adaptive management system based on identification of the technological system-manufacturing process is not done currently at the available technological systems
- It finds that through the current control techniques of management process, real values of parameters are not optimal, which shows that there are enough reserves to increase performance indicators of the process through better management and without significant additional costs.

References

- 1) S. Hemmati, M. Rabbani, “Make-to-order/make-to-stock partitioning decision using the analytic network process”, *Int J Adv Manuf Technol*, DOI 10.1007/s00170-009-2312-4, 2009.
- 2) A. Garcia-Crespo, B. Ruiz-Mezcua, J.L. Lopez-Cuadrado, I. Gonzales-Carrasco, “A review of conventional and knowledge based systems for machining price quotation”, *J Intel Manuf*, DOI 10.1007/s10845-009-0335-1, 2009.
- 3) Niazi, A., Dai, J., Balabani, S., & Seneviratne, L. “Product cost estimation: Technique classification and methodology review”, *Journal of Manufacturing Science Engineering*, 128(2), 563–575, 2006.
- 4) E. Shehab and H. Abdalla, “An Intelligent Knowledge-Based System for Product Cost Modelling”, *Int J Adv Manuf Technol*, 2002, 19:49–65.
- 5) Fehmi H'mida, Patrick Martin, Francois Vernadat, “Cost estimation in mechanical production: The Cost Entity approach applied to integrated product engineering”, *Int. J. Production Economics*, 2006, 103: 17–35.
- 6) Z. Bouaziz, J. B. Younes and A. Zghal. “A Fast and Reliable Tool for Estimates for Plastic Blowing Moulds”, *Int J Adv Manuf Technol*, 2002, 20:545–550.
- 7) Z. Bouaziz, J. Ben Younes, A. Zghal, “Cost estimation system of dies manufacturing based on the complex machining features”, *Int J Adv Manuf Technol*, 2006, 28: 262–271, DOI 10.1007/s00170-004-2179-3.

The Influence Study of The Mole Ratio Reactant in Ceftriaxone Sodium Synthesis Against The Yield of The Production

Rohimmahtunnissa A., Alfian D.A., Agus S., Firdayani

Pharmaceutical and Biomedical Technology Center
 Agency for The Assessment and Application of Technology
 South Tangerang, Indonesia

ABSTRACT

Ceftriaxone is one of the third generations of cephalosporin antibiotics and commercially found as a sodium salt. The market demand for it is still high in recent years, including in Indonesia. However, there is no local production manufacture yet. A high yield of ceftriaxone sodium would be an advantage in industrial scale. Ceftriaxone was synthesized by reacting 7-amino-3-[(2,5-dihydro-6-hydroxy-2-methyl-5-oxo-1,2,4-triazin-3-yl) thiomethyl] cephalosporanic acid (7-ACT) with 2-Mercaptobenzothiazolyl (Z)-2-(2-Aminothiazole-4-yl)-2-Methoxyimino Acetate (MAEM) then with sodium salt in basic condition. The product was generated by solventing-out using acetone. The products were analyzed by HPLC quantitatively and the structure was confirmed using FTIR, MS and NMR. In this research, the variation in the mole ratio of reactants against the yield of product was evaluated. The result showed that the variations in mole ratio reactants affect the yield production. The higher ratio of MAEM would be the higher yield is obtained. The results show that the yield was 72,17% at mole ratio 1:2 which has 99,32% purity. This result could be a consideration in industrial production scale in ceftriaxone sodium preparation.

Keywords—*ceftriaxone sodium; mole ratio; yield*

I. Introduction

Ceftriaxone has white to yellowish-orange odourless crystalline powder. It has obtained high status among the cephalosporin drugs. Like other third-generation cephalosporins, it is considerably less active than first-generation drugs against gram-positive bacteria but has a much broader spectrum of activity against gram-negative organisms. It is also effective against gram-negative anaerobes and Enterobacteriaceae (*Echeria coli*, *Enterobacter*, *Klebsiella pneumoniae*) [1].

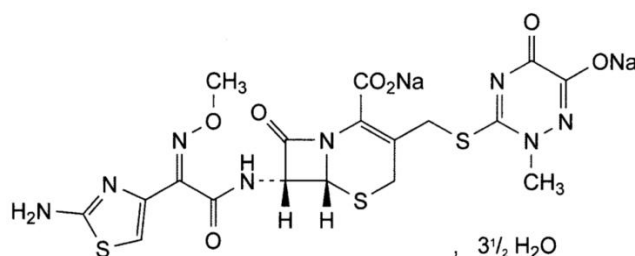


Fig. 1. Chemical structure of ceftriaxone disodium hemiheptahydrate [2]

Ceftriaxone is effective in the treatment of various infections caused by susceptible organisms including those of the bone and joint, abdomen, lower respiratory tract, meninges, pelvic area, skin and soft tissue, and the urinary tract. It is also effective in the treatment of septic arthritis, bacteremia, and gonorrhea, caused by organisms susceptible to the antibiotic [1, 3, 4].

Ceftriaxone sodium (Fig. 1) could be obtained by reacting 7-ACT with MAEM then the suspension reacts with sodium salts such as Sodium acetate, sodium carbonate and sodium 2-ethyl hexanoate.

The reaction between ceftriaxone and sodium salts occurred at the basic condition, $\text{pH} \leq 8$. If the pH above 8, ceftriaxone sodium could be dissolved and it is disadvantage the process [1]. There are other methods to obtained ceftriaxone by substituted the starting material, 7-ACT substituted with 7-aminocephalosporanic acid (7-ACA) [1] or substituted MAEM with other Active esters [5]. However, these methods profitable less in step process which needs a lot of steps and supporting materials.

One of the factors to make a profitable industry is a high yield production. The yield production depends on the reaction process which is the reaction condition affects the yield. There are some factors in reaction; temperature, pressure, concentration, surface area and catalysts. Hence, this research has evaluated the variation in the mole ratio of reactants against the yield of the product. Increasing a mole ratio of reactant could accelerate the reaction rate at some typical reaction. The variation in the mole ratio of 7-ACT: MAEM is 1:1; 1:1.25; 1:1.5 and 1:2. The higher concentration of reactants could accelerate the reaction. Therefore, increasing 7-ACT would not favorable because the solubility characteristic as same as ceftriaxone sodium which it would be a matter to remove the excess 7-ACT. So, increasing concentration of MAEM could lead to a higher yield production.

II. Methodology

A. Materials

The chemicals that used in this research are purchased, MAEM and 7-ACT from Hefei Joye Import & Export Co., Ltd, China, Triethylamine and Sodium acetate trihydrate from Merck. The working standard is Ceftriaxone disodium hemiheptahydrate from Santa Cruz Biotechnology, Inc. for comparison.

B. Variables

There are 3 variables in this research. First, the independent variables was mole ratio of MAEM, 1; 1,25; 1,5; 2. Second, the dependent variables was the yield and the purity of the product. Third, the control variables was temperature reaction between MAEM, 7-ACT, and Triethylamine at 15°C , the other steps of the process at ambient pressure.

C. Methods

The method of ceftriaxone sodium synthesis in this research based on US Patent No. 5574155 in 1996, Example 1 [6] and used 1/10 reactants as a basis in the reaction. The amount of MAEM based on mole ratio was dissolved in the mixture distilled water and acetone in the Erlenmeyer flask 250 mL then 7-ACT was added. The Triethylamine solution was added to suspension and stirred at 15°C . Sodium acetate trihydrate was added to form a sodium salt of ceftriaxone. Acetone was added with rate 2 ml/min [7] and slow down the rate 1 ml/min to solvating-out the solid product from the solution. The products were centrifuged, washed by the mixture of distilled acetone and water [2,8] then dried in desiccator vacuum.

The synthesis product was analyzed by HPLC (UFLC Shimadzu 20A) to check the purity of the product in and the structure was confirmed by FTIR (Thermo Scientific, Nicolet iS10), proton NMR and MS spectra with ESI-positive ion method.

III. Results

A. The Qualitative Test Results

The product sample tested by FT-IR Spectroscopy, the results can be seen in Table 1 for similarity and Fig. 2.

Table 1. Similarity percentage of ceftriaxone sodium synthesis product

| Ratio Mole 7-ACT | Ratio Mole MAEM | % Similarity |
|------------------|-----------------|--------------|
| 1 | 1 | 88,41 |
| 1 | 1,25 | 89,36 |

| | | |
|-----------------------------|-----|-------|
| 1 | 1,5 | 88,55 |
| 1 | 2 | 92,71 |
| Working standard Santa Cruz | | 95,10 |

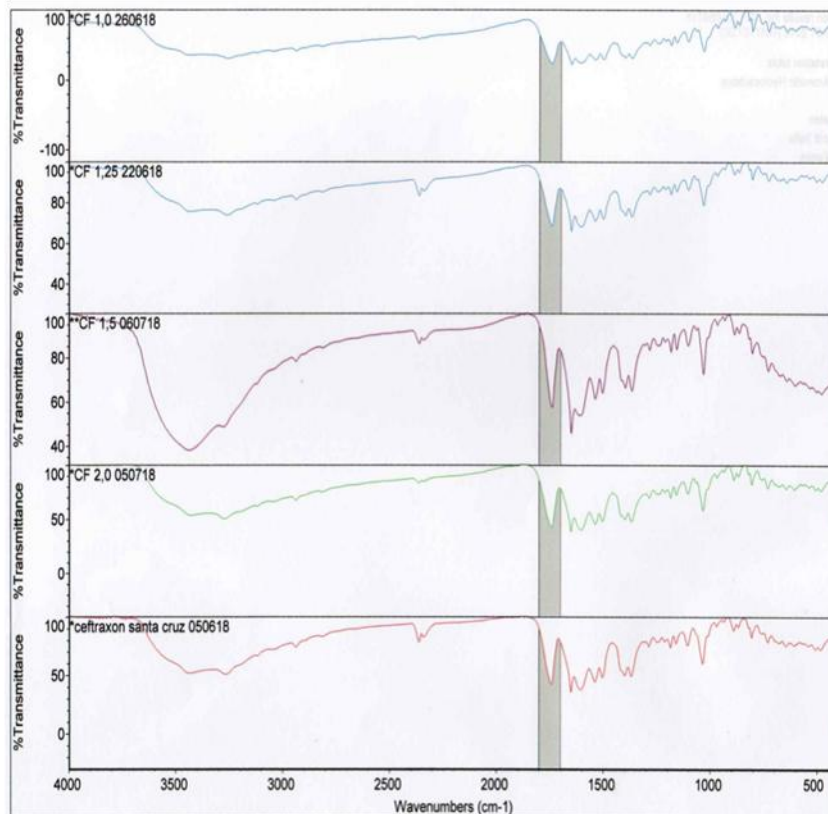


Fig. 2. IR-Spectra of the synthesis product and the RDS Santa Cruz

The product also tested by NMR and LC-MS. The results can be seen in Fig. 3 and Fig. 4. The qualitative test done for certainty the product is sodium ceftriaxone.

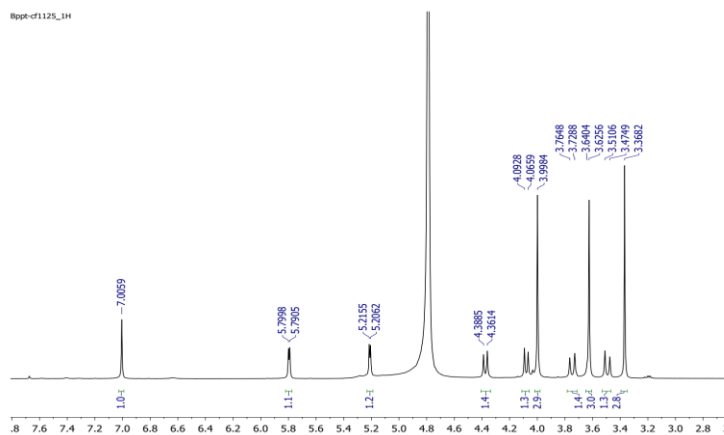


Fig. 3. 1H-NMR Spectrum of the synthesis product

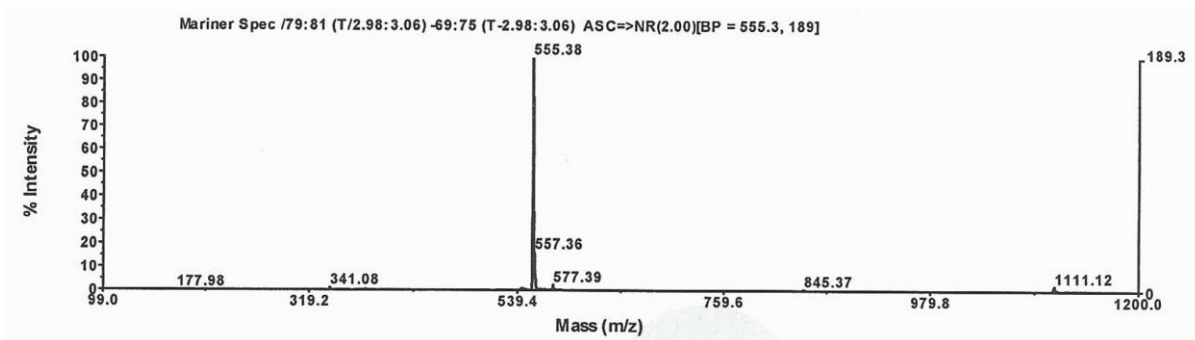


Fig. 4. LC-MS spectrum of synthesis product

B. The Quantitative Test Results

The synthesis products tested by HPLC to acquire the purities and calculated the yield.

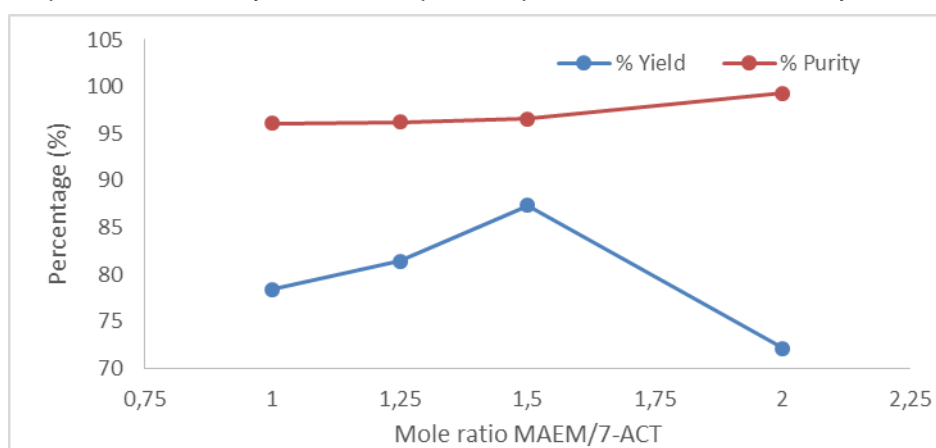
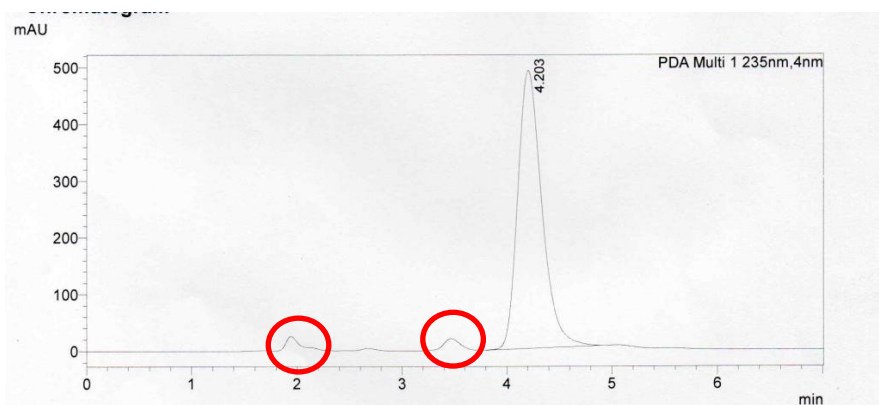


Fig. 5. The yield and purity of the synthesis product

The purity of working standard also tested by HPLC for a comparison with the sample products.



(Figure 3 chromatogram of RDS Santa Cruz)

IV. Discussion

A. The Qualitative Test Results

The sample product analyzed by FT-IR Spectroscopy to confirm the sample is ceftriaxone sodium. The IR Spectral of the variable samples and standard has compared. In the Table 1 can be seen that 1:2 in mole ratio has the highest similarity with the standard, 92,71%. It compared with the data in the

system library HR Georgia State Forensic Drugs as ceftriaxone meanwhile the working standard Santa Cruz 95,10% in similarity.

Trindade (2017) reported that the carbonyl present in the region between 1800 and 1700 cm^{-1} is specific and useful in the determination of ceftriaxone sodium in powder for injection [9]. Fig. 4 showed the carbonyl band in the region between 1800 and 1700 cm^{-1} which indicated the sample was confirmed as ceftriaxone sodium.

The product was analyzed by $^1\text{H-NMR}$ and the spectrum data confirm the structure of ceftriaxone sodium. $^1\text{H-NMR}$ (500 MHz, $\text{C}_3\text{D}_6\text{O}$, δ , ppm): 7.00 (s, 1H, aromatic C-H), 5.79-5.80 (d, 1H, $J = 5.0$ Hz), 5.20-5.21 (d, 1H, $J = 5.0$ Hz), 4.00 (s, 3H, NO-CH_3), 3.63 (s, 3H, N-CH_3), 3.37 (s, 2H, S-CH_2). Some of the spectra had shifted compared to Owens [1] and Dash cited in their report which could be caused by the impurities of the product. There were some protons did not show up completely such as NH_2 and NH . In addition, the CH_2 band could overlap with another CH_2 band because there was only one spectrum detected.

The product also analyzed by LC-MS with 5 μL volume injection, 0.2 mL/min in flowrate, methanol mobile phase in C-8 (15 mm x 2 mm) column. The spectrum in Figure 4 indicated that the product is sodium ceftriaxone which ceftriaxone has 554.53 in molecular weight. The mass peak show at 555.38 m/z for $\text{M}+\text{H}$ so that the molecular weight is 554.38 which is similar with molecular weight of ceftriaxone.

B. The Yield and Purity of The Product

The product from all variable in mole ratio has yellowish powder in appearance. The yield and the purity can be seen in Fig 2. The results showed that the yield increased then decreased to 70,12% at 1:2 in 7-ACT:MAEM mole ratio while the purity still increased, significantly at 1:2 in mole ratio. It might happen when added more reactant could increase the yield but at a certain point the excess reactant could inhibit the reaction or interfere the solventing-out process. Jagadale (2012) also had the same phenomenon, at the certain mole ratio, the yield product decreased because the excess reactant interferes in the separation process which made solubility increased [10].

The purity was analyzed by HPLC then compared the sample results with the standard from Santa Cruz. All of the synthesis product had more than 96% in purity which above the USP standard 79,5%. The chromatogram showed that the standard had more than one peak. So, the samples were compared to highest peak only then calculated by a single point of view. Shrestha (2013) reported that the ceftriaxone sodium standard only had one peak and the impurities showed up after a few treatment variables [11].

V. conclusion

Based on the results, the synthesis product is ceftriaxone sodium, confirmed by spectra FT-IR, spectrum H-NMR, and spectrum LC-MS. The yield of ceftriaxone sodium could be improved by increased a mole ratio of MAEM at certain point although the purity could still be increased by added more mole of MAEM.

Acknowledgment

The authors thanks to Ms Raodhatul Jannah as laboratory assistant for technical support and Laboratory Synthesis of LAPTIB BPPT.

References

- [1] Owens HM, Dash AK. Ceftriaxone sodium: comprehensive profile. Profiles of Drug Substances, Excipients, and Related Methodology. 2003, vol. 30, pp. 21–57.
- [2] British Pharmacopeia. British Pharmacopeia. London: Her Majesty's Stationary Office. 2012.

- [3] Mantu FNK, Goenawi LR, Bodhi W. Evaluation of antibiotic application to urinary infection patients in RSUP Prof. Dr. R. D. Kandaou Manado; July 2013-June 2014. PHARMACON Journal of Scientific Pharmacy–UNSRAT 2015, vol. 4(4), pp. 196-202. (In Indonesian).
- [4] Furdianti NH, Maharani NA, Saputri M. Analysis of Drug Related Problems (DRP'S) in antibiotics application to children inpatients in Klinik Sari Medika Ambarawa. Journal of Pharmaceutical and Natural Remedies 2016, vol. 5, pp. 49-58. (In Indonesian).
- [5] Zhao WL, Yue XP, Zhao ZD. One-pot synthesis method of ceftriaxone sodium. China Patent 105061472A. 2015.
- [6] Danklmaier J, Ingolf M, Prager Bernhard. Process for the synthesis of the disodium salt hemiheptahydrate of ceftriaxone. US Patent No. 5574155. 1996.
- [7] Zhang CT, Wang HR, Wang YL. Internally generated seeding policy in anti-solvent crystallization of ceftriaxone sodium. Chemical Engineering and Processing 2010, vol. 49, pp. 396–401.
- [8] Zhang CT, Wang JK, Wang YL. Solubility of ceftriaxone disodium in acetone, methanol, ethanol, N,N-dimethylformamide, and formamide between 278 and 318 K. J. Chem. Eng. Data 2005, vol. 50, pp. 1757–1760.
- [9] Trindade MTd, Salgado HRN. Development and Validation of a Modern and Stability-Indicating Method for the Quantification of Ceftriaxone Sodium in Powder for Injection by Infrared Spectroscopy. Physical Chemistry 2017, vol. 7(3), pp. 55-62.
- [10] Jagadale SS, Jugulkar LM. Review of Various Reaction Parameters and Other Factors Affecting on Production of Chicken Fat Based Biodiesel. International Journal of Modern Engineering Research 2012, vol. 2(2), pp. 407-411.
- [11] Bhupendra S., Nihar RB, and Barij NS. Simultaneous determination of Ceftriaxone and Tazobactam in injectables by UPHPLC method. Pharmaceutical Methods 2013. vol. 4, pp. 46–51.

MHD Newtonian and non-Newtonian Nano Fluid Flow Passing On A Magnetic Sphere with Mixed Convection Effect

Basuki Widodo, Yolanda Norasia, Dieky Adzkiya

Department of Mathematics, Faculty of Mathematics, Computing, and Data Sciences
Institut Teknologi Sepuluh Nopember
Indonesia

ABSTRACT

This paper considers the problem of magneto-hydrodynamics (MHD) Newtonian and non-Newtonian nano fluid flow passing on a magnetic sphere with mixed convection effect. Nano Fluid is a combination of liquid fluid as a base fluid with small solid nano particles. Water is chosen as Newtonian base fluid and oil is chosen as non-Newtonian base fluid. Then, Alumina and Copper are chosen as solid particle in nano fluid. We further construct governing equation by applying continuity equation, momentum equation, and energy equation to obtain dimensional governing equations. The dimensional governing equations that have been obtained are converted into non-dimensional governing equations by substituting non-dimensional variables. The non-dimensional governing equations are further transformed into similarity equations using stream function and solved numerically using Euler Implicit Finite Difference method. We further analyse the effect of magnetic parameter towards velocity and temperature in MHD nano fluid flow. The results show that the increases of magnetic parameter impacts to the decrease of velocity and temperature. Then, the velocity and temperature of Newtonian nano fluid are higher than the velocity and temperature of non-Newtonian nano fluid. Also, the velocity and temperature of copper-water are higher than the velocity and temperature of Alumina-water.

Keywords—Newtonian and non-Newtonian nano fluid; MHD; Sphere; Euler Implicit Finite Difference.

I. INTRODUCTION

Nano fluid is a combination of liquid fluid as a base fluid with small solid nano particles [1]. Nano fluid is divided into two types, i.e. Newtonian nano fluid and non-Newtonian nano fluid. Newtonian nano fluid is a base fluid in nano fluid which has a linear relationship between viscosity and shear stress. However, non-Newtonian nano fluid is the opposite of Newtonian nano fluid. In this paper, water is chosen as Newtonian base fluid and oil is chosen as non-Newtonian base fluid. Then, Alumina (Al_2O_3) and Copper (Cu) are chosen as solid particle in nano fluid. Alumina (Al_2O_3) contains metal oxide and copper (Cu) contains metal. These types of fluids are used in industrial area that needs for heating and cooling based on heat transfer [2].

Because of those, we conduct a research how to analyse MHD nano fluid flow problem using numerical simulation based on mathematical modelling. Putra et al [3] have illustrated the natural convection of nano-fluids. Their investigations stated that the thermal conductivity of solid nano particles can be increased when mixed with base fluid. Wen and Ding [4] have discussed about experimental investigation into convection heat transfer of nano fluids at the entrance region under laminar flow conditions. Akbar et al [5] have investigated unsteady MHD nano fluid flow through a channel with moving porous walls and medium by using Runge Kutta. The results show that the heat transfer rate increases and mass transfer rate decreases with the increase of Reynolds number. Mahat et al [6] also have observed mixed convection boundary layer flow past a horizontal circular cylinder in visco-elastic nano fluid with constant wall temperature and solved numerically by using the Keller-Box

method. The results indicate that the velocity and temperature are increased by increasing the values of nano particles volume fraction and mixed convection parameter. Juliyanto et al [7] also have solved the problem of the effect of heat generation on mixed convection in nano fluids over a horizontal circular cylinder numerically by using Keller-Box method. The result of their investigations show that the velocity increase and temperature decrease when mixed convection parameter increases. In the present paper, we are interested to develop mathematical modelling of the problem of MHD newtonian and non-newtonian nano fluid flow passing on a magnetic sphere with mixed convection effect. The influence of magnetic parameter (M), mixed convection parameter (λ), and volume fraction (χ) towards velocity and temperature in Newtonian and non-Newtonian nano fluid are investigated.

II. MATHEMATICAL FORMULATION

The unsteady MHD Newtonian and non-Newtonian nano fluid flow passing on a magnetic sphere with mixed convection effect is considered. *Fig. 1* illustrates the physical model of the problem and the coordinate system used to develop the mathematical model. The fluid used is Newtonian nano fluid and non-Newtonian nano fluid. The bluff body used is a magnetic sphere with radius a . The flow of nano fluid is assumed laminar flow and incompressible. The magnetic Reynolds number is assumed to be very small. Therefore, there is no electrical voltage which makes electric field. With potential theory, where the velocity potential is perpendicular with stream function, so the 3D dimensional governing equations can be transform into 2D dimensional governing equations.

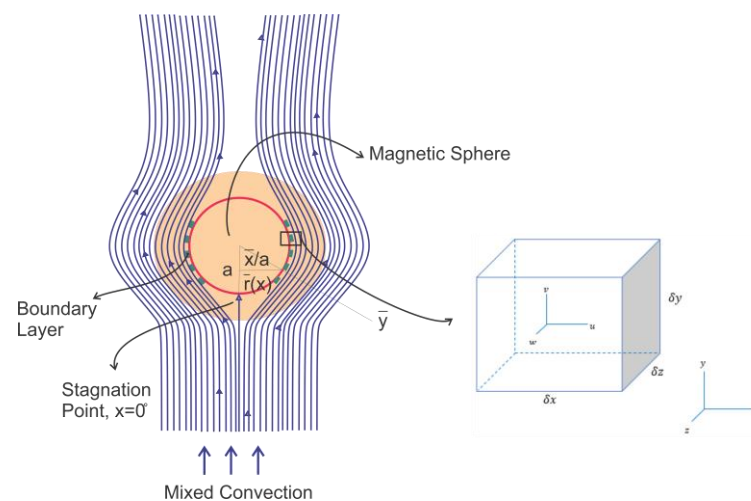


Fig. 1 Physical model and coordinate system

Based on the physical model and coordinate system, unsteady MHD Newtonian and non-Newtonian nano fluid flow passing on a magnetic sphere is illustrated in *Fig. 1*. The 2D dimensional governing equations are developed from the law of conservation mass, the second law of Newton, and the first law of Thermodynamics. We further obtain continuity equation, momentum equation, and energy equation, which can be written as follows:

Continuity Equation:

$$\frac{\partial \bar{r}\bar{u}}{\partial \bar{x}} + \frac{\partial \bar{r}\bar{v}}{\partial \bar{y}} = 0 \quad (1)$$

Momentum Equation :

at x axis

$$\rho_{fn} \left(\frac{\partial \bar{u}}{\partial \bar{t}} + \bar{u} \frac{\partial \bar{u}}{\partial \bar{x}} + \bar{v} \frac{\partial \bar{u}}{\partial \bar{y}} \right) = -\frac{\partial \bar{p}}{\partial \bar{x}} + \mu_{fn} \left(\frac{\partial^2 \bar{u}}{\partial \bar{x}^2} + \frac{\partial^2 \bar{u}}{\partial \bar{y}^2} \right) + \sigma B_0^2 \bar{u} - \rho_{fn} \beta (\bar{T} - T_\infty) g_{\bar{x}} \quad (2)$$

at y axis

$$\rho_{fn} \left(\frac{\partial \bar{u}}{\partial \bar{t}} + \bar{u} \frac{\partial \bar{u}}{\partial \bar{x}} + \bar{v} \frac{\partial \bar{u}}{\partial \bar{y}} \right) = -\frac{\partial \bar{p}}{\partial \bar{x}} + \mu_{fn} \left(\frac{\partial^2 \bar{u}}{\partial \bar{x}^2} + \frac{\partial^2 \bar{u}}{\partial \bar{y}^2} \right) + \sigma B_0^2 \bar{u} - \rho_{fn} \beta (\bar{T} - T_\infty) g_{\bar{y}} \quad (3)$$

Energy Equation :

$$\left(\frac{\partial \bar{T}}{\partial \bar{t}} + \bar{u} \frac{\partial \bar{T}}{\partial \bar{x}} + \bar{v} \frac{\partial \bar{T}}{\partial \bar{y}} \right) = \alpha_{fn} \left(\frac{\partial^2 \bar{T}}{\partial \bar{x}^2} + \frac{\partial^2 \bar{T}}{\partial \bar{y}^2} \right) \quad (4)$$

With the initial and boundary condition as follows :

$$\begin{aligned} \bar{t} = 0: \bar{u} = \bar{v} = 0, \bar{T} = T_\infty, \text{ for every } \bar{x}, \bar{y} \\ \bar{t} > 0: \bar{u} = \bar{v} = 0, \bar{T} = T_w, \text{ for } \bar{y} = 0 \\ \bar{u} = \bar{u}_e(\bar{x}), \bar{u} = \bar{v} = 0, \bar{T} = T_\infty \text{ as } \bar{y} \rightarrow \infty \end{aligned}$$

where ρ_{fn} is density of nano fluid, μ_{fn} is dynamic viscosity of nano fluid, g is the gravitational acceleration, and α_{fn} is thermal diffusivity of nano fluid. In addition, the value of r is defined as $\bar{r}(\bar{x}) = a \sin(\bar{x}/a)$.

Further, the 2D dimensional governing equations (1)-(4) are transformed into non-dimensional equations by using both non-dimensional parameters and variables. In this problem, the non-dimensional variables are given as in [7], i.e.:

$$\begin{aligned} x = \frac{\bar{x}}{a}; y = Re^{1/2} \frac{\bar{y}}{a}; t = \frac{U_\infty \bar{t}}{a}; u = \frac{\bar{u}}{U_\infty} \\ v = Re^{1/2} \frac{\bar{v}}{U_\infty}; r(x) = \frac{\bar{r}(\bar{x})}{a} \end{aligned}$$

where g_x and g_y are defined as in [7]

$$\begin{aligned} g_x = -g \sin \left(\frac{\bar{x}}{a} \right) \\ g_y = g \cos \left(\frac{\bar{x}}{a} \right) \end{aligned}$$

Boundary layer theory [8] is applied to non-dimensional governing equation. We obtain the following results

Continuity Equation

$$\frac{\partial(ru)}{\partial x} + \frac{\partial(rv)}{\partial y} = 0 \quad (5)$$

Momentum Equation

at x axis

$$\frac{\partial u}{\partial t} + u \frac{\partial u}{\partial x} + v \frac{\partial u}{\partial y} = -\frac{\partial p}{\partial x} + \frac{\nu_{nf}}{\nu_f} \frac{\partial^2 u}{\partial y^2} + Mu + \lambda T \sin x \quad (6)$$

at y axis

$$-\frac{\partial p}{\partial y} = 0 \quad (7)$$

Energy Equation

$$\left(\frac{\partial T}{\partial t} + u \frac{\partial T}{\partial x} + v \frac{\partial T}{\partial y} \right) = \frac{1}{Pr} \frac{\alpha_{fn}}{\alpha_f} \frac{\partial^2 T}{\partial y^2} \quad (8)$$

where these nano fluid constants are defined as [9], i.e. :

Density of nanofluid :

$$\rho_{fn} = (1 - \chi)\rho_f + \chi\rho_s$$

Dynamic viscosity :

$$\mu_{nf} = \mu_f \frac{1}{(1 - \chi)^{2.5}}$$

Specific heat :

$$(\rho C_p)_{nf} = (1 - \chi)(\rho C_p)_f + \chi(\rho C_p)_s$$

Heat conductivity :

$$k_{nf} = \frac{k_s + 2k_f - 2\chi(k_f - k_s)}{k_s + 2k_f + \chi(k_f - k_s)} k_f$$

The thermo-physical properties of nano particles and base fluid is given in Table 1 [10].

TABLE I. THERMO-PHYSICAL PROPERTIES

| <i>Properties</i> | <i>Water</i> | <i>Oil</i> | <i>Cu</i> | <i>Al₂O₃</i> |
|---|--------------|------------|-----------|------------------------------------|
| <i>density</i> | 997.1 | 884 | 8933 | 3970 |
| <i>specific heat of constant pressure</i> | 4179 | 1900 | 385 | 765 |
| <i>thermal conductivity</i> | 0.613 | 0.145 | 400 | 40 |

We substitute those nano fluid constants into (6) and (8). We obtain

Momentum Equation :

$$\frac{\partial u}{\partial t} + u \frac{\partial u}{\partial x} + v \frac{\partial u}{\partial y} = -\frac{\partial p}{\partial x} + \left(\frac{1}{(1-\chi)^{2.5}} \frac{1}{(1-\chi)+\chi\left(\frac{\rho_s}{\rho_f}\right)} \right) \frac{\partial^2 u}{\partial y^2} + Mu + \lambda T \sin x \tag{9}$$

And

Energy equation :

$$\left(\frac{\partial T}{\partial t} + u \frac{\partial T}{\partial x} + v \frac{\partial T}{\partial y} \right) = \frac{1}{Pr} \frac{k_s + 2k_f - 2\chi(k_s - k_f)}{k_s + 2k_f + \chi(k_s - k_f)} \frac{1}{(1-\chi)+\chi\left(\frac{\rho C_p)_s}{(\rho C_p)_f}\right)} \frac{\partial^2 T}{\partial y^2} \tag{10}$$

Further, by converting (9) and (10) into non-similarity equations using stream function, which is given as follows [11]

$$u = \frac{1}{r} \frac{\partial \psi}{\partial y}$$

$$v = -\frac{1}{r} \frac{\partial \psi}{\partial x}$$

Where

$$\psi = t^{\frac{1}{2}} u_e(x) r(x) f(x, \eta, t),$$

$$\eta = \frac{y}{t^{\frac{1}{2}}}$$

$$T = s(x, \eta, t)$$

The equation (9) and (10) are modified by substituting stream function as follows:

Momentum Equation :

$$\left[\frac{1}{(1-\chi)^{2.5} \left[(1-\chi) + \left(\frac{\rho_s}{\rho_f} \right) \right]} \right] \frac{\partial^3 f}{\partial \eta^3} + \frac{\eta \partial^2 f}{2 \partial \eta^2} + t \frac{\partial u_e}{\partial x} \left[1 - \left(\frac{\partial f}{\partial \eta} \right)^2 + f \frac{\partial^2 f}{\partial \eta^2} \right] = t \frac{\partial^2 f}{\partial \eta \partial t} + t u_e \left(\frac{\partial f}{\partial \eta} \frac{\partial^2 f}{\partial x \partial \eta} - \frac{\partial f}{\partial x} \frac{\partial^2 f}{\partial \eta^2} - \frac{1}{r} \frac{\partial r}{\partial x} f \frac{\partial^2 f}{\partial \eta^2} \right) + Mt \left(1 - \frac{\partial f}{\partial \eta} \right) - \frac{\lambda st}{u_e} \sin x \tag{11}$$

Energy Equation :

$$\left(\frac{k_s + 2k_f - 2\chi(k_s - k_f)}{k_s + 2k_f + \chi(k_s - k_f)} \frac{1}{(1-\chi) + \chi \left(\frac{\rho C_p s}{\rho C_p f} \right)} \right) \frac{\partial^2 s}{\partial \eta^2} + Pr \frac{\eta \partial s}{2 \partial \eta} + Pr t \frac{\partial u_e}{\partial x} f \frac{\partial s}{\partial \eta} = Pr t \left[\frac{\partial s}{\partial \eta} + u_e \left(\frac{\partial f}{\partial \eta} \frac{\partial s}{\partial x} - \frac{\partial f}{\partial x} \frac{\partial s}{\partial \eta} - \frac{1}{r} \frac{\partial r}{\partial x} f \frac{\partial s}{\partial \eta} \right) \right]$$

(12) With the initial and boundary condition are as follows :

$$t = 0 : f = \frac{\partial f}{\partial \eta} = s = 0 \text{ untuk setiap } x, \eta$$

$$t > 0 : f = \frac{\partial f}{\partial \eta} = 0, s = 1 \text{ ketika } \eta = 0$$

$$\frac{\partial f}{\partial \eta} = 1, s = 0 \text{ ketika } \eta \rightarrow \infty$$

By substituting local free stream for sphere case [12], $u_e = \frac{3}{2} \sin x$ into (11) and (12) respectively, we obtain

Momentum Equation :

$$\left[\frac{1}{(1-\chi)^{2.5} \left[(1-\chi) + \left(\frac{\rho_s}{\rho_f} \right) \right]} \right] \frac{\partial^3 f}{\partial \eta^3} + \frac{\eta \partial^2 f}{2 \partial \eta^2} + \frac{3}{2} t \cos x \left[1 - \left(\frac{\partial f}{\partial \eta} \right)^2 + 2f \frac{\partial^2 f}{\partial \eta^2} \right] = t \frac{\partial^2 f}{\partial \eta \partial t} + \frac{3}{2} t \sin x \left(\frac{\partial f}{\partial \eta} \frac{\partial^2 f}{\partial x \partial \eta} - \frac{\partial f}{\partial x} \frac{\partial^2 f}{\partial \eta^2} \right) + Mt \left(1 - \frac{\partial f}{\partial \eta} \right) - \frac{2}{3} \lambda st \tag{13}$$

Energy Equation :

$$\left(\frac{k_s + 2k_f - 2\chi(k_s - k_f)}{k_s + 2k_f + \chi(k_s - k_f)} \frac{1}{(1-\chi) + \chi \left(\frac{\rho C_p s}{\rho C_p f} \right)} \right) \frac{\partial^2 s}{\partial \eta^2} + Pr \frac{\eta \partial s}{2 \partial \eta} + 3 \cos x Pr t f \frac{\partial s}{\partial \eta} = Pr t \frac{\partial s}{\partial \eta} + Pr t \frac{3}{2} \sin x \left(\frac{\partial f}{\partial \eta} \frac{\partial s}{\partial x} - \frac{\partial f}{\partial x} \frac{\partial s}{\partial \eta} \right) \tag{14}$$

III. NUMERICAL PROCEDURES

MHD Newtonian and non-Newtonian nano fluid flow passing on a magnetic sphere with mixed convection effect have been investigated numerically by using Euler Implicit Finite Difference method. he set of similarity equation and boundary condition are discretized by a second order central difference method and solved by a computer program which has been developed.

Momentum Equation :

$$\left[\frac{1}{(1-\chi)^{2.5} \left[(1-\chi) + \chi \left(\frac{\rho_s}{\rho_f} \right) \right]} \right] \frac{\partial^2 u}{\partial \eta^2} + \frac{\eta \partial u}{2 \partial \eta} + \frac{3}{2} t \left(1 - (u)^2 + f \frac{\partial u}{\partial \eta} \right) = t \frac{\partial u}{\partial t} + Mt (1 - u) - \frac{2}{3} \lambda st$$

by using Euler implicit finite difference method we obtain

$$\begin{aligned} & \left[\frac{1}{(1-\chi)^{2.5}((1-\chi) + \chi \frac{\rho_s}{\rho_f})} \right] \frac{1}{\Delta \eta^2} (u_{i+1}^{n+1} - 2u_i^{n+1} + u_{i-1}^{n+1}) + \frac{\eta_i}{2} \left(\frac{3u_{i+1}^{n+1} - 4u_i^{n+1} + u_{i-1}^{n+1}}{2\Delta \eta} \right) \\ & + \frac{3}{2} t^{n+1} \left(1 - (u_i^{n+1})^2 + 2 \frac{1}{2\Delta \eta} f_i^n (3u_{i+1}^{n+1} - 4u_i^{n+1} + u_{i-1}^{n+1}) \right) \\ & = t^{n+1} \frac{1}{2\Delta t} (3u_{i+1}^{n+1} - 4u_i^n + u_{i-1}^{n+1}) + M t^{n+1} (1 - u_i^{n+1}) - \frac{2}{3} \lambda s_i^n t^{n+1} \end{aligned}$$

where K_i

$$\begin{aligned} K_i = & \left[\frac{1}{(1-\chi)^{2.5}((1-\chi) + \chi \frac{\rho_s}{\rho_f})} \right] \frac{1}{\Delta \eta^2} (u_{i+1}^n - 2u_i^n + u_{i-1}^n) + \frac{\eta_i}{4} \frac{1}{\Delta \eta} (3u_{i+1}^n - 4u_i^n + u_{i-1}^n) \\ & + \frac{3}{2} t^{n+1} \left(1 - (u_i^n)^2 + \frac{f_i^n}{\Delta \eta} (3u_{i+1}^n - 4u_i^n + u_{i-1}^n) \right) - t^{n+1} M (1 - u_i^n) + \frac{2}{3} \lambda s_i^n t^{n+1} \end{aligned}$$

and for

$$A_0 = \frac{1}{4} \frac{\eta_i}{\Delta \eta} + \frac{3}{2} t^{n+1} \frac{f_i^n}{\Delta \eta}$$

$$A_1 = \frac{\left[\frac{1}{(1-\chi)^{2.5}((1-\chi) + \chi \frac{\rho_s}{\rho_f})} \right]}{\Delta \eta^2} + A_0$$

$$A_2 = \frac{3}{2} \frac{t^{n+1}}{\Delta t} + 2 \frac{\left[\frac{1}{(1-\chi)^{2.5}((1-\chi) + \chi \frac{\rho_s}{\rho_f})} \right]}{\Delta \eta^2} - t^{n+1} M + 3 t^{n+1} u_i^n + 4A_0$$

$$A_3 = \frac{\left[\frac{1}{(1-\chi)^{2.5}((1-\chi) + \chi \frac{\rho_s}{\rho_f})} \right]}{\Delta \eta^2} + 3A_0$$

Energy Equation :

$$\text{Pr } t \frac{\partial s}{\partial t} = \left[\frac{(k_s + 2k_f) - 2\chi(k_f - k_s)}{((k_s + 2k_f) + \chi(k_f - k_s))((1-\chi) + \left(\frac{\chi \rho(Cp)_s}{\rho(Cp)_f}\right))} \right] \frac{\partial^2 s}{\partial \eta^2} + \text{Pr} \frac{\eta}{2} \frac{\partial s}{\partial \eta} + 3 \text{Pr } t \frac{\partial s}{\partial \eta}$$

by using implicit finite difference method we get

$$\begin{aligned} & \text{Pr } t^{n+1} \frac{1}{2\Delta t} (3s_i^{n+1} - 4s_i^n + s_i^{n-1}) \\ & = \left[\frac{(k_s + 2k_f) - 2\chi(k_f - k_s)}{((k_s + 2k_f) + \chi(k_f - k_s))((1-\chi) + \left(\frac{\chi \rho(Cp)_s}{\rho(Cp)_f}\right))} \right] \frac{1}{\Delta \eta^2} (s_{i+1}^{n+1} - 2s_i^{n+1} + s_{i-1}^{n+1}) \\ & + \text{Pr} \frac{\eta_i}{\Delta \eta} \frac{1}{2} (3s_{i+1}^{n+1} - 4s_i^{n+1} + s_{i-1}^{n+1}) + 3 \text{Pr } t^{n+1} f_i^n \frac{1}{2\Delta \eta} (3s_{i+1}^{n+1} - 4s_i^{n+1} + s_{i-1}^{n+1}) \end{aligned}$$

Where L_i

$$L_i = \left[\frac{(k_s + 2k_f) - 2\chi(k_f - k_s)}{((k_s + 2k_f) + \chi(k_f - k_s))((1 - \chi) + \left(\frac{\chi \rho(Cp)_s}{\rho(Cp)_f}\right))} \right] \frac{1}{\Delta\eta^2} (s_{i+1}^n - 2s_i^n + s_{i-1}^n) + \frac{1}{4} Pr \frac{\eta_i}{\Delta\eta} (3s_{i+1}^n - 4s_i^n + s_{i-1}^n) + 3 Pr \frac{t^{n+1}}{2\Delta\eta} f_i^n (3s_{i+1}^n - 4s_i^n + s_{i-1}^n)$$

and for

$$B_0 = \frac{1}{4} \frac{\eta_i}{\Delta\eta} + \frac{3}{2} Pr t^{n+1} \frac{f_i^n}{\Delta\eta}$$

$$B_1 = \left[\frac{(k_s + 2k_f) - 2\chi(k_f - k_s)}{((k_s + 2k_f) + \chi(k_f - k_s))((1 - \chi) + \left(\frac{\chi \rho(Cp)_s}{\rho(Cp)_f}\right))} \right] \frac{1}{\Delta\eta^2} + B_0$$

$$B_2 = \frac{3}{2} Pr \frac{t^{n+1}}{\Delta t} + 2 \left[\frac{(k_s + 2k_f) - 2\chi(k_f - k_s)}{((k_s + 2k_f) + \chi(k_f - k_s))((1 - \chi) + \left(\frac{\chi \rho(Cp)_s}{\rho(Cp)_f}\right))} \right] \frac{1}{\Delta\eta^2} + 4B_0$$

$$B_3 = \left[\frac{(k_s + 2k_f) - 2\chi(k_f - k_s)}{((k_s + 2k_f) + \chi(k_f - k_s))((1 - \chi) + \left(\frac{\chi \rho(Cp)_s}{\rho(Cp)_f}\right))} \right] \frac{1}{\Delta\eta^2} + 3B_0$$

IV. RESULTS AND DISCUSSION

In this research, the effect of magnetic parameter (M) to velocity and temperature in Newtonian and non-Newtonian nano fluid are analyzed.

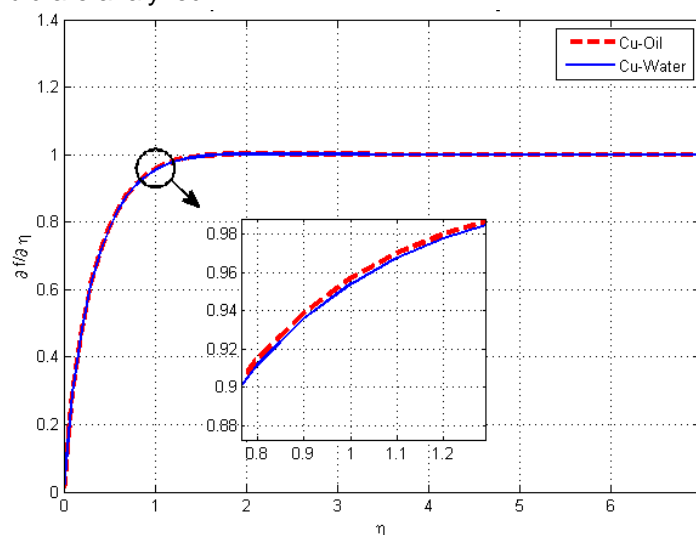


Fig. 2 Velocity Profile of Cu-Oil and Cu-Water with Magnetic Influence

Water is chosen as Newtonian base fluid and oil is chosen as non-Newtonian base fluid. Then, Alumina (Al_2O_3) and Copper (Cu) are chosen as solid particle in nano fluid. The numerical results of the velocity and temperature with respect to the position in front of the lower stagnation at

the point $x = 0^\circ$ with value of magnetic parameters $M = 1$ are depicted in Fig. 2 and Fig. 3 respectively.

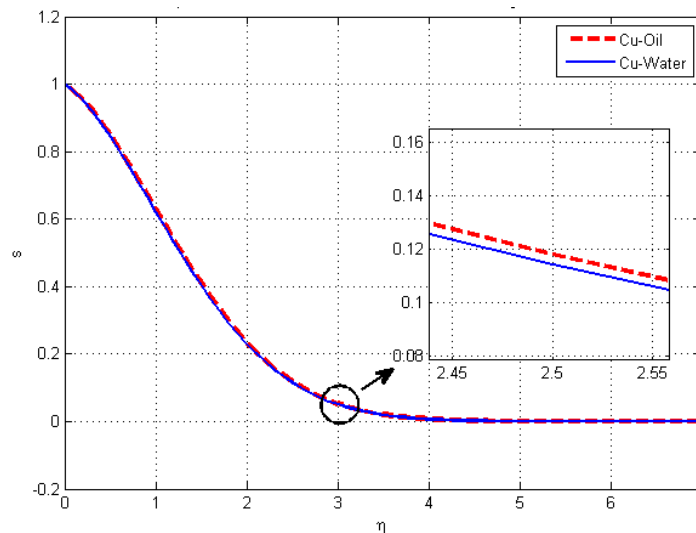


Fig. 3 Temperature Profile of Cu-Oil and Cu-Water with Magnetic Influence

Fig. 2 shows the velocity profiles of the MHD Newtonian and non-Newtonian nano fluid flow passing on a magnetic sphere with mixed convection effect. *Cu-oil* is used as non-Newtonian nano fluid and *Cu-water* is used as Newtonian nano fluid. The results show that the velocity of Newtonian nano fluid is higher than the velocity of non-Newtonian nano fluid. Also, Fig. 3 shows that the temperature of Newtonian nano fluid is higher than the temperature of non-Newtonian nano fluid.

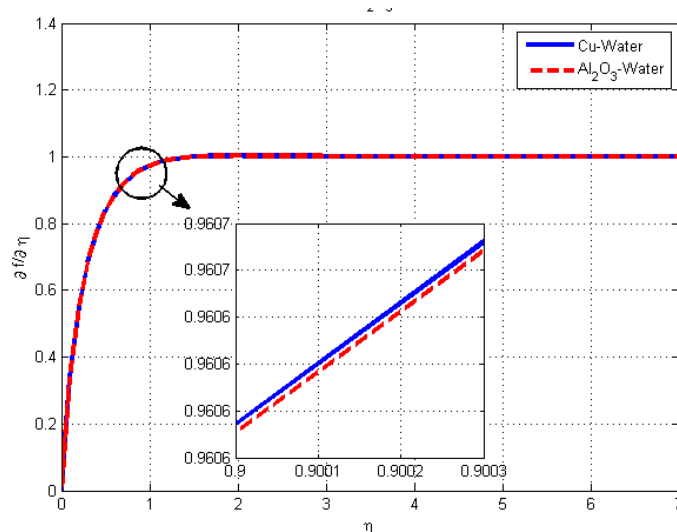


Fig. 4 Velocity Profile of Cu-Water and Al_2O_3 -Water with Magnetic Influence

Fig. 4 and Fig. 5 show the velocity profiles and temperature profiles of *Cu-Water* and *Al₂O₃-water* respectively. Alumina (Al_2O_3) contains metal oxide and copper (*Cu*) contains metal. The results show that the velocity of *Cu-Water* is higher than the velocity of *Al₂O₃-water*. Fig. 5 also shows that the temperature of *Cu-water* is higher than the temperature of *Al₂O₃-water*.

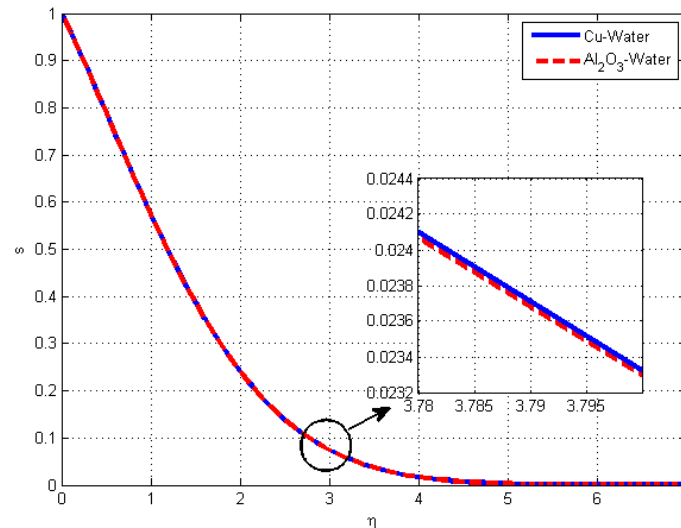


Fig. 5 Temperature Profile of Cu-Water and Al_2O_3 -Water with Magnetic Influence

The numerical results of the velocity and temperature in Newtonian nano fluid *Cu*-Water with respect to the position in front of the lower stagnation at the point $x = 0^\circ$ with various value of magnetic parameters $M = 0, 1, 3,$ and 5 are illustrated in *Fig. 6* and *Fig. 7* respectively.

Fig. 6 shows the velocity profiles of the MHD Newtonian nano fluid *Cu*-Water flow passing on a magnetic sphere at various M when mixed convection parameter $\lambda = 1$ and volume fraction $\chi = 0.1$. The results show that velocity and temperature of Newtonian nano fluid *Cu*-Water in *Fig. 6* and *Fig. 7* decrease when magnetic parameter increases. The magnetic parameter represents the presence of Lorentz force in a magnetic sphere. Therefore, when magnetic parameter increases, then the Lorentz force also increases. It impacts to decrease of the velocity and temperature in Newtonian nano fluid *Cu*-Water.

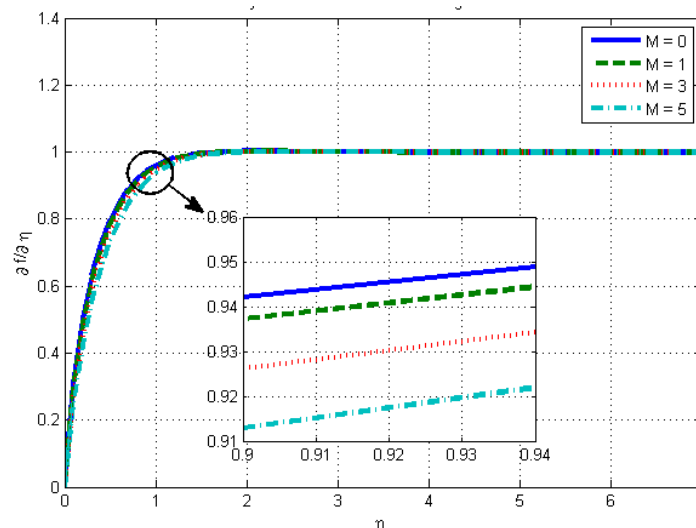


Fig. 6 Velocity Profile for various M of *Cu*-Water

The numerical results of the velocity and temperature in non-Newtonian nano fluid *Cu*-Oil with respect to the position in front of the lower stagnation at the point $\chi = 0.1$ with various value of magnetic parameters $M = 0, 1, 3,$ and 5 are illustrated in *Fig. 8* and *Fig. 9* respectively.

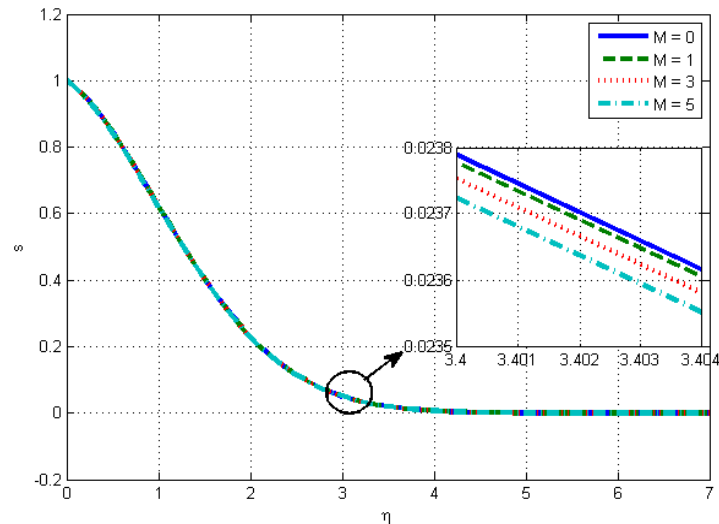


Fig. 7 Temperature Profile for various M of Cu-Water

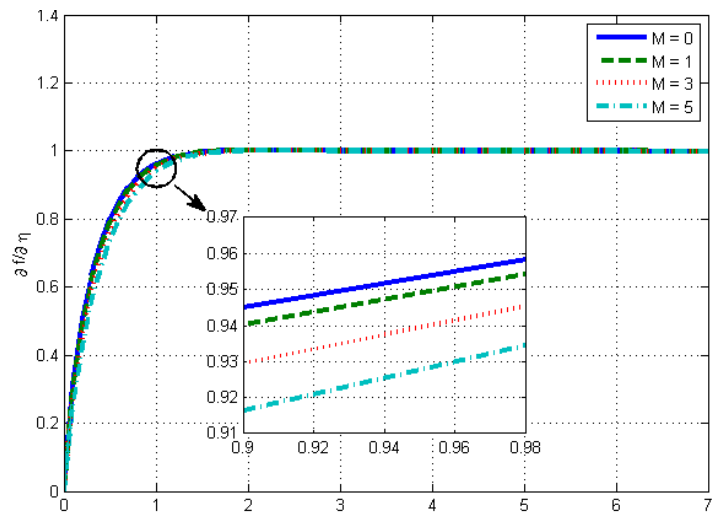


Fig. 8 Velocity Profile for various M of Cu-O

Fig. 8 shows the velocity of the MHD non Newtonian nano fluid *Cu-Oil* flow passing on a magnetic sphere at various M when mixed convection parameter $\lambda = 1$ and volume fraction $\chi = 0.1$. *Fig. 9* shows the temperature of the MHD non Newtonian nano fluid *Cu-Oil* flow passing on a magnetic sphere at various M when mixed convection parameter $\lambda = 1$ and volume fraction $\chi = 0.1$. The results in *Fig. 8* and *Fig. 9* show that velocity profiles and temperature profiles of non-Newtonian nano fluid *Cu-Oil* decrease when magnetic parameter increases.

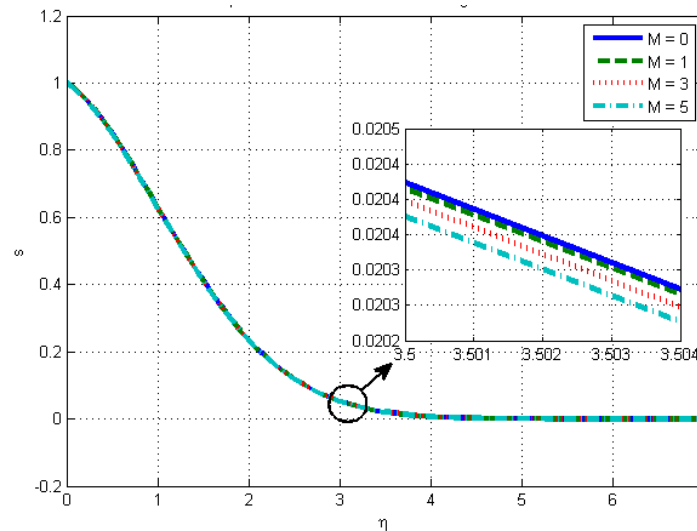


Fig. 9 Temperature Profile for various M of Cu-Oil

V. CONCLUSIONS

MHD Newtonian and non-Newtonian nano fluid flow passing on a magnetic sphere with mixed convection effect have been investigated numerically by using Euler Implicit Finite Difference method. We have considered water as Newtonian base fluid and oil is chosen as non-Newtonian base fluid. Further, Alumina (Al_2O_3) and Copper (Cu) are chosen as solid particle in nano fluid. We further obtain numerical results that when effects of magnetic parameter, mixed convection parameter, and volume fraction are included, the velocity and temperature profiles change. It is concluded that the velocity and temperature of Newtonian nano fluid Cu -water are higher than the velocity and temperature of non-Newtonian nanofluid Cu -Oil. The velocity and temperature of copper-water Cu -Water also are higher than the velocity and temperature of Alumina-water Al_2O_3 -Water. Further, the velocity profiles and temperature profiles of Newtonian Cu -Water and non-Newtonian nano fluid Cu -Oil decrease when magnetic parameter increases.

ACKNOWLEDGMENT

This research is supported by the Institute for Research and Community Services, Institut Teknologi Sepuluh Nopember (ITS) Surabaya, Indonesia with Funding Agreement Letter number 970/PKS/ITS/2018. We further are very grateful to LPPM-ITS for giving us a chance to submit this paper in an International Journal.

REFERENCES

- [1] Y. Ding, Y. Chen, Y. He, A. Lapkin, M. Yeganeh, L. Siller, Y. V. Butenko, "Heat Transfer Intensification Using Nanofluids", *Advanced Powder Technol*, 2007, pp.813-24.
- [2] S. Das, S. Chakraborty, R. N. Jana, O. D. Makinde, "Entropy analysis of unsteady magneto-nanofluid flow past accelerating stretching sheet with convective boundary condition" *Appl. Math. Mech.*, 2015, pp.1593-610.
- [3] Putra N, Roetzel W, Das S K, "Natural convection of nano-fluids", *Heat and Mass Transfer*, 2003, pp.775-84.
- [4] D. Wen and Y. Ding, "Experimental Investigation into Convective Heat Transfer of Nanofluids at the Entrance Region under Laminar Flow Conditions", *International journal of heat and mass transfer*, 2004, pp.5181-8.
- [5] M. Z. Akbar, M. Ashraf, M. F. Iqbal, K. Ali, "Heat and mass transfer analysis of unsteady MHD nanofluid flow through a channel with moving porous wall and medium.", *AIP Conf Proc*, 2016, 045222.

- [6] R. Mahat, N. A. Rawi, A. R. M. Kasim, S. Shafie, "Mixed convection boundary layer flow past a horizontal circular cylinder in viscoelastic nanofluid with constant wall temperature", *Malaysian Journal of Fundamental and Applied Sciences*, 2017, 13(4-1).
- [7] B. Juliyanto, B. Widodo, C. Imron, "The effect of heat generation on mixed convection flow in nano fluids over a horizontal circular cylinder", *IOP Conf. Series*, 2018, 012001
- [8] B. Widodo, I. Anggriani, C. Imron, "The Characterization of Boundary Layer Flow in The Magnetohydrodynamic Micropolar Fluid Past A Solid Sphere", *International Journal of Advances in Science Engineering and Technology*, 2016, pp. 2321-9009.
- [9] A. Karimipour, A. H. Nezhad, A. D'Orazio, E. Shirani, "The effects of inclination angle and Prandtl number on the mixed convection in the inclined lid driven cavity using lattice Boltzmann method", *Journal of Theoretical and Applied Mechanics*, 2013, pp.447-62.
- [10] A. Zaib, A. R. M. Kasim, N. F. Mohammad, S. Shafie, "Unsteady MHD Mixed Convection Stagnation Point Flow in A Micropolar Fluid on A Vertical Surface in A Porous Medium with Soret and Dufour Effects", *Heat Transfer Research*, 2013, pp.603-20.
- [11] B. Widodo, D. K. Arif, D. Aryany, N. Asiyah, F. A. Widjajati, Kamiran, "The effect of magnetohydrodynamic nano fluid flow through porous cylinder", *AIP Conference Proceedings*, 2017, 020069.
- [12] N. Freidoonimehr, M. M. Rashidi, S. Mahmud, "Unsteady MHD free convective flow past a permeable stretching vertical surface in a nano-fluid", *International Journal of Thermal Sciences*, 2015, pp.136-45.

Parameters calculation of turbulent fluid flow in a pipe of a circular cross section

Denis Chemezov, Svetlana Tyurina, Irina Medvedeva, Lyudmila Smirnova, Elena Bogomolova, Margarita Bakhmeteva, Alexandra Strunina, Nina Melenteva

Vladimir Industrial College
Vladimir, Russian Federation

ABSTRACT

The dependencies of total pressure, velocity, vorticity, turbulent length, turbulent dissipation, turbulent viscosity, turbulent energy and turbulent time of moving fluid from a straight pipe length of a circular cross section are presented in graphical and mathematical forms. Changing analysis of considered parameters was performed at mass flow rates of 0.45, 1.0 and 1.5 kg/s. A transition boundary of laminar flow of fluid to turbulent flow is at the distance of $\frac{2}{5}$ of length from the inlet of the pipe (at accepted total length of the pipe of 1000 mm).

Keywords – fluid, turbulent flow, a pipe, a model, a section.

I. INTRODUCTION

At present, a question of sustainability of laminar/transient flow regimes of fluid in pipelines has not been fully studied. According to numerous experimental data, it is determined that even in small straight sections of the pipeline, fluid flow changes from laminar to turbulent [1 – 7].

Flow pattern of fluid is determined by viscosity, flow velocity, a cross-sectional area of the pipe, composition of fluid mixture and other parameters. Also, flow pattern of fluid depends on the ratio of accelerating force and viscous friction force.

Conducting of experiments on a research of fluid flow regimes in the production, and even in the laboratory conditions, is difficult. A computer simulation of hydrodynamic processes of fluid flow in the pipelines allows not only to present a visual model of fluid flow, but also to obtain accurate or approximate mathematical equations describing pattern of each flow regime.

II. MATERIAL AND METHOD

Intensity changing of the parameters of turbulent fluid flow in the pipe of the circular cross section was determined by calculations in the *Flow Simulation* special computer program. Three solid-state pipe models with the same overall dimensions (internal diameter is 30 mm and total length is 1000 mm) were built for the computer simulation.

Different mass of the incompressible fluid model (water) at temperature of 293.2 K was supplied per unit of time (second) in the inlet of the pipe models. Specified mass flow rates for three pipe models are presented in the table I.

TABLE I. MASS FLOW RATES OF FLUID.

| The pipe model | The first | The second | The third |
|--------------------------------------|-----------|------------|-----------|
| Mass flow rate of fluid Q_m , kg/s | 0.45 | 1.0 | 1.5 |

Fluid flow direction was taken normal to a face of the inlet of the pipe model. Turbulence intensity I_t (2%) and turbulence length L_t (0.0008 m) were taken as the basic parameters of developed turbulent fluid motion in the pipe model. Turbulence intensity of fluid flows depends on characteristics of the pipe and the Reynolds number Re . Fluid pressure at the outlet of the pipe model was taken of 101325 Pa. Laminar and turbulent fluid flows were taken into account in the calculation. The cavitation process in the calculation was not accepted.

An inner wall of the pipe model had the properties of the adiabatic wall with the perfectly smooth surface (the surface roughness is 0 μm). Initial temperature of the inner surface of the pipe model was taken of 293.2 K.

Accuracy of the calculation results was average when a number of finite elements of the fluid model equal to 3264 and the pipe model equal to 528.

III. RESULT AND DISCUSSION

Flow pattern of fluid in the pipe model of the circular cross section is presented in the form of vectors (the Fig. 1).

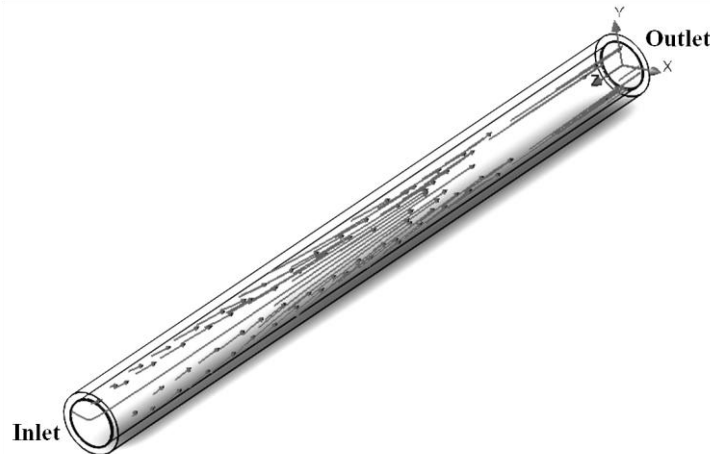


Fig. 1. Water flow at the straight section of the three-dimensional pipe model of the circular cross section.

Vortex formation of fluid flows is observed in a center part of a calculated field of the pipe model, laminar regime prevails at the inlet and the outlet.

The dependencies of the changing values of the turbulent fluid flow parameters from length of the model pipe of the circular cross section are presented in the Fig. 2 – 5. The data were obtained from the axial line of fluid motion in the pipe model.

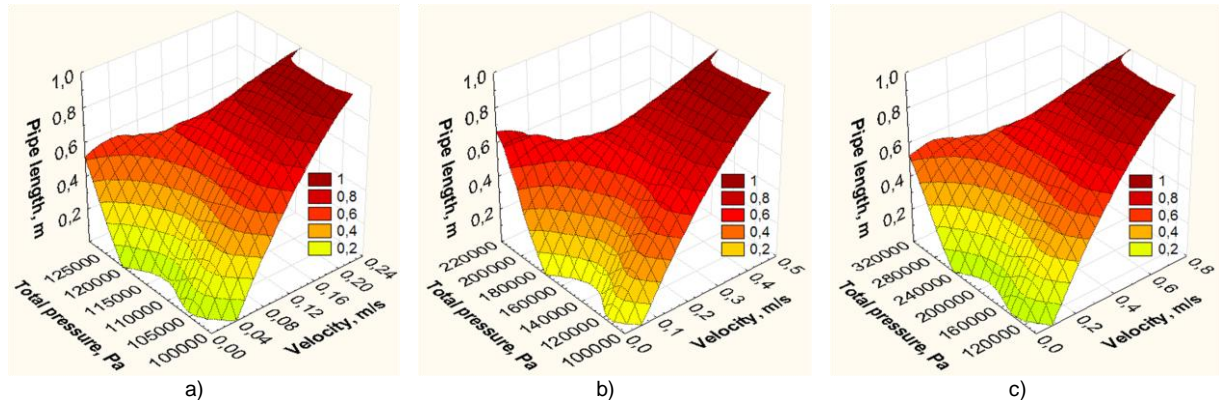


Fig. 2. The dependencies of flow velocity and total pressure of fluid from the pipe length: a) at $Q_M = 0.45$ kg/s; b) at $Q_M = 1.0$ kg/s; c) at $Q_M = 1.5$ kg/s.

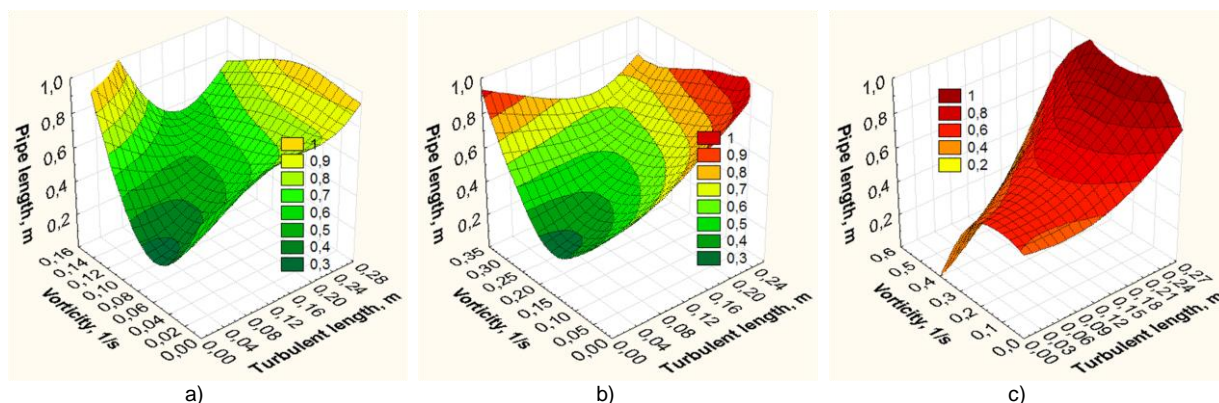


Fig. 3. The dependencies of turbulent length and vorticity of fluid from the pipe length: a) at $Q_M = 0.45$ kg/s; b) at $Q_M = 1.0$ kg/s; c) at $Q_M = 1.5$ kg/s.

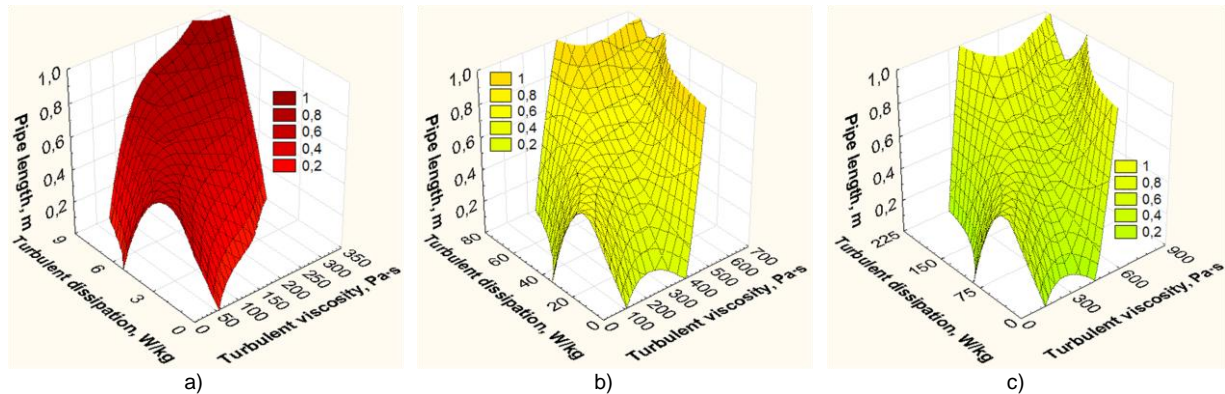


Fig. 4. The dependencies of turbulent viscosity and turbulent dissipation of fluid from the pipe length: a) at $Q_M = 0.45$ kg/s; b) at $Q_M = 1.0$ kg/s; c) at $Q_M = 1.5$ kg/s.

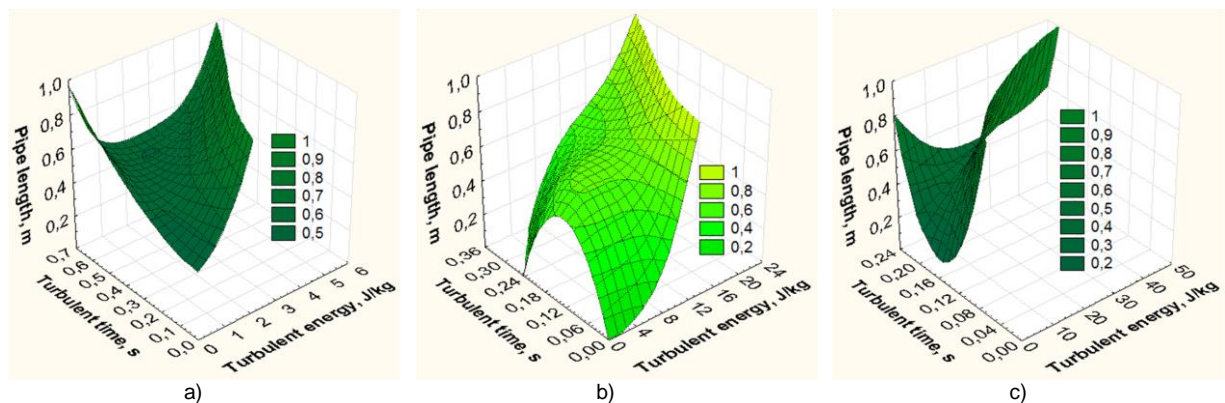


Fig. 5. The dependencies of turbulent energy and turbulent time of fluid from the pipe length: a) at $Q_M = 0.45$ kg/s; b) at $Q_M = 1.0$ kg/s; c) at $Q_M = 1.5$ kg/s.

Based on the analysis of the dependencies graphs of flow velocity and total fluid pressure, turbulent length and vorticity of fluid, turbulent viscosity and turbulent dissipation of fluid, turbulent energy and turbulent time of fluid flow from length of the pipe model, it could be argued that:

1. The values of the considered parameters of turbulent fluid flow increase with increasing of mass flow rate at the distance from the inlet to the outlet of the pipe model. Herewith, turbulent time of fluid in the each section of the pipe model decreases.
2. Pressure, flow velocity, turbulent dissipation and turbulent viscosity of moving fluid have almost the same pattern of changing over entire length of the pipe model. The other parameters of turbulent fluid flow in the pipe model have different regularities.

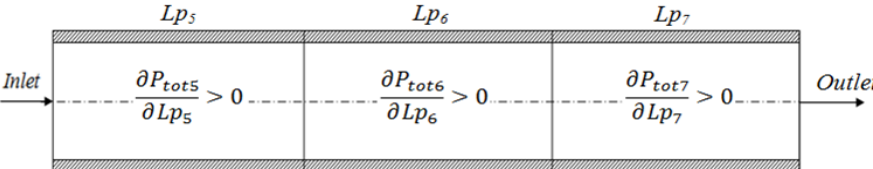
Let us consider flow pattern of fluid in the second pipe model. Total length of the pipe model was divided into 10 equal sections. Length of the each section was 100 mm (0.1 m). Herewith, 0 was taken by the inlet of the pipe model, and 1 was taken by the outlet. Let us write down the parameters changing of turbulent fluid flow in the each section of the pipe model in the functions form (the tables II – IV): $P_{tot}(L_p)$, $\epsilon_t(L_p)$, $L_t(L_p)$, $u(L_p)$, $t_t(L_p)$, $v_t(L_p)$, $k_t(L_p)$ and $\omega(L_p)$.

TABLE II. THE PARAMETERS CHANGING OF TURBULENT FLUID FLOW IN THE FIRST TO THE FOURTH SECTIONS OF THE PIPE MODEL.

| | Lp_1 | Lp_2 | Lp_3 | Lp_4 |
|--------|---|--|--|---|
| Inlet | 0 | | | |
| | $\frac{\partial P_{tot1}}{\partial Lp_1} = 0$ | $\frac{\partial P_{tot2}}{\partial Lp_2} = 0$ | $\frac{\partial P_{tot3}}{\partial Lp_3} = 0$ | $\frac{\partial P_{tot4}}{\partial Lp_4} = 0$ |
| | $P_{tot1} = 202950e^{9.9557 \cdot 10^{-10} Lp_1}$ | $P_{tot2} = 202950e^{1.0151 \cdot 10^{-9} Lp_2}$ | $P_{tot3} = 202950e^{1.0382 \cdot 10^{-9} Lp_3}$ | $P_{tot4} = 202950e^{1.1346 \cdot 10^{-9} Lp_4}$ |
| | $\epsilon_{t1} = 0.2983e^{0.0002 Lp_1}$ | $\epsilon_{t2} = 0.2984e^{0.0001 Lp_2}$ | $\epsilon_{t3} = 0.2989e^{0.0001 Lp_3}$ | $\epsilon_{t4} = 0.3008e^{1.1637 \cdot 10^{-5} Lp_4}$ |
| Outlet | | | | |

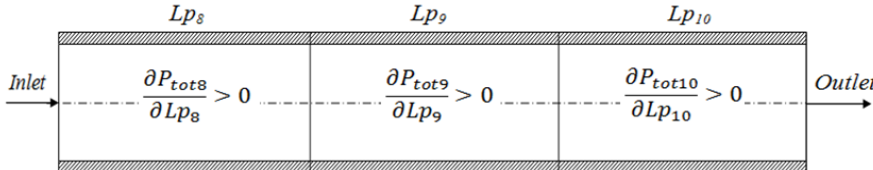
| | | | |
|---|---|---|---|
| $L_{t1} = 0.0017e^{-9.3762 \cdot 10^{-6} Lp_1}$ | $L_{t2} = 0.0017e^{-7.9763 \cdot 10^{-6} Lp_2}$ | $L_{t3} = 0.0017e^{-6.2387 \cdot 10^{-6} Lp_3}$ | $L_{t4} = 0.0017e^{-3.9188 \cdot 10^{-6} Lp_4}$ |
| $u_1 = 0.0036e^{0.0029 Lp_1}$ | $u_2 = 0.0037e^{0.0028 Lp_2}$ | $u_3 = 0.0037e^{0.0027 Lp_3}$ | $u_4 = 0.0038e^{0.0024 Lp_4}$ |
| $t_{t1} = 0.0711e^{-6.6033 \cdot 10^{-5} Lp_1}$ | $t_{t2} = 0.0711e^{-5.3932 \cdot 10^{-5} Lp_2}$ | $t_{t3} = 0.0711e^{-3.9038 \cdot 10^{-5} Lp_3}$ | $t_{t4} = 0.0709e^{-2.6339 \cdot 10^{-6} Lp_4}$ |
| $v_{t1} = 0.1475e^{3.6208 \cdot 10^{-5} Lp_1}$ | $v_{t2} = 0.1475e^{2.9879 \cdot 10^{-5} Lp_2}$ | $v_{t3} = 0.1475e^{2.2173 \cdot 10^{-5} Lp_3}$ | $v_{t4} = 0.1478e^{-8.4752 \cdot 10^{-7} Lp_4}$ |
| $k_{t1} = 0.022e^{0.0001 Lp_1}$ | $k_{t2} = 0.022e^{8.3904 \cdot 10^{-5} Lp_2}$ | $k_{t3} = 0.022e^{6.2324 \cdot 10^{-5} Lp_3}$ | $k_{t4} = 0.0221e^{6.6643 \cdot 10^{-6} Lp_4}$ |
| $\omega_1 = 0.1942e^{0.0017 Lp_1}$ | $\omega_2 = 0.1944e^{0.0017 Lp_2}$ | $\omega_3 = 0.1951e^{0.0016 Lp_3}$ | $\omega_4 = 0.193e^{0.0017 Lp_4}$ |

TABLE III. THE PARAMETERS CHANGING OF TURBULENT FLUID FLOW IN THE FIFTH TO THE SEVENTH SECTIONS OF THE PIPE MODEL.



| | | |
|--|---|---|
| $P_{tot5} = 202950e^{1.3425 \cdot 10^{-9} Lp_5}$ | $P_{tot6} = 206630e^{-6.5981 \cdot 10^{-5} Lp_6}$ | $P_{tot7} = 735640e^{-0.0026 Lp_7}$ |
| $\epsilon_{t5} = 0.3067e^{-0.0002 Lp_5}$ | $\epsilon_{t6} = 0.0034e^{0.0181 Lp_6}$ | $\epsilon_{t7} = 0.5027e^{0.0088 Lp_7}$ |
| $L_{t5} = 0.0017e^{-2.6022 \cdot 10^{-7} Lp_5}$ | $L_{t6} = 2.7591 \cdot 10^{-5} e^{0.0167 Lp_6}$ | $L_{t7} = 0.059e^{0.0026 Lp_7}$ |
| $u_5 = 0.0043e^{0.0012 Lp_5}$ | $u_6 = 0.0002e^{0.0131 Lp_6}$ | $u_7 = 0.0033e^{0.0089 Lp_7}$ |
| $t_{t5} = 0.0704e^{7.6711 \cdot 10^{-5} Lp_5}$ | $t_{t6} = 0.0202e^{0.0051 Lp_6}$ | $t_{t7} = 0.6355e^{-0.0012 Lp_7}$ |
| $v_{t5} = 0.1485e^{-5.4355 \cdot 10^{-5} Lp_5}$ | $v_{t6} = 0.0001e^{0.0279 Lp_6}$ | $v_{t7} = 18.214e^{0.0063 Lp_7}$ |
| $k_{t5} = 0.0224e^{-0.0001 Lp_5}$ | $k_{t6} = 7.3856 \cdot 10^{-5} e^{0.023 Lp_6}$ | $k_{t7} = 0.3194e^{0.0076 Lp_7}$ |
| $\omega_5 = 0.1961e^{0.0017 Lp_5}$ | $\omega_6 = 0.4569e^{-0.0031 Lp_6}$ | $\omega_7 = 0.0874e^{0.0024 Lp_7}$ |

TABLE IV. THE PARAMETERS CHANGING OF TURBULENT FLUID FLOW IN THE EIGHTH TO THE TENTH SECTIONS OF THE PIPE MODEL.



| | | |
|--|--|--|
| $P_{tot8} = 14195000e^{-0.0038 Lp_8}$ | $P_{tot9} = 2162300e^{-0.0046 Lp_9}$ | $P_{tot10} = 7624400e^{-0.0067 Lp_{10}}$ |
| $\epsilon_{t8} = 6.6458e^{0.004 Lp_8}$ | $\epsilon_{t9} = 21802e^{0.0019 Lp_9}$ | $\epsilon_{t10} = 34.5148e^{0.0011 Lp_{10}}$ |
| $L_{t8} = 0.1082e^{0.0014 Lp_8}$ | $L_{t9} = 0.1879e^{0.0004 Lp_9}$ | $L_{t10} = 0.2273e^{0.0001 Lp_{10}}$ |
| $u_8 = 93.1834e^{-0.01 Lp_8}$ | $u_9 = 0.0442e^{0.0036 Lp_9}$ | $u_{10} = 0.0396e^{0.0038 Lp_{10}}$ |
| $t_{t8} = 0.4028e^{-0.0004 Lp_8}$ | $t_{t9} = 0.3915e^{-0.0003 Lp_9}$ | $t_{t10} = 0.3813e^{-0.0003 Lp_{10}}$ |
| $v_{t8} = 96.7102e^{0.0032 Lp_8}$ | $v_{t9} = 300.0135e^{0.0012 Lp_9}$ | $v_{t10} = 450.542e^{0.0005 Lp_{10}}$ |
| $k_{t8} = 2.6755e^{0.0036 Lp_8}$ | $k_{t9} = 8.5355e^{0.0016 Lp_9}$ | $k_{t10} = 13.1607e^{0.0008 Lp_{10}}$ |
| $\omega_8 = 3236300e^{-0.0297 Lp_8}$ | $\omega_9 = 7.6045e^{-0.0078 Lp_9}$ | $\omega_{10} = 0.0003e^{0.0092 Lp_{10}}$ |

In the presented functions are conditionally designated: $P_{tot1}, P_{tot2}, P_{tot3}, \dots, P_{tot10}$ – total pressure of fluid in the first, the second, the third, ..., the tenth sections of the pipe model, Pa; $L_{p1} = (0;0.1], L_{p2} = (0.1;0.2], L_{p3} = (0.2;0.3], L_{p4} = (0.3;0.4], L_{p5} = (0.4;0.5], L_{p6} = (0.5;0.6], L_{p7} = (0.6;0.7], L_{p8} = (0.7;0.8], L_{p9} = (0.8;0.9], L_{p10} = (0.9;1.0]$ – the length ranges of the each section of the pipe model, m (the values in the range are location coordinates of the corresponding section, starting from the inlet of the pipe model); $\epsilon_{t1}, \epsilon_{t2}, \epsilon_{t3}, \dots, \epsilon_{t10}$ – turbulent dissipation of fluid in the first, the second, the third, ..., the tenth sections of the pipe model, W/kg; $L_{t1}, L_{t2}, L_{t3}, \dots, L_{t10}$ – turbulent length of fluid flow in the first, the

second, the third, ..., the tenth sections of the pipe model, m; $u_1, u_2, u_3, \dots, u_{10}$ – flow velocity of fluid in the first, the second, the third, ..., the tenth sections of the pipe model, m/s; $t_{t1}, t_{t2}, t_{t3}, \dots, t_{t10}$ – turbulent time of fluid flow in the first, the second, the third, ..., the tenth sections of the pipe model, s; $\nu_{t1}, \nu_{t2}, \nu_{t3}, \dots, \nu_{t10}$ – turbulent viscosity of fluid in the first, the second, the third, ..., the tenth sections of the pipe model, Pa·s; $k_{t1}, k_{t2}, k_{t3}, \dots, k_{t10}$ – turbulent energy of fluid in the first, the second, the third, ..., the tenth sections of the pipe model, J/kg; $\omega_1, \omega_2, \omega_3, \dots, \omega_{10}$ – vorticity of fluid in the first, the second, the third, ..., the tenth sections of the pipe model, 1/s.

In the first four sections, non-gradient flow is observed, i.e. fluid in these sections does not completely fill the cross section of the pipe model. Thickness of a boundary layer (the thin near-wall layer) increases at non-gradient flow of fluid. In the remaining sections of the pipe model, an area with positive pressure gradient was determined in which fluid flow was slowing down. Fluid flow slows in the boundary layer and in the flow core (external flow). Fluid slowing is more quickly in the boundary layer by increasing its thickness.

The general analytical formula was obtained after the analysis of the calculated mathematical equations for determining of the parameters of turbulent fluid flow in the pipe model of the circular cross section:

$$\int A e^{kx} dx = \frac{A}{k} (e^{kx} - 1),$$

where A is numerical coefficient of the function; k is power coefficient of the function.

IV. CONCLUSION

1. Changing pattern of flow velocity and total pressure, and, consequently, turbulent dissipation and viscosity of moving fluid does not depend on mass flow rate.
2. The more mass flow rate of fluid, the more strongly signs of turbulence are observed (the Fig. 3, c and the Fig. 5, c).
3. At the distance of $2/5$ of length from the inlet of the pipe, fluid flow is closer to laminar. At the distance of $3/5$ of length from the outlet of the pipe, interaction of direct and reverse fluid flows occurs, which causes vortices, and, consequently, laminar regime turns into turbulent.

REFERENCES

- [1] D. Chemezov, Calculation of pressure losses of liquid at a cylindrical straight pipeline section, ISJ Theoretical & Applied Science, 12 (56), 2017, 19 – 22. DOI [10.15863/TAS.2017.12.56.5](https://doi.org/10.15863/TAS.2017.12.56.5)
- [2] D.A. Chemezov, Hydrodynamic characteristics of water flow in straight and curved sections of a pipeline, Modern materials, equipment and technology [Text]: Materials of the 4th International scientific and practical conference, South-West State University, CJSC «University book», Kursk, 2015, 468 – 471. ISBN 978-5-9906195-4-8.
- [3] D. Chemezov, N. Palev, Analytical models of the turbulent fluid flow in a circular pipe, ISJ Theoretical & Applied Science, 09 (41), 2016, 77 – 84. DOI [10.15863/TAS.2016.09.41.12](https://doi.org/10.15863/TAS.2016.09.41.12)
- [4] V. Oshovskiy, A. Dyubanov, Computer modelling of the hydrodynamic effects arising in the narrowing device, Scientific Works of Donetsk National Technical University, 2(21), 2013, 168 – 169. ISSN 2074-6652.
- [5] I. Tsukanov, V. Shapiro, S. Zhang, A Mesh free Method for Incompressible Fluid Dynamics Problems, Int. J. Numer. Meth. Eng., 2003, Vol. 58.
- [6] D.S. Henningson, P.J. Schmid, Stability and transition in shear flows, New-York, 2001.
- [7] A.V. Proskurin, A.M. Sagalakov, Viscous Fluid Flow in a Coaxial Pipe, Izvestiya of Altai State University Journal, 2016, 62 – 68. DOI [10.14258/izvasu\(2016\)1-10](https://doi.org/10.14258/izvasu(2016)1-10)

HIGGS BOSON RADIUS of ACTION

Antonio Puccini

Neurophysiologist of Health Ministry, Naples – Italy

ABSTRACT

As we are all aware, the recent discovery of the Higgs boson has revealed a highly massive particle, the value of which lies between 125 and 126.5 GeV/c².

According to the basic concepts of Quantum Mechanics, and in full compliance with the Uncertainty Principle and Yukawa intuitions, we were able to calculate the maximum limit of the Higgs boson's field of action.

From the calculations show that the Higgs boson presents a range of action really very small, namely $9.8828 \cdot 10^{-16}$ [cm], that is slightly smaller than 10^{-15} [cm].

This value is justified by the considerable mass that the Higgs boson acquires, in perfect agreement with the Uncertainty Principle.

Keywords: Higgs boson (HB); Standard Model (SM); Heisenberg Uncertainty Principle (HUP); Wave Function (WF); Higgs field (HF).

I. INTRODUCTION

As it is known, the Standard Model (SM) of elementary particles is made up of a basic principle, known as 'local Gauge Invariance' or 'local Gauge Symmetry'.

1.1 The GAUGE SYMMETRY

According to Noether the behavior of nature is *invariant* under certain transformations on its fundamental constituents, such as the fields of fundamental particles [1][2].

The conservation of various physical quantities comes from this *invariance*. Applying this procedure to the *fields*, we have that in case of a *gauge-invariance*, we will have a charge conservation: e.g. in the case of the *gauge invariance* of the electromagnetic (EM) field.

As Chandrasekhar reminds us "the dualism wave-particle is an universal and fundamental property of the matter" [3]. In line with de Broglie [4], this dualism can be solved with the Quantum Mechanics living to the particles a *wave function* (WF) of their own, indicated with Ψ , which describes correctly both their wave and particle character.

In the case of the EM field, we will have a conservation of the electrical charge, respect to:

$$\Psi \rightarrow e^{i\theta} \Psi \quad (1)$$

This *unobservable* transformation is the most famous *gauge transformation* where Ψ represents the WF of an electrically charged particle (such as the electron), $e^{i\theta}$ is a *complex unit number* (with θ real), expressing a *complete* phase, and i is the *imaginary unit*.

Penrose points out: "If the WF describes a charged particle, then we can make *gauge transformations* of the form expressed by equation (1) where θ is an arbitrary real position function, allowing us to change the way the phase varies!" [5].

Maxwell's equations do not change, that is, they are *covariant*, so Weyl believed that it was possible to extend this *covariance* to the gravitational field too, as well as to General Relativity, thus trying to unify electromagnetism and gravity. In fact, in line with the Noether theorem, in 1918 Weyl formulated a *gauge theory* to be applied to General Relativity [6]. However, "Along with Weyl's theory, the way a clock measures time does not depend solely on its current position, but also on the previously positions. Likewise, the emission frequencies of a hydrogen atom will depend both on its current and past positions. It is like saying: the behavior of the atom will depend on its history, despite contradicting experimental evidence" [7].

II. DISCUSSION

In short, "Weyl's idea contained a fatal mistake, which Einstein clearly saw from the beginning"[7]. Pauli also pointed out with regret that error[8][9].

2.1 The MASS BREAKS the SYMMETRY

Thus the introduction of a simple mass parameter, necessary to describe the mass of a particle, is in contradiction with the existence of the *gauge symmetry*: it is said, that is, that the *mass breaks the gauge symmetry*, thus risking to make insubstantial the entire theory of the *SM*.

According to *SM* the problem can be solved by assuming that all particles have a null intrinsic mass and postulating the existence of a *complex scalar field* permeating the space.

The re-introduction of the mass parameter causes the gauge symmetry is not more explicit, but that is spontaneously broken: *Spontaneous Symmetry Breaking*[10][11][12]. It is in this case a *symmetry hidden from the mass*.

So it was conjectures more or less at the same time, and independently by Englert and Brout, [13] by Higgs [14], Guralnik, Hagen and Kibble[15] that particles would tend to interact, to mate with this *complex scalar field*, now known as Higgs field (HF), acquiring an energy at rest which is not null, which for almost all respects is analogous to a value of mass at rest, then describable as a parameter mass. As it is well known, the mechanism just described is the so-called *Higgs Mechanism*.

The *Higgs Mechanism* requires the intervention of a permeating particle the HF, i.e. the Higgs Boson (HB).

It is interesting to note that the coupling between the various particles (to be exact "only those bearers of weak charge"[16][17]) and HF (steeped in weak charge) complies with the *gauge symmetry* and explains the presence of non-null restmasses.

2.2 HIGGS BOSON HUNTING

As we all know the research of the HB was delayed for a long time.

Frequent were its probable measurements in particle accelerators, but it reached a value of reliability (or *confidence level*) of 2 sigma (σ) and then to 3 σ : still a too low value to be able to proclaim a discovery [16], since a signal at 3 σ it corresponds to a *confidence level* of 99.7%, that is, to a probability of 0.3% that the signal is actually due to the case [18].

Subsequently, when the CERN of Geneva began operating with an energy of collisions of 7 and 8 TeV, it was possible to reach the much longed 5 σ .

In short, as you will be aware, to be able to announce the discovery of a new particle, it is required a signal with a *confidence level* $\geq 5 \sigma$ [16], as a signal to 5 σ corresponds to a *confidence level* of 99.9999% [18].

2.3 HIGGS BOSON DISCOVERY

Finally, at the Congress of the CERN on 4 July 2012 it was announced a series of reliable surveys for HB [19].

As everyone knows, the first to speak was Joe Incandela, head of the study group working with the detector Compact Muon Solenoid (CMS). He announced that, working with an energy of collision of 7 and 8 TeV, they carried out repeated surveys, with a *confidence level* to 5 σ , of a particle of mass apparently equal to 125.5 GeV/c².

Next was the turn of Fabiola Gianotti, head of the study group working with the ATLAS (A Thoroidal LHC ApparatuS) detector. She announced that, working with the same energy used by CMS, they had found numerous surveys, with 5 σ of reliability, of a particle of mass approximately between 125 and 126.5 GeV/c².

Both study groups communicated that the decay products of the particle detected could match those of HB.

So: we have the HB, and we know its mass, which we could consider between the values measured with the CMS and ATLAS, which is roughly equal to 125.5 GeV /c².

2.4 HIGGS BOSON RANGE

At which point we would like to know its range of action, its operating field: this is the purpose of our work.

One wonders: where does the HB take all this *mass-energy*? From its field, that is the field in which it is immersed: the HF. According to the Quantum Field Theory the higher the value of the mass of the particle, i.e. the more the energy (ΔE) taken from the field, the sooner (Δt) the energy must be returned to the field itself. This is an inviolable rule of Quantum Mechanics, dictated by the Heisenberg Uncertainty Principle (HUP)[20][21]:

$$\Delta E \cdot \Delta t \geq h \quad (2),$$

where h is Planck's constant, equal to $6.626 \cdot 10^{-27}$ [erg · sec].

Applying the HUP to HB, we have that the ΔE of equation (2) corresponds to the energy value of HB, i.e. 125.5 GeV/c².

Obviously, what we do not know, in this case, is the value of Δt , i.e. of duration (t) of the HB's life, before it returns to the field all the energy (E) taken, so to speak, *borrowed*.

The duration of this energy loan, in favor of HB, is provided by equation(2), from which we have:

$$t = \frac{h}{E} \quad (3).$$

Observing the equation (3), we notice that *time* and *energy* are inversely proportional.

That's why the higher the energy value borrowed, as saying subtracted from the field, the sooner this energy must be returned.

To this point we take into account the Principle of Equivalence Mass-Energy:

$$E = m c^2 \quad (4).$$

Hence, by replacing the value of *E* in equation (3) with that of equation (4), we obtain:

$$t = \frac{h}{m c^2} \quad (5).$$

Equation (5), as Fermi reminds us "it is the *time*(*t*) in which the boson issued may remain in free space. If then it is assumed that its speed is the maximum speed at which a particle can move, that is the speed of light (*c*), it is seen that the maximum distance (*d*) it can reach, before being recalled to weld the debt, is given, as order of magnitude, by the product of time (*t*) for the maximum rate at which the particle can move" [22], namely:

$$d = t c \quad (6).$$

So we put in equation (6) the value of *t* expressed by equation(5):

$$d = \frac{h}{m c^2} \cdot c \quad (7),$$

namely:

$$d = \frac{h}{m c} \quad (8).$$

And interesting to note that the *distance* (*d*) expressed by the latter equation corresponds exactly to the radius of action (*R₀*) obtainable from the *Yukawa* potential[23]:

$$R_0 = \frac{h}{2 \pi m c} \quad (9).$$

Thus one expressed by equation(8) is the maximum distance the HB can take, ie the upper limit of its *action field*. It comes more useful to express in grams [g] the mass HB, using the *cgs system*. Since $1 \text{ GeV}/c^2 = 1.782 \cdot 10^{-24} \text{ [g]}$, so the mass of HB will be:

$$m_{\text{HB}} = 125.5 \cdot (1.782 \cdot 10^{-24} \text{ [g]}) \quad (10),$$

that is:

$$m_{\text{HB}} = 2.23641 \cdot 10^{-22} \text{ [g]} \quad (11).$$

So we replace this value to *m* of Eq. (8):

$$d = 6.626 \cdot 10^{-27} \text{ [erg} \cdot \text{s]} / (2.23641 \cdot 10^{-22} \text{ [g]}) (2.99792 \cdot 10^{10} \text{ [cm/s]}) \quad (12).$$

Since $1 \text{ erg} = \text{g} \cdot \text{cm}^2/\text{s}^2$, we can write:

$$d = 6.626 \cdot 10^{-27} \text{ [g} \cdot \text{cm}^2/\text{s]} / 6.7045782 \cdot 10^{-12} \text{ [g} \cdot \text{cm/s]} \quad (13),$$

$$d_{\text{HB}} = 9.8828 \cdot 10^{-16} \text{ [cm]} \quad (14).$$

III. CONCLUSIONS

In short, the value expressed by equation (14) represents the maximum limit of the *radius of action* of the HB, i.e. the maximum distance (*d*) passable by HB, before it returns the energy to the field in which it is immersed, namely the HF.

Our calculations reveal a *range of action* of HB really very small, slightly smaller than 10^{-15} [cm] , but this value is justified by the considerable mass that the HB acquires, perfectly along with the known fact that the action range of a *force* is inversely proportional to the mass of the bosons the force conveys.

This is certainly a very small value, which shows a very marked space limitation of this boson, but these are the rules imposed by Quantum Mechanics, through one of its most profound concepts: the HUP.

In closing, the *range* of HB will never exceed the distance expressed by equation (14), otherwise the HUP would be violated and as Feynman specifies: "No one has ever found (or even thought of) a way around the Uncertainty Principle. So we must assume that it describes a basic characteristic of nature" [24].

Hawking adds: "HUP is a fundamental, inescapable property of the world"[25].

REFERENCES

- [1.] Noether E., "Invariante variationsprobleme", Math.-phys. Klasse, 235-257(1918).
- [2.] Noether E., "Gleichungen mit vorgeschriebener Gruppe", Mathematische Annalen, 78, 221-229 (1918).
- [3.] Chandrasekhar B.S., "Why Things Are the Way They Are", Cambridge University Press, 1998; Il Saggiatore ed., Milano, 72 (2004).
- [4.] de Broglie L., "Ondes et quanta", Comtes Rendus, Vol.177, 507-510 (1923).

- [5.] Penrose R., "The Road to Reality", 2004 Roger Penrose; RCS ed., Milano, 453 (2005).
- [6.] Weyl H., "Gravitation und Elektrizität", Sitzungsber Akademie der Wissenschaften, Berlin, 465, 480 (1918).
- [7.] Quirantes A., "Lo Spazio-Tempo Quantistico", ©2015 RBA, Contenidos ed., Spagna; © RBA Italia, Milano, 78-79 (2016).
- [8.] Pauli W., "Zur Theorie der Gravitation und der Elektrizität von Hermann Weyl", Physikalische Zeitschrift, vol.20, 457-467 (1919).
- [9.] Pauli W., "Merkurperihelbewegung und Strahlenablenkung in Weyls Gravitationstheorie", Verhandlungen der Deutschen Physikalischen Gesellschaft, vol.21, 742-750 (1919).
- [10.] Nambu Y. and Jona-Lasinio G., "Dynamical Model of Elementary Particles Based on an Analogy with Superconductivity. I", Phys.Rev., 122, 345-358 (1961).
- [11.] Nambu Y. and Jona-Lasinio G., "Dynamical Model of Elementary Particles Based on an Analogy with Superconductivity. II", Phys.Rev., 124, 246-254 (1961).
- [12.] Goldstone J., Salam A., Weinberg S., "Broken Symmetries", Phys.Rev., 127, 965-970 (1962).
- [13.] Englert F., Brout R., "Broken Symmetry and the Mass of Gauge Vector Mesons", Phys.Rev. Lett., 13, 321-323 (1964).
- [14.] Higgs P.W., "Broken Symmetries and the Masses of Gauge Bosons", Phys.Rev.Lett. 13, 508-509 (1964).
- [15.] Guralnik G.S., Hagen C.R. and Kibble T.W.B., "Global Conservation Laws and Massless Particles", Phys.Rev.Lett., 13, 585-587 (1964).
- [16.] Randall L., "Knocking on Heaven's Door", ©Lisa Randall 2011, 2012; il Saggiatore ed., Milano, 293, XIV (2012).
- [17.] Puccini A., "On the Bosons' Range of the Weak Interaction", Journal of Advances in Physics, Vol.14, 3, 5865-5868 (2018).
- [18.] Baggott J., "Higgs: The Invention and Discovery of the God Particle", 2012; Adelphi Ed., Milano, 172 (2013).
- [19.] CERN Seminar, "Latest update in the search for the Higgs boson", Geneva, July 4th (2012).
- [20.] Heisenberg W., "Über den anschaulichen Inhalt der quantentheoretischen Kinematik und Mechanik", Zeitschrift für Physik, Vol.43, 172-198 (1927).
- [21.] Puccini A., "Uncertainty Principle and Electromagnetic Waves", Journal of Electromagnetic Waves and Applications, Vol.19, N°7, 885-890 (2005).
- [22.] Fermi E., "Atomi Nuclei Particelle", a cura di V. Barone, Boringhieri ed. (Torino), 140, 2009.
- [23.] Yukawa H., "On the Interaction of Elementary Particles", Proc. Phys. Math. Soc. Japan., 17, 48-57 (1935).
- [24.] Feynman R.P., Lectures on Physics, 1965 Caltech; Zanichelli Ed. (Bologna), Vol 3, 1-11 (2001).
- [25.] 25) Hawking S., "A Brief History of Time", ©1988 by Stephen W. Hawking, Bantam Books ed.; Rizzoli Ed. (Milano), 73 (1993).

Modeling and Simulation of a Water Gas Shift Reactor operating at a low pressure

Wail El Bazi^{1,*}, Abderrahim El-Abidi^{2,3}, Moulay Saddik Kadiri¹, Said Yadir^{2,3}

¹Laboratory of Process Engineering and Industrial Systems Optimization (LIPOSI)
ENSAKhouribga, Sultan Moulay Slimane University,
BéniMellal, Morocco

²Laboratory of Materials, Processes, Environment and Quality (LMPEQ),
ENSA Safi, Cadi Ayyad University,
Marrakech, Morocco

³Laboratory of Electronics, Instrumentation and Energy (LEIE),
Faculty of Science, Chouaib Doukkali University,
El Jadida, Morocco

ABSTRACT

In order to study the WGS on an industrial scale at a low pressure, the modeling and simulation of a WGS reactor operating at a pressure close to P_{atm} and processing an industrial charge in the presence of a high temperature shift catalyst (Fe_2O_3/Cr_2O_3) were performed. The Profiles of the carbon monoxide conversion, temperature and pressure along the reactor were obtained. The effect of several operating parameters (inlet temperature, H_2O/CO ratio) on the conversion of carbon monoxide along the reactor has been determined. The estimated catalytic mass to convert 60.5% of the carbon monoxide contained in the inlet is 170.76 t. The pressure drops in the reactor are not negligible and the maximum temperature reached is without any harmful effect on the catalyst. The choice of an optimal inlet temperature and a high H_2O/CO ratio improves the conversion of carbon monoxide.

Keywords—Packed bed reactor, catalyst, water gas shift reaction

I. INTRODUCTION

Hydrogen is an important source of energy and is involved in various industrial processes such as: ammonia synthesis, methanol synthesis, etc. [1]. The production of this molecule can be carried out through several ways: Production from methane [2], biological production [3], water electrolysis [4], chemical production of aluminum and sodium hydroxide [5], or WGS (water gas shift reaction) which is a chemical reaction converting a mixture of carbon monoxide (CO) and water vapor (H_2O) into a mixture of carbon dioxide (CO_2) and hydrogen (H_2):



This slightly exothermic reaction discovered by the Italian physicist Felice Fontana in 1780 [1] can occur in the presence of catalysts based on several metals such as Cu, Fe, Ni, Pd, Pt, Rh, Ru [6] or even metal oxide [7]. At high temperatures (350-450°C) catalysts based on iron oxides and chromium oxide III (Cr_2O_3) can be used [7]. At low temperatures (120-240°C) copper or copper oxide catalysts can be used with promoters of alumina oxide (Al_2O_3) [7] and zinc oxide (ZnO) [8]. WGS can occur at pressures ranging from 1 to 83.75 bars [7-10]. But often industrial reactors operate at high pressures [8,11-12]. Numerous models of the water gas shift reactors have been published to date. Elnashaie et al developed a steady-state one-dimensional heterogeneous model to study the behavior of industrial reactors operating at high temperatures [11]. Their work also focused on the effect of temperature on the conversion of carbon monoxide. Adams et al used a dynamic two-dimensional heterogeneous model to study the behavior of reactors operating at both high and low temperatures [13]. Adams was also interested in the effect of important parameters on X_{CO} (H_2O/CO - temperature ratio). Falleiros

Barbosa Lima et al investigated an industrial reactor operating at high temperatures, using different one-dimensional pseudo homogeneous models [14]. The effect of catalyst deactivation on reactor performance was also investigated. A steady-state one-dimensional pseudo-homogeneous model was also used by Shokry et al to predict the evolution of molar flow rate along and at the outlet of an industrial WGS reactor operating at low temperatures [12]. These authors also studied the effect of pressure, inlet temperature, H₂O/CO ratio on X_{CO}. The major disadvantage of operating at high pressures is the enormous energy costs that it would be interesting to reduce them by carrying out the WGS at low pressures. In addition, the operating life of the catalyst can reach 15 years if the reactor operates at a low pressure [15]. Indeed, several papers have been carried out to study this reaction and to determine its kinetic expressions in the presence of catalysts allowing its activation at pressures close to the atmospheric pressure [8,16-23]. It would therefore be interesting to use these expressions in the simulation and study of the behaviour of reactors operating at pressures on the order of 1 atm. In fact, the work of Maklavany et al has been interested in this topic. These authors used the kinetic expression of WGS in the presence of a low temperature shift catalyst (CuO/ZnO/Al₂O₃) to simulate a laboratory reactor operating at 1.2 bar. Two models were used: a steady state 2D homogeneous isothermal model [24] and a 1D homogeneous isothermal model with axial dispersion [25]. The effect of temperature on the variation of several parameters along the reactor (CO concentration, pressure, reaction rate, superficial velocity) was also studied. In our study, we also carried out the simulation of a reactor operating at a low pressure. But in our case, it is in the presence of a high temperature shift catalyst (Fe₂O₃/Cr₂O₃) and for a large reactor. This will allow the industrial-scale study of the reaction at a low pressure and clarified the strengths and weaknesses of the realization of WGS under this condition. The model we used to simulate the fixed catalytic bed is the steady state one-dimensional pseudo homogeneous model that is widely used in the study of the behaviour of industrial catalytic convertors, sites of the WGS [12,14,26] or other gas phase reactions [27,28,29]. In the first part of this study, we used the kinetic rate expression corresponding to this catalyst in the modeling and simulation of an industrial WGS reactor. This allowed the prediction of profiles of the carbon monoxide conversion, temperature and pressure along the reactor. Then, the work was continued by studying the effects of the operating parameters (inlet temperatures, H₂O/CO ratios) on the conversion of carbon monoxide in order to define the optimal conditions of the reaction realization.

II. DESCRIPTION

A. Description of the studied catalyst and the operating conditions for establishing the kinetic rate expression

The kinetic rate expression corresponding to the chosen catalyst was carried out by Keiski et al [18]. The characteristics of the catalyst, as well as the operating conditions under which the kinetic rate expression was established, are presented in Table I [7,13,18].

TABLE I. CATALYST CHARACTERISTICS AND OPERATING CONDITIONS FOR THE ESTABLISHMENT OF THE WGS KINETICS [7,13,18]

| Catalyst | Composition | Operating conditions for the establishment of WGS kinetics | Equivalent spherical diameter, d _p (μm) | Shape | Catalyst density, ρ _c (kg/m ³) |
|------------------------------|---|---|--|----------|---|
| CCE C12 Ref: [7,13,18] | Fe ₂ O ₃ /Cr ₂ O ₃ (89/9%) | T : [575-675 K], P : 1 atm H ₂ O/CO (molar) : [2.4-12.1] Gas mixture of different fractions of: CO, CO ₂ , H ₂ O, H ₂ , N ₂ | 2800 | Cylinder | 3730 |

B. Description of the reactor and the operating conditions considered in the simulation

The characteristics of the simulated reactor are presented in Table II.

TABLE II. REACTOR CHARACTERISTICS

| Packed bed diameter D (m) | Packed bed length, L (m) | Number of packed beds (tubes) | Thermal property of the packed bed | void fraction in the packedbed ϵ |
|---------------------------|--------------------------|-------------------------------|------------------------------------|---|
| 0.09 | 2.2 | 6000 | Adiabatic | 0.4 |

The first simulations were run to predict the profiles of carbon monoxide conversion, temperature and pressure along the reactor operating at a low pressure and for a feed flow of an industrial nature. We ran these Simulations under the operating conditions presented in Table III.

TABLE III. OPERATING CONDITIONS USED FOR THE PREDICTION OF X(Z), T(Z) AND P(Z)

| Molar flow rate of the feed gas mixture, $F_{i0}(\text{mol. s}^{-1})$ | Inlet pressure, P_0 (atm) | Inlet temperature, T_0 (K) |
|--|-----------------------------|------------------------------|
| CO : 23.28 CO ₂ : 94.19 H ₂ : 364.149 H ₂ O : 228.93 N ₂ : 134.354 | 1.12 | 590 |

The compositions and the inlet pressure of the gas mixture of table 3 are close to those studied when establishing the kinetic rate expression of the WGS [18]. The temperatures remain within the temperature range of the kinetic study [18]. At the same time, in order to evaluate the WGS at low pressures in a situation close to an industrial case, each partial molar flow rate of WGS reagent (CO, CO₂, H₂O, H₂) presented in Table 3 is equal to 30% of the actual partial molar flow rate of the same reagent feeding the high pressure WGS reactor of the Alexandria Fertilizers Company (AlexFert) [12]. The molar flow rate of nitrogen shown in this table is equal to 30% of the real molar flow rate of the inerts feeding the company's reactor.

To study the effect of temperature on the carbon monoxide conversion along the reactor, other simulations were performed for other inlet temperatures (575 K, 605 K, 620 K) while keeping the other operating conditions (Table 3) and the same reactor characteristics (Table 2).

Finally, the study of the effect of the H₂O/CO ratio on the X_{CO} profile along the reactor required further simulations for [H₂O]/[CO]=3 which corresponds to $F_0(\text{H}_2\text{O}) = 69.84 \text{ mol.s}^{-1}$ and $F_0(\text{CO}) = 23.28 \text{ mol.s}^{-1}$ and for [H₂O]/[CO]=5 which corresponds to $F_0(\text{H}_2\text{O}) = 116.4 \text{ mol.s}^{-1}$ and $F_0(\text{CO}) = 23.28 \text{ mol.s}^{-1}$. These last simulations were established by varying only the molar flow rate of the water vapor. While the other operating conditions (Table III) and reactor characteristics (Table II) have not been changed.

III. EQUATIONS

A. kinetic expression

The kinetic expression used is a simple power-law model [7,18]:

$$-r_{co} (\text{mol. kg cata}^{-1} . \text{h}^{-1}) = 2623447 \exp\left(\frac{-79759}{RT}\right) C_{co}^{0.74} C_{H_2O}^{0.47} C_{CO_2}^{-0.18} [1 - \beta] \quad (1)$$

Where $-r_{CO}$ is the CO conversion rate, C_i is the molar concentration of species i (mol.dm^{-3}) and β is the reversibility factor:

$$\beta = \frac{C_{CO_2} C_{H_2}}{C_{CO} C_{H_2O} K_e}$$

The equilibrium constant, K_{eq} , is given by the equation 2 [7,18]:

$$K_{eq} = \exp\left(\frac{4577.8}{T} - 4.33\right) \quad (2)$$

B. Process modeling and numerical solution

The following assumptions were made to develop the used mathematical model for the packed bed reactor simulation:

- Adiabatic reactor.
- Steady state condition.
- Axial dispersion is neglected, because the flow rate is sufficiently high to create a turbulent flow ($Re = \frac{G \cdot d_p}{\mu} > 40$) and ($L/d_p > 150$) [30]. Where Re is the Reynolds number, G is the superficial mass velocity ($\text{kg} \cdot \text{m}^{-2} \cdot \text{s}^{-1}$) and μ is the dynamic viscosity of the mixture (Pa.s).
- Radial dispersion is neglected, because the tube diameter is narrow, the reactor is adiabatic and the WGS is a moderately exothermic. Under these conditions, radial gradients of concentrations and temperatures are not important [30,31,32].
- The heat and mass transfer as well as the diffusion in the catalyst were lumped in the rate constant.

The system of differential equations used is as follows [14]:

$$\frac{dX_{CO}}{dz} = \frac{-r_{CO} F_{Pres} \rho_B S}{F_{CO,0}} \quad (3)$$

$$\sum F_i C_{pi} \frac{dT}{dz} = \Delta H_R r_{CO} F_{Pres} \rho_B S \quad (4)$$

$$\frac{dp}{dz} = -f \frac{\rho_g u_s^2}{d_p} \quad (5)$$

C_i is expressed using the perfect gas equation:

$$C_i = \frac{P_i}{RT} \quad (6)$$

Where P_i is the partial pressure (Pa), expressed as follows: $P_i = \frac{F_i}{\sum_{i=0}^n F_i} \cdot P = y_i \cdot P$

With y_i is the molar fraction of the species i

The expression of the molar flow rate, F_i ($\text{mol} \cdot \text{s}^{-1}$), of each component depends on its nature, be it a reagent, a product or an inert:

- For the reagent:

$$F_i = F_{i,0} - F_{CO,0} * X_{CO} \quad (7)$$

- For the product:

$$F_i = F_{i,0} + F_{CO,0} * X_{CO} \quad (8)$$

- For the inert:

$$F_i = F_{i,0} \quad (9)$$

The kinetic expression rate presented in equation 1 is applicable at $P=1$ atm, while the pressures in the reactor are slightly above the atmospheric pressure. To consider this difference between the reactor pressures and the atmospheric pressure, a pressure scale-up factor (F_{pres}) can be used to apply the kinetic equation derived at $P=1$ atm to higher pressures [13]:

$$F_{pres} = P(atm)^{(0,5 - \frac{P(atm)}{250})} \quad (10)$$

The catalyst bulk density, ρ_B ($\text{kg}\cdot\text{m}^{-3}$), is expressed by equation 11:

$$\rho_B = (1 - \varepsilon) \cdot \rho_c \quad (11)$$

The molar specific heat capacity of each component, C_{p_i} ($\text{J}\cdot\text{mol}^{-1}\cdot\text{K}^{-1}$), as a function of temperature is given by the empirical equation:

$$C_{p_i} = \alpha + \beta \cdot T + \gamma \cdot T^2 \quad (12)$$

The values of α , β and γ are provided in Table IV:

TABLE IV. CONSTANTS EXPRESSING C_{p_i} ACCORDING TO TEMPERATURE

| Speciesi | α | $\beta \times 10^3$ | $\gamma \times 10^6$ |
|------------------|----------|---------------------|----------------------|
| H ₂ | 29.3 | -0.84 | 2.09 |
| CO ₂ | 32.22 | 22.18 | -3.35 |
| CO | 27.62 | 5.02 | 0 |
| H ₂ O | 30.13 | 10.46 | 0 |
| N ₂ | 27.62 | 4.19 | 0 |

The heat of the reaction, ΔH_R ($\text{J}\cdot\text{mol}^{-1}$), is expressed by equation 13:

$$\Delta H_R = -4,12 \times 10^4 + \int_{298}^T (C_{pCO_2} + C_{pH_2} - C_{pCO} - C_{pH_2O}) \cdot dT \quad (13)$$

The friction factor f , presented in equation 5 can be calculated using Ergun's equation [33]:

$$f = \frac{1 - \varepsilon}{\varepsilon^3} \left(a + b \frac{1 - \varepsilon}{Re} \right) \quad (14)$$

with $a=1.75$ and $b=150$.

G is calculated by equation 15:

$$G = \sum_{i=1}^{i=n} \frac{F_i M_i}{S} \quad (15)$$

Where S (m^2) is the cross section of the reactor ($S = \frac{\pi D^2}{4}$) and M_i is the molecular weight of the species i ($\text{kg}\cdot\text{mol}^{-1}$)

μ is expressed by equation 16 [34]:

$$\mu = \sum_{i=1}^n \frac{\mu_i}{1 + \frac{1}{y_i} \sum_{\substack{j=1 \\ j \neq i}}^n \frac{y_j [1 + \frac{\mu_i}{\mu_j}]^{1/2} [\frac{M_j}{M_i}]^{1/4}}{2\sqrt{2} [1 + \frac{M_i}{M_j}]^{1/2}}} \quad (16)$$

When the pressure level is moderate, its impact on the viscosity of the gas is low. In this case, the parameter that most impacts viscosity is mainly temperature [35].

The dynamic viscosity of species i , μ_i (Pa.s), is expressed as a function of temperature by the empirical equation 17:

$$\mu_i = \frac{AT^B}{1 + \frac{C}{T} + \frac{D}{T^2}} \quad (17)$$

Table V below gives the values of A, B, C and D for each species i :

TABLE V. CONSTANTS EXPRESSING μ_i ACCORDING TO TEMPERATURE

| species i | A x 10 ⁷ | B | C | D |
|------------------|---------------------|-------|--------|--------|
| H ₂ | 1.797 | 0.685 | -0.59 | 140 |
| CO ₂ | 2.148 | 0.46 | 290 | 0 |
| CO | 1.113 | 0.534 | 94.7 | 0 |
| H ₂ O | 6.1839 | 0.678 | 847.23 | -73930 |
| N ₂ | 6.56 | 0.608 | 54.71 | 0 |

The density of the gas mixture, ρ_g (kg.m⁻³), is expressed by equation 18:

$$\rho_g = \frac{P}{RT} \sum_{i=1}^{i=n} y_i M_i \quad (18)$$

The superficial velocity, u_s (m.s⁻¹), is defined as:

$$u_s = \frac{G}{\rho_g} \quad (19)$$

The catalyst mass corresponding to a longitudinal position z in the reactor, $w(z)$ (kg), is expressed by equation 20:

$$w(z) = S \cdot z \cdot \rho_B \quad (20)$$

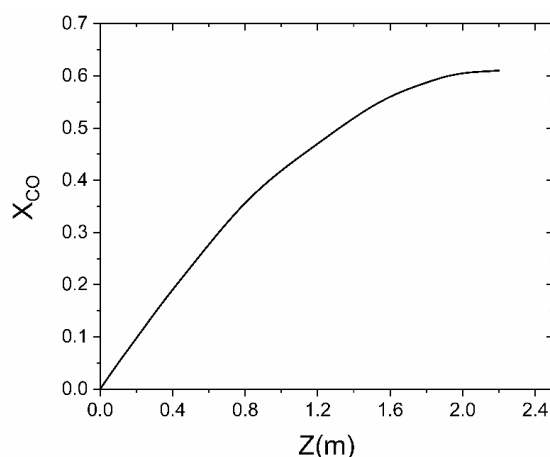
Differential equations (3-5) were numerically solved by MATLAB by using the fourth-order Runge-Kutta method. The boundary conditions are: $X_{CO}(Z=0) = 0$, $P_0(Z=0) = 1,134 \cdot 10^5$ Pa, $T_0(Z=0) =$ The inlet temperature.

IV. RESULTS AND DISCUSSIONS

A. Profile of the carbon monoxide conversion along the reactor

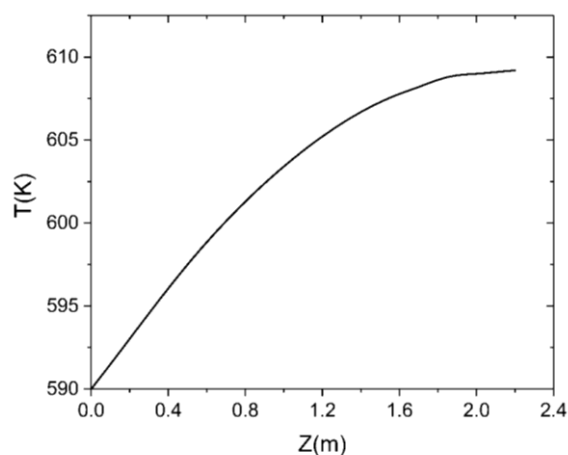
Figure 1 has an asymptotic shape. From $Z=0$ m to $Z= 1.8$ m, the conversion of carbon monoxide increases along the reactor until a value of $X_{CO} = 0.6$. From 1.8 m to 2 m, the increase of X_{CO} according to the longitudinal position is very weak and X_{CO} obtained at $Z= 2$ m is 0.605. Beyond 2 m, X_{CO} remains constant. Under the conditions studied, the equilibrium conversion would be 0.605. The catalytic mass required to reach this conversion is 170.76t. In order to increase the conversion of carbon monoxide or/and lower the necessary catalytic mass, several possibilities remain to be explored:

- Determination of optimal operating conditions (inlet temperature, H₂O/CO ratio, etc.).
- Optimization of the catalyst composition (choice of the promoter or/ and promoter fraction increasing catalytic activity [7]),
- ...etc.

Fig. 1. $X_{CO}=f(Z)$.

B. Variation of temperature, along the reactor height

The curve showing the temperature variation along the reactor also has an asymptotic shape. From $Z=0$ m to $Z=1.8$ m, the temperature increases along the reactor until it reaches 608.95 K. From $Z=1.8$ m to $Z=2$ m, the temperature increase along the reactor is very slight. T obtained at $Z=2$ m is 609 K. Beyond 2m, the temperature remains constant. In fact, at this longitudinal position the equilibrium is reached and since the reactor is an adiabatic one, the temperature rise stops.

Fig. 2. $T=f(Z)$.

The maximum temperature reached in the case studied has no damaging effect on the catalyst. In fact, when the temperature exceeds 823 K, the catalyst will quickly be deactivated by sintering and the thermodynamic limitation becomes very important [8].

C. Pressure profile across the catalyst bed

The pressure drops from 1.12 atm to 1.021 atm ($\Delta P=8.8\%$ of inlet pressure). This loss of pressure is not negligible [24] and can affect the good functioning of the reactor. In fact, the decrease in pressure between the inlet and outlet of the reactor causes an increase in the superficial velocity, which leads to a decrease in contact time and therefore in catalytic activity. In addition, it is necessary to compress the inlet flow when its pressure is low in order to overcome the pressure drop along the reactor and ensure a downstream flow at a pressure higher than the atmospheric pressure. If the pressure in the reactor is lower than the atmospheric pressure, it is necessary to use a vacuum pump in order to evacuate the reactor.

Several solutions can be studied to reduce pressure drops, including:

- The selection of the catalyst shape offering the lowest possible pressure loss. In fact, several studies have demonstrated that the shape of the catalyst has an important effect on the pressure loss [36, 37].
- The use of a foamsince it limits the pressure drops compared to a conventional fixed bed [38].
- ...etc

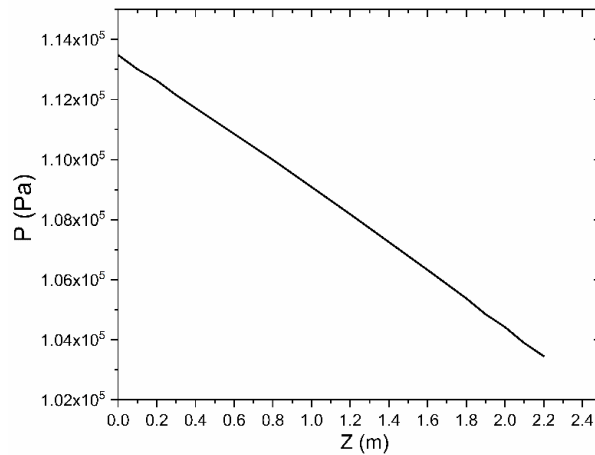


Fig. 3. $P = f(Z)$.

D. The effect of inlet temperature on carbon monoxide conversion

Figure 4 shows that the increase in the inlet temperature from 575 K to 590 K causes an increase in the CO conversion along the reactor. It should also be noted that the equilibrium is not reached in the reactor when the inlet temperature is 575 K. For the inlet temperature range between 590 K and 620 K, the conversion of CO is thermodynamically limited. The higher the inlet temperature, the faster the equilibrium is reached (located in the most remote longitudinal positions) and the lower the equilibrium conversion. In fact, according to Le Chatelier's principle, to counter the constraint of a temperature increase, the equilibrium is shifted following the reverse reaction, which leads to this decrease in the carbon monoxide conversion. According to Figure 4, the inlet temperature giving the highest conversion at the reactor outlet ($X_{CO} = 0.605$) is 590 K.

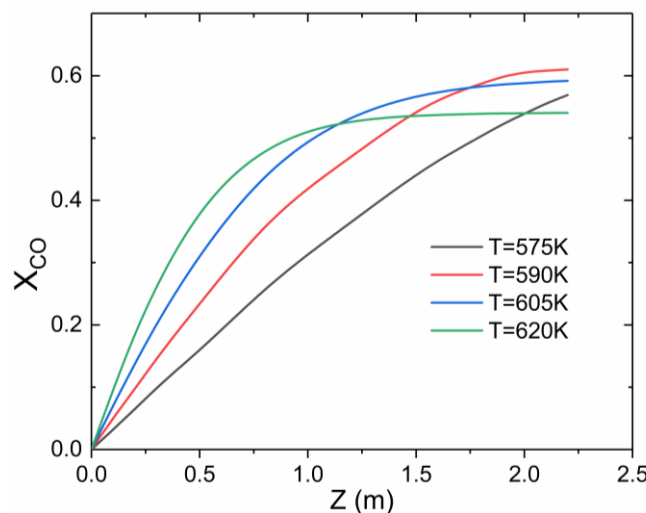


Fig. 4. The effect of inlet temperatures on X_{CO} along the reactor

E. The effect of H_2O/CO ratio on X_{CO}

It is clear from figure 5 that the higher the H_2O/CO ratio, the more carbon monoxide conversion is important. The highest conversion is obtained for a ratio of $H_2O/CO=10$. In fact, in the studied case, the reaction rates accelerated with the increase in water concentration (see Equation 1) and therefore the H_2O/CO ratio. The same effect of this ratio on X_{CO} has been observed in experimental studies conducted at the atmospheric pressure, at high temperatures (573 K-773 K) and in the presence of catalyst also composed of Fe_2O_3 and Cr_2O_3 [39]. In fact, the role of the water vapour is extremely important, because its use with sufficiently high flow rates prevent over reducing of the catalyst [7]. If the WGS is conducted with low H_2O/CO ratios, this results in methanation, Fischer Tropsch reaction and carbon deposition on the catalyst [7]. However, it should be noted that the carrying out of WGS with high H_2O/CO ratios requires significant energy costs related to the water vapor production.

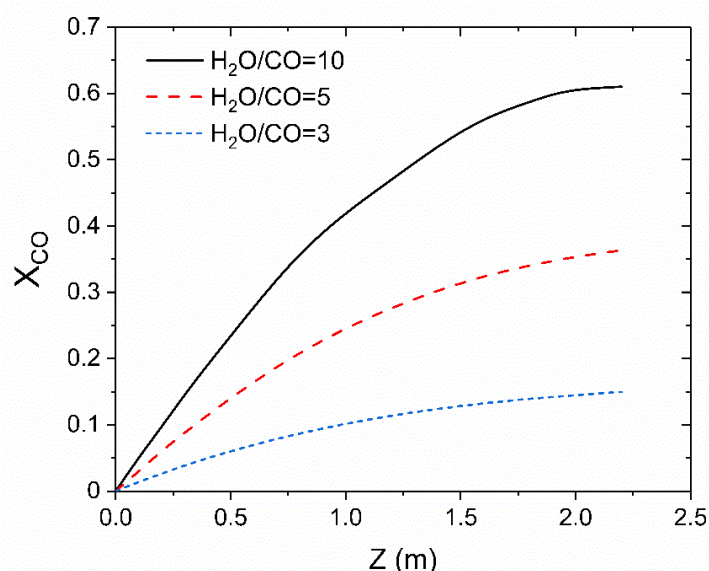


Fig. 5. The Effect of H_2O/CO ratios on X_{CO} along the reactor.

V. CONCLUSION

This study investigated the modeling and simulation of a WGS reactor processing an industrial load operating at a low pressure. The model used to predict the profiles of carbon monoxide conversion, temperature and pressure along reactor is the steady state one-dimensional pseudo homogenous model and the kinetic rate expression of the WGS corresponding to the catalyst used is taken from the literature. The estimated catalytic mass to convert 60.5% of carbon monoxide contained in inlet flow is 170.76 t. To lower the catalytic mass needed and/or increase the conversion of carbon monoxide there are several paths to explore such as the choice of promoter or a fraction of promoter allowing to improve catalytic activity. The pressure drop is not negligible ($\Delta P = 8.8\% P_{inlet}$) which can have many harmful effects on the proper functioning of the installation. The use of foam, for example, should limit pressure drops. The maximum temperature reached (609 K) has no damaging effect on the catalyst. This work confirmed the important role of choosing an optimal inlet temperature and a high H_2O/CO ratio in increasing the conversion of carbon monoxide at the reactor outlet. The best conversion ($X=0.605$) is obtained for a ratio $H_2O/CO=10$ and for an inlet temperature of 590 K.

REFERENCES

- [1] W. Li, Theoretical investigation on hydrogen production using metal-oxide catalysts: TiO₂ and CeO₂, Ph.D. thesis, Jacobs-Brême University, Germany, 2015.
- [2] A. Rakib, Valorisation du méthane en hydrogène par reformage catalytique, Ph.D. thesis, Université du littoral-côte d'Opale, France, 2012.
- [3] S. Chader, H. Hacene, M. Belhamel, "Etudes des procédés de production biologiques de l'hydrogène", *Revue des Energies Renouvelables*, 2007(4), 497 – 505.
- [4] J. W. Richards, V. Engelhardt, *The Electrolysis of Water : Processes and Applications*, The Chemical Publishing Company, 2010.
- [5] H.Z. Wang, D.Y.C Leung, M.K.H. Leung, "A review on hydrogen production using aluminium and aluminium alloys", *Renewable and sustainable energy reviews*, 2009(13), 845-853.
- [6] C. A. Callaghan, Kinetics and Catalysis of the Water-Gas-Shift Reaction: A Microkinetic and Graph Theoretic Approach, Ph.D. thesis, Worcester Polytechnic Institute, USA, 2006.
- [7] B. Smith RJ, M. Loganathan, M. Shekhar Shantha, "A Review of the Water Gas Shift Reaction Kinetics", *International Journal Of Chemical Reactor Engineering*, 2010(8), 1-32.
- [8] C. Lang, Développement de catalyseurs pour la réaction de conversion du gaz à l'eau dans le cadre de la production d'hydrogène par vapogazéification de la biomasse, Ph.D. thesis, Université de Strasbourg, France, 2016.
- [9] C. V. Ovesen, B. S. Clausen, B. S. Hammershøi, "A Microkinetic Analysis of the Water-Gas Shift Reaction under Industrial Conditions", *Journal Of Catalysis*, 1996(158), 170–180.
- [10] J. R. Ladebeck, J. P. Wagner, *Handbook of Fuel Cells – Fundamentals, Technology and Applications*, John Wiley & Sons, Ltd, Chichester, 2003.
- [11] S. S. E. H. Elnashaie, F. M. Alhabdan, "Mathematical modelling and computer simulation of industrial Water-Gas Shift Converters", *Mathl Comput Modelling*, 1989(12), 1017-1034.
- [12] F. Shokry, Y. A. El-Tawil, A. S. Shehata, "Modeling and simulation of low temperature water gas shift reactor", *Proceedings of International conference of chemical and Biochemical engineering*, 2015, 155.
- [13] T. A. Adams, Paul I. Barton, A dynamic two-dimensional heterogeneous model for water gas shift reactors: *international journal of hydrogen energy*, 2009(34), 8877 – 8891.
- [14] www.intechopen.com/books/petrochemicals/modeling-and-simulation-of-water-gas-shift-reactors-an-industrial-case
- [15] B. Bishara Hallac, Kinetic Experimental and Modeling Studies on Iron-Based Catalysts Promoted with Lanthana for the High-Temperature Water-Gas Shift Reaction Characterized with *Operando* UV-Visible Spectroscopy and for the Fischer-Tropsch Synthesis, Ph.D. thesis, Brigham Young University, Canada, 2014.
- [16] T. Salmi, R. Hakkarainen, "Kinetic Study of the Low-Temperature Water-Gas Shift Reaction over a Cu-ZnO Catalyst", *Applied Catalysis*, 1989(49), 285-306.
- [17] R. L. Keiski, T. Salmi, "Desactivation of the high-temperature water-gas shift catalyst in nonisothermal conditions", *Applied Catalysis*, 1992(87), 185-203.
- [18] R. L. Keiski, T. Salmi, V. J. Pohjola, "Development and verification of a simulation model for a nonisothermal water-gas shift reactor", *The Chemical Engineering Journal*, 1992(48), 17-29.
- [19] Y. Choi and H. G. Stenger, "Water gas shift reaction kinetics and reactor modeling for fuel cell grade hydrogen", *Journal of Power Sources*, 2003(124), 432–439.
- [20] S. S. Hla, D. Park, G. J. Duffy, "Kinetics of high-temperature water-gas shift reaction over two iron-based commercial catalysts using simulated coal-derived syngases", *Chemical Engineering Journal*, 2009(146), 148–154.
- [21] D. Mendes, V. Chibante, A. Mendes, "Determination of the Low-Temperature Water-Gas Shift Reaction Kinetics Using a Cu-Based Catalyst", *Ind. Eng. Chem. Res.*, 2010(49), 11269–11279.
- [22] D.M. Maklavany, K. Nikou, M. Reza, "Kinetic Modeling of Low Temperature Water-Gas Shift Reaction using gPROMS", *American Journal of Oil and Chemical Technologies*, 2016(4), 70-80.
- [23] E. Poggio-Fraccari, P. Giunta, G. Baronetti, F. Marino, "Cu and/or Ni catalysts over CePr oxide for the water gas shift reaction: an experimental study, kinetic fitting and reactor simulation", *Reac Kinet Mech Cat*, 2017(121), 607–628.
- [24] D.M. Maklavany, K. Nikou, M. Reza, "2-D Homogeneous Modeling and Simulation of Catalytic WGS Reactor", *American Journal of Oil and Chemical Technologies*, 2016(4), 81-89.
- [25] D. M. Maklavany, A. Shariati, K. Nikou, B. Roozbehani, "Hydrogen Production via Low Temperature Water Gas Shift Reaction: Kinetic Study, Mathematical Modeling, Simulation and Optimization of Catalytic Fixed Bed Reactor using gPROMS", *Chemical Product and Process Modeling*, 2017.
- [26] H. Er-rbib, C. Bouallou, "Modelling and Simulation of Methanation Catalytic Reactor for Renewable Electricity Storage", *Chemical Engineering Transactions*, 2013(35), 541-546.
- [27] M. Alavi, H. Jazayeri-rad, R. M. Behbahani, "Optimizing the Feed Conditions in a DME Production Process to Maximize the Methanol Conversion", *Science and Technology*, 2013(3), 61-66.
- [28] P.N. Panahi, S.M. Mousavi, A. Niaei, A. Farzi, D. Salari, "Simulation of methanol synthesis from synthesis gas in fixed bed catalytic reactor using mathematical modeling and neural networks", *International Journal of Scientific & Engineering Research*, 2012(3), 1-7.

- [29] S. Bahrami, M. Seifolahi, F. Ghanaat and S. Rahmani, "Modeling of Fixed-Bed Reactor for Hydrogenation of Acetylene in the Olefin Unit's", International Proceedings of Chemical, Biological and Environmental Engineering, 2015, 54-58.
- [30] M. E. Davis, R. J. Davis, Fundamentals of Chemical Reaction Engineering, McGraw-Hill Companies, New York, 2003.
- [31] A. Aboudheir, A. Akande, R. Idem, A. Dalai, "Experimental studies and comprehensive reactor modeling of hydrogen production by the catalytic reforming of crude ethanol in a packed bed tubular reactor over a Ni/Al₂O₃ catalyst", International Journal of Hydrogen Energy, 2006(31), 752 – 761.
- [32] S Z Saw, J Nandong, "Simulation and control of water-gas shift packed bed reactor with inter-stage cooling", IOP Conf. Series: Materials Science and Engineering, 2016(121), 1-10.
- [33] J. Villermaux, Génie de la réaction chimique, Tec & Doc- Lavoisier, Paris, 1993.
- [34] C.R. Wilke, "A viscosity equation for gas mixtures", chem. Phys, 1950(18), 517-519.
- [35] John. J. Bloomer, Practical fluid mechanics for engineering applications, Marcel Deeker, New York, 2000.
- [36] B. Elvers, S. Hawkins, G. Schulz, Ullmann's encyclopedia of industrial chemistry, Vol B4, VCH Publishers, New York, 1992.
- [37] N. Portin, V. Hanus, "Détermination des pertes de charge à travers les biocarburants solides", Revue Scientifique des Ingénieurs Industriels, 2016(30), 253-271.
- [38] M. Lacroix, P. Nguyen, D. Schweich, "Pressure drop measurements and modelling on SIC Foams", Chem. Eng. Sci, 2007 (62), 3259-3267.
- [39] W.-H. Chen, T.-H. Hsieh, T. L. Jiang, "An experimental study on carbon monoxide conversion and hydrogen generation from water gas shift reaction", Energ. Convers. Manage, 2008(49), 2801-2808.

Properties of Geopolymer Bricks Exposed To High Temperatures

Ghada D. Abdel-Hameed¹

1- Associated Professor, Materials Building and Quality Control Institute, Housing and Building National Research Center, Giza, Egypt

ABSTRACT

Green concrete are generally composed of recycling materials as full or partial substitutes for aggregate, cement, and admixture in concrete. To reduce greenhouse gas emissions, efforts are needed to develop environmentally friendly construction materials. Using fly ash based geopolymer as an alternative binder can help reduce CO₂ emission of cement. This paper presents the results of a study to compare the properties of geopolymer bricks prepared using class C fly ash. Also, utilization of cement kiln dust (by-pass) with its high alkali content in the activation of geopolymer bricks specimens to create nonconventional cementitious binders was investigated. Many different geopolymer mortar mixtures were tested. Mixture evaluation was based upon replacing the fly ash with cement kiln dust (by-pass). The cement kiln dust (by-pass) content percentages were 50%, 75%, and 100% by weight of fly ash as a partial replacement. Geopolymer mortar specimens were prepared using different concentrations of NaOH solution of M10, and M16 and were cured at air until test date. The manufactured bricks were exposed to 300°C and 600°C for two hours after 28 days of curing. Tests were conducted according to both Egyptian Standard Specifications (ESS) and American Society for Testing and Materials (ASTM) in order to determine compressive strength, absorption percentage, and oven-dry weight. Also, loss in weight was performed. In this study, the Local Alkaline Activator in Egypt and Natural River sand as fine aggregate, in fly ash based-geopolymer bricks was used. This paper illustrates the development of mechanical properties. Hence it has been found that the cement kiln dust (by-pass) as geopolymer base can be used to manufacture both load-bearing and non-load-bearing units at room temperature with high molarity.

Keywords: Geopolymer; molarity; temperature; solid bricks, cement kiln dust, compressive strength, water absorption, weight.

I. INTRODUCTION

In recent years, green concrete has drawn serious attention of researchers and investigators because of a concept of "thinking environmentally friendly" [1]. The contribution of ordinary Portland cement production worldwide to greenhouse gas emissions is estimated to be approximately 1.35 billion tons annually [2]. To keep the global environment safe from the consequence of cement production, it is essential to explore alternative materials that can completely or partially eliminate the use of cement in concrete and cause no environmental destruction [3]. Geopolymers are formed when various alumina and silica containing materials react under highly alkaline conditions and forms a three dimensional network of Si–O–Al–O bonds [4]. The most commonly used raw materials in geopolymer are clay and metakaolin [5]. Cement kiln dust (by-pass) is a fine-grained, particulate material easily entrained in the combustion gases moving through the kiln. It is composed primarily of variable mixtures of calcined and uncalcined feed materials, fine cement clinker, fuel combustion by-products and condensed alkali compounds. Cement kiln dust (by-pass) generation is responsible for a significant financial loss to the cement industry in terms of the value of raw materials, processing, energy usage, dust collection and disposal. Cement manufacturing plants generate approximately 30 million tons of cement kiln dust (by-pass) worldwide per year. According to, Dyer et al., [6] and Zainab H. A., [7] the compressive strength increase in the concrete mixtures that include 10% and 20% CKD (as an addition of cement weight). A decrease in the compressive strength was noticed in the concrete mixtures that include 10% and 20% CKD (as a replacement of cement weight). A similar trend was noticed in the splitting tensile strength and the increase in splitting tensile strength was less pronounced than that in compressive strength. Khater. H.M, [8] concluded that the compressive strength increased in concrete mixtures that include 10% and 20% cement kiln dust (by-pass) as an

addition of cement weight. A reduction in compressive strength was noticed in concrete mixtures that include 10% and 20% cement kiln dust (by-pass) as a replacement of cement weight. Wallah and Rangan [9] reported that geopolymer concrete specimens exhibit extremely small changes in length and also show very little increase in mass after one year in sulphate solution. In another study by Bakharev [10] the author used various concentrations of sulphate solution to immerse the geopolymer materials prepared using different types of activating solutions. This study was conducted to reveal the behavior of green geopolymer bricks incorporating various percentages of cement kiln dust (by-pass) as a partial/ full replacement and evaluate its compressive strength, water absorption, and oven-dry weight.

II. EXPERIMENTAL PROGRAM

The experimental program consists of ten different mixes; four geopolymer mixes with molarity of M10, four geopolymer mixes M16 and two mixes as control. The two controlled mixture were normal bricks mixture, one with Portland cement and the other one by Cement kiln dust (by-pass). Furthermore, the effect of the different contents of cement kiln dust (by-pass) content percentages of 50%, 75%, and 100% by weight of fly ash as a partial/full replacement for the remain eight mixtures. The mechanical properties of green bricks were studied. Test specimens were prepared from the local materials. These include natural siliceous sand from Suez area and clean rounded fine aggregate of size of 0.15 to 5 mm that was used. The physical properties of fine aggregate are shown in Table (1). CEMI 42.5 N was used from Suez Cement Company; the physical properties of ordinary Portland cement are shown in Table (2). Sodium hydroxide in flake form was used (NaOH with 98-99% purity). The fly ash used in this research is class F fly ash according to the requirement of ASTM C618 Class F [13], its physical properties and XRF analysis are given in table (3) and table (4), respectively. Cement kiln dust (by-pass) was obtained from EL-Suez Cement Company where the percentage retained on sieve #170 was less than 9%. Accordingly the cement was expected to have particles surface area in the range of 2980 cm²/gm. Tables (5) and (6) show the physical and chemical properties of cement kiln dust (by-pass), respectively.

Table 1: Physical properties of fine aggregate

| Property | Results | Limits |
|--|---------|--------------------|
| Specific Weight | 2.63 | 2.5-2.75 ** |
| Bulk Density (t/m ³) | 1.78 | ----- |
| Fineness Modulus | 2.89 | ----- |
| Clay and Fine Dust Content (% By Volume) | 0.85 | Not more Than 3 ** |

** Egyptian Standard Specifications ESS 1106 [11].

Table 2: Physical properties of Ordinary Portland Cement.

| Property | | Results | Specifications Limits* |
|--|---------|---------|------------------------|
| Compressive Strength of Standard Mortar (Mpa) | 2 days | 21.4 | Not less than 18 |
| | 28 days | 39.7 | Not less than 36 |
| Fineness in terms of S.S.A** (cm ² /gm) | | 3185 | >2750 |
| Setting Time (min) | Initial | 75 | Not less than 45 |
| | Final | 480 | Not more than 600 |

* Egyptian Standard Specifications ESS 4756-1/2009 [12].

Table (3): Physical properties of the used fly ash

| Property | Test Results |
|--|--------------|
| Specific surface area (cm ² /gm) | 3950 |
| Bulk density (kg/m ³) | 1250 |
| Specific gravity | 2.5 |
| Color | Light gray |

Table (4): XRF Analysis of the used fly ash

| Oxide | Content % | Limits % * |
|--------------------------------|-----------|------------|
| SiO ₂ | 61.30 | Min. 70% |
| Al ₂ O ₃ | 29.40 | |
| Fe ₂ O ₃ | 3.27 | |
| CaO | 1.21 | ----- |
| MgO | 0.75 | ----- |
| K ₂ O | 1.20 | ----- |
| SO ₃ | 0.003 | Max. 3% |
| TiO ₂ | 0.01 | ----- |
| Na ₂ O | 0.73 | Max. 1.5% |
| Cl | 0.04 | Max. 0.05% |
| LOI | 0.67 | Max. 6% |

* According to ASTM C618 Class F [13].

Table (5): Physical properties of the used cement kiln dust (by-pass).

| Property | Test Results |
|--|--------------|
| Specific surface area (cm ² /gm) | 2980 |
| Bulk density (kg/m ³) | 1150 |
| Specific gravity | 2.81 |
| color | Light gray |
| Physical Form | Powder |

Table (6): XRF Analysis of used cement kiln dust (by-pass).

| Oxide | Content % |
|--------------------------------|-----------|
| SiO ₂ | 16.65 |
| Al ₂ O ₃ | 4.48 |
| Fe ₂ O ₃ | 2.08 |
| CaO | 41.87 |
| MgO | 2.33 |
| K ₂ O | 5.20 |
| SO ₃ | 2.15 |
| Na ₂ O | 4.16 |
| Cl | 3.36 |
| LOI | 11.82 |

III. MIXING, MOLDING, AND CURING

Table (7), represents the mix proportions of the tested mixes by weight quantities for geopolymer bricks. The control mix design for the manufactured product was designed and tested at age 28 days (as specified by the Egyptian Standard Specification). For 28 days after casting, all specimens were sprayed twice daily. Geopolymer mixture proportions, different molarity and exposure temperatures are given in Table 7. Solid cement bricks 26x 12x 6 cm were manufactured by conventional equipment. The manufacturing process involves compaction of the mixed constituent materials in a mold followed immediately by extrusion of the pressed product so that the mold can be used repeatedly. Since the finished product is required to be self-supporting and able to withstand any movement and vibration from the moment they are extruded, very much drier, and leaner mixes are used than in the normal concrete work. The demoulding ability is an essential criterion for manufacturing solid cement bricks. The molarity contents of the solid cement bricks were adjusted to maintain an almost zero slump. Crushed stone was not washed prior to mixing. A series of tests were carried out after 28 days of curing according to ASTM C 67-03a [14] to determine compressive strength, oven dry-weight and absorption values of the brick samples. Also, the mass loss was performed before and after the specimens exposed to high temperatures. Three specimens were tested for each test. After curing for 28 days, the samples which were exposed to elevated temperatures were heated in an electric oven up to 300, and 600°C. The temperature was maintained at the

respective temperature for 2 hours to achieve a thermally steady-state. Then, the furnace door was opened and the samples were allowed to cool naturally to room temperature.

Table (7): Mixture proportions, molarity and cement kiln dust

| Mix No. | Molarity | cement (kg) | FA (kg) | Sand (kg) | Dolomite (kg) | cement kiln dust (by-pass) (kg) | water |
|---------|----------|-------------|---------|-----------|---------------|---------------------------------|-------|
| 1 | 0 | 250 | 0 | 1086.66 | 1086.66 | 0 | 125 |
| 2 | 0 | 0 | 0 | 1086.66 | 1086.66 | 250 | 125 |
| 3 | M10 | 0 | 250 | 1086.66 | 1086.66 | 0 | - |
| 4 | M10 | 0 | 0 | 1086.66 | 1086.66 | 250 | - |
| 5 | M10 | 0 | 125 | 1029.3 | 1029.3 | 125 | - |
| 6 | M10 | 0 | 187.33 | 1029.3 | 1029.3 | 62.6 | - |
| 7 | M16 | 0 | 250 | 1086.66 | 1086.66 | 0 | - |
| 8 | M16 | 0 | 0 | 1086.66 | 1086.66 | 250 | - |
| 9 | M16 | 0 | 125 | 1029.3 | 1029.3 | 125 | - |
| 10 | M16 | 0 | 187.33 | 1029.3 | 1029.3 | 62.6 | - |

IV. RESULTS AND DISCUSSION

The effects of molarity, fly ash, and cement kiln dust (by-pass) in the activation on geopolymer bricks properties due to exposure to elevated temperatures are herein presented.

Compressive Strength: The effects of the cement kiln dust (by-pass) in the activation of geopolymer bricks specimens and elevated temperatures on average product compressive strength are presented in Figure 1. The limits of both load-bearing and non-load bearing units are shown in Table 8. Ordinary Portland cement class 42.5N and cement kiln dust (by-pass) was used in mixes 1 and 2 respectively. The results show that mix 1 satisfied the limit of average product compressive strength concerning load-bearing units up till 300°C tested temperature. However, at 600°C, the limit of non-load bearing units was met. Mix 2, on the other hand, satisfied the requirement of load-bearing units at room temperature only. The loss in compressive strength using cement kiln dust (by-pass) can be related to the chemical effects. Moreover, the percentage of free calcium hydroxide during the reaction of cement and cement kiln dust (by-pass) increase similarly.

In other words, both could be used as load-bearing units at room temperature. It should be noted that there are two phenomena that govern the behavior of bricks when exposed to various temperatures: firstly, the increase in the rate of cement hydration and secondly, the thermal incompatibility between the cement paste and the aggregates, the dehydration of the matrix and the thermal expansion of the aggregates give rise to internal stresses and beginning at 300°C, micro-cracks begin to pierce through the material [19, 20]. In some cases, the first factor becomes the governing factor, while in other cases; second factor becomes the overriding factor.

Mixes 3, 4, 7 and 8 produced geopolymer bricks specimens of different base and molarity. The mixes provided average compressive strength satisfied that the requirement for load-bearing units at room temperature except mix 4 which contained cement kiln dust (by-pass) base. According to these results, the compressive strength of geopolymer mixes containing sodium silicate solution of molarity 16 is higher than that of mixes of molarity 10. At room temperature only, using cement kiln dust (by-pass) as geopolymer base with high molarity satisfy the load-bearing requirements. The results of the remaining mixes containing cement kiln dust (by-pass) as partial replacement by 25% and 50% of fly ash by weight in geopolymer mixes of different molarity, showed using cement kiln dust (by-pass) with high molarity can satisfy the load-bearing requirements at room temperature.

Table (8): Strength and Absorption Requirements [15-17]

| | | | |
|---|--|----------------|------------------|
| Compressive strength, min, (kg/cm ²) | Water absorption, max, (kg/cm ³) Average of 3 Units | | |
| Average net area | Weight classification-oven-dry weight of concrete(kg/cm ³) | | |
| Average of 3 Units | Light weight | Medium weight | Normal weight |
| Loadbearing units | Less than 1680 | 1680 288 (240) | 2000 or more 208 |
| 131 | 288 | | |
| | Non-loadbearing units | | |
| | 41.4 | | |

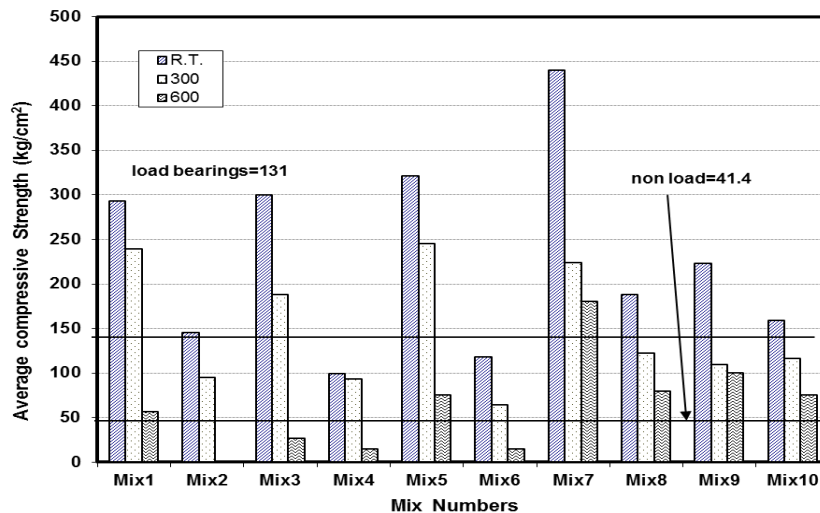


Fig. (1): Effects of geopolymer base and elevated temperatures on compressive strength

Oven-Dry Weight and Water Absorption Percentage:

There are three classes of solid cement bricks: normal weight, medium weight and light weight according to both ESS 1292-1/2005 [16] and ASTM C90-03 [15]. The two criteria that specify the categorization of weight are water absorption and the Oven-Dry weight. The effects of the geopolymer base at room temperature on absorption and unit weight are presented in Fig. 2 and 3, respectively. The limits of water absorption and Oven-Dry weight are given in table 8. The criterion regarding normal weight for absorption was satisfied by the ten mixes at the tested temperatures. In other words, all mixes at tested temperatures had values of water absorption less than 208 Kg/m³. Thus, the Oven-Dry weight of the specimens becomes the decisive factor with regard to the categorization of weight. At different temperatures tested, all mixes satisfied the criteria of normal weight, while mixes 2 and 7 met the criteria of medium weight at elevated temperatures. From the above results, it may be concluded, that irrespective of the different geopolymer base, the weight classification generally ranged from medium to normal weight at elevated temperatures.

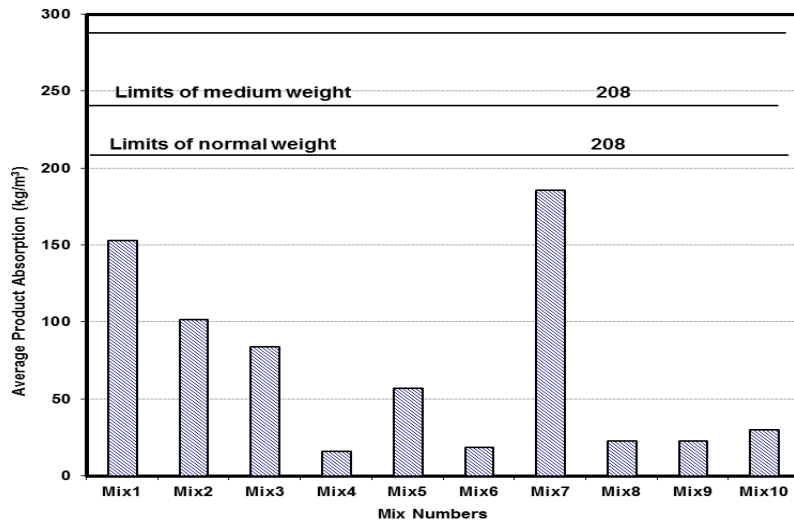


Fig. (2): Effects of geopolymer base on water absorption

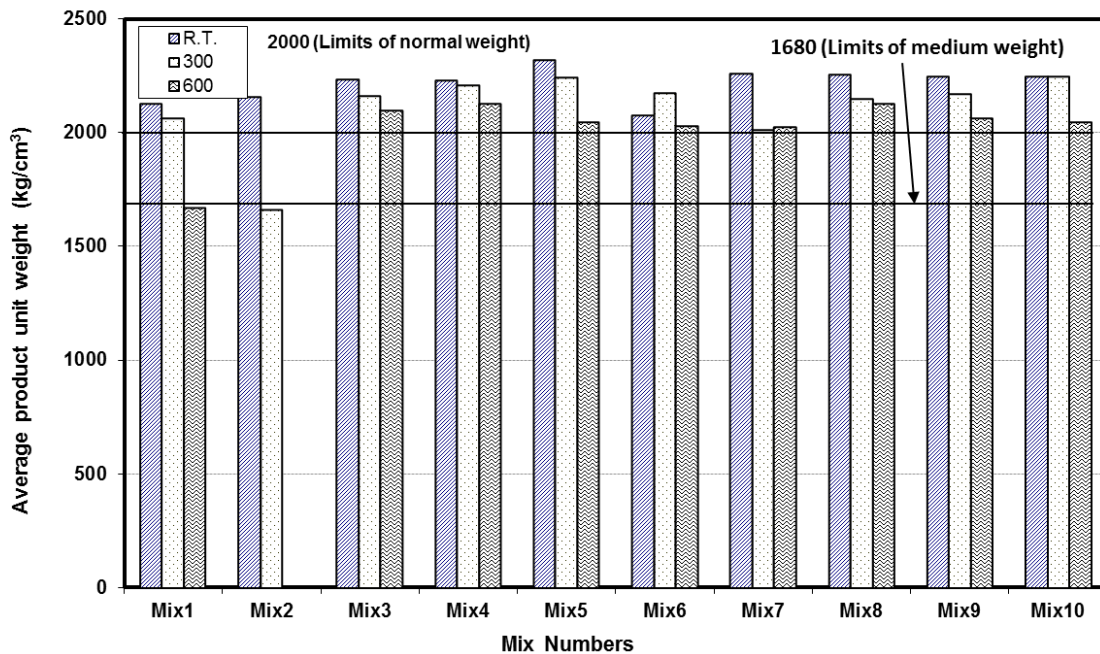


Fig. (3): Effects of geopolymer base and elevated temperatures on unit weight

Mass Loss: The effects of cement types and elevated temperature on mass loss are shown in Fig. 4. When comparing mixes 1 and 2, at 300°C, mix2 resulted in lower mass. However, there was a pronounced increase in mass loss regarding mix 2 at temperature 600°C. from the figure it can be observed that, using cement kiln dust (by-pass) as base in geopolymer mixes increase the mass loss for this specimens. The highest mass loss was obtained for mix 2 at 300°C of 22.9%. Weight reduction occurs due to the release of bound water from the cement paste. Consequently, air voids are formed and the structural integrity of the specimens deteriorates. Thus, the reduction in weight confirms the loss of mass by the concrete material and the increase in the proportion of air voids [18].

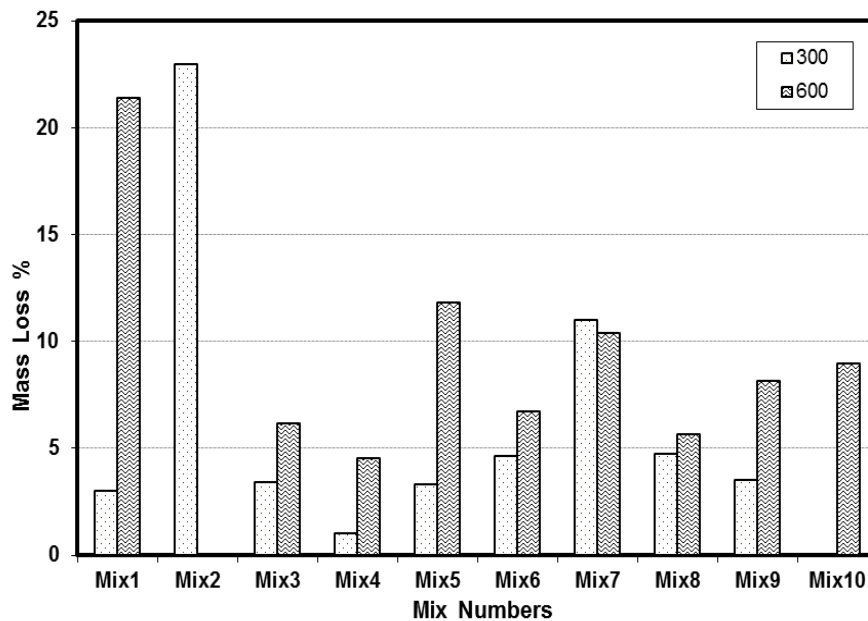


Fig. (4): Effects of geopolymer base and elevated temperatures on mass loss

V. CONCLUSIONS

Based on the experimental results obtained from this study, the following conclusions can be drawn:

- Concerning using OPC and cement kiln dust (by-pass) can be used for load-bearing units in room temperature only.
- Using cement kiln dust (by-pass) as geopolymer base cannot be used for load-bearing units with lower molarity.
- Using cement kiln dust (by-pass) as partial replacement for geopolymer base can be used for non-load-bearing units with high molarity even when subjected to temperature up to 600°C.
- At room temperature, bricks incorporating cement kiln dust (by-pass) full or partial replacement geopolymer base satisfied the criteria of normal weight even when subjected to temperature up to 600°C.
- Bricks incorporating cement kiln dust (by-pass) resulted in the highest mass loss.
- The tested cement kiln dust (by-pass) as geopolymer base can be used to manufacture both load-bearing and non-load-bearing units at room temperature with high molarity.

REFERENCES

- 1) O. M. Omar, G. D. Abd Elhameed, M. A. Sherif, and H. A. Mohamadien, “Influence of limes tone waste as partial replacement material for sand and marble powder in concrete properties” HBRC Journal Vol. 8, pp. 193–203 May 2012.
- 2) P. K. Sarker, R. Haque, and K. V. Ramgolam, Fracture behaviour of heat cured fly ash based geopolymer concrete. Materials and Design Vol. 44, pp.580–586 August 201.
- 3) S. Demie, M. F. Nuruddin, and N. Shafiq, “Effects of micro-structure characteristics of interfacial transition zone on the compressive strength of self-compacting geopolymer concrete” Construction and Building Materials Vol. 41, pp. 91–98 January 2013.
- 4) D. Hardjito, Studies on Fly Ash-Based Geopolymer Concrete. Ph. D. thesis, Curtin University of Technology, Australia, November 2005.
- 5) B. V. Rangan, “Fly Ash-Based Geopolymer Concrete” International Workshop on Geopolymer Cement and Concrete, Allied Publishers Private Limited, Mumbai, India, 68-106, December 2010.
- 6) T. D. Dyer, J. E. Halliday, R. K. Dhir, An investigation of the hydration chemistry of ternary blends containing cement kiln dust. Journal of Materials Science, Vol. 34, pp 4975-4983.
- 7) Z. H. Abdulabbas, Utilization of Cement Kiln Dust in Concrete Manufacturing. Jordan Journal of Civil Engineering, 2013 Vol. 7, pp. 111-125.

- 8) Khater. H.M, Effect of cement kiln dust on Geopolymer composition and its resistance to sulphate attack. International journal of civil and structural engineering, 2012, Vol. (2), PP. 749-762.
- 9) S. E. Wallah and B. V. Rangan, Low calcium fl ash based geopolymer concrete: Long term properties, Research report GC2, Curtin University of Technology, Australia (2006).
- 10) T. Bakharev, Durability of geopolymer materials in sodium and magnesium sulphate solutions, Cement and Concrete Research 35 (2005) 1233-1246.
- 11) Egyptian Standard Specifications ESS 1106
- 12) Egyptian Standard Specifications ESS 4756-1/2009.
- 13) ASTM C618 Class F, Standard Specification for Coal Fly Ash and Raw or Calcined Natural Pozzolan for Use in Concrete.
- 14) ASTM C67-03. Standard Test Methods for Sampling and Testing Brick and Structural Clay Tile. Philadelphia, PA: American Society for Testing and Materials.
- 15) ASTM, C., 90-03. Standard Specification for Loadbearing Concrete Masonry Units.
- 16) ESS1292-1, 2005. Concrete Masonry Units, Part 1: Loadbearing Concrete Masonry Units.
- 17) ESS1292-2, 2005. Concrete Masonry Units, Part 2: Non-loadbearing Concrete Masonry Units.
- 18) Demirel, B. and O. Kelestemur, 2010. Effect of Elevated Temperature on the Mechanical Properties of Concrete Produced with Finely Ground Pumice and Silica Fume. Fire Safety Journal, 45: 385-391.

In vitro Evaluation of the Antimicrobial and Antioxidant activities of *Juniperus oxycedrus* essential oil (Cade oil)

Fatiha Abdellah*, Boukraa Laid, Si Mohamed Hammoudi and Rachida Benaraba

Laboratory of Research on Local Animal Products Ibn-Khaldoun University, Tiaret, Algeria

ABSTRACT

Aromatic oils from junipers have been used since antiquity for fragrance, flavoring, and medicinal, insecticidal, and cosmetic purposes. Cade essential oil is produced from destructive distillation of *Juniperus oxycedrus* (Cade tree) wood which is native to the Mediterranean region. This empyreumatic oil contains mostly sesquiterpenes and phenols and is used in both human and veterinary dermatology to treat chronic eczema and other skin diseases. The objective of this study is the evaluation of the antibacterial, antifungal and antioxidant activities of *Juniperus oxycedrus* essential oil (Cade oil). The results of the antimicrobial effect reveals that the Cade oil possess an antibacterial and antifungal effect against all tested strains, *Staphylococcus aureus* is the most sensitive species with an MIC value of 0.05% and *Escherichia coli* is the species the most resistance with an MIC value of 0.6%. The result of the antioxidant effect showed that the Cade oil has a strong antioxidant activity compared to standard antioxidants, ascorbic acid and gallic acid. From the above study it may be concluded that *Juniperus oxycedrus* essential oil (Cade oil) has a potential source of biological activity including, antibacterial, antifungal and antioxidants of natural origins.

Key words: *Juniperus oxycedrus*, Essential oil, Antibacterial, Antifungal, Antioxydant

I. INTRODUCTION

Natural products have been used for thousands of years in folk medicine for several purposes. They are both fundamental sources of new chemical diversity and integral components of today's pharmaceutical compendium [1]. In recent years, essential oils and plant extracts have attracted a great deal of scientific interest due to their potential as a source of natural antioxidants and biologically active compounds, such as antibacterial, antifungal and insecticidal substances [2]. The genus *Juniperus* is considered as an important medicinal plant largely used in traditional medicine. Its leaves are used in the form of decoction to treat diabetes, diarrhea, and rheumatism [3]. Furthermore, this plant is also used as a folk remedy to treat various ailments, such as hyperglycemia, obesity, tuberculosis, bronchitis, and pneumonia [4]. Some juniper species have strong anti-termite, antibacterial, and antifungal properties [5]. Aromatic oils from junipers have been used since antiquity for fragrance, flavoring, medicinal, insecticidal, and cosmetic purposes [6]. *Juniperus oxycedrus* which is native to the Mediterranean region is used to prepare an empyreumatic oil (Cade oil) by destructive distillation of the branches and wood of the plant, Cade oil is dark, aromatic oil with a strong smoky smell [7]. which is widely used in human and veterinary dermatology to treat chronic eczema and other skin diseases [8]. Cade essential oil have also been in use since the ancient times in the treatment of pain, joint aches, leprosy, toothaches, snake bites, dandruff, cancer, peptic ulcer, pneumonia, high blood pressure, skin irritation, bronchitis, diarrhea, itching and few other infections. Rectified Cade oil, employed as a fragrance component in soaps, detergents, creams, lotions, and perfumes is also produced. In regard to pharmacology or biological activities, Cade oil has been reported to have keratolytic and antipruritic properties, and antimicrobial activities *in vitro* [9]. The present study was conducted to investigate the antimicrobial and antioxidant properties of the Cade oil.

II. Material and Methods

A. *Juniperus oxycedrus* essential oil sample (Cade oil)

The Cade oil was purchased from distillerie des cévennes - claret-France

B. Evaluation of the Antimicrobial Activity

- *Bacterial strains and inoculums standardization*

Pseudomonas aeruginosa ATCC 27853, *Escherichia coli* ATCC 25922, *Bacillus cereus* ATCC 10876, *Staphylococcus aureus* OXA R ATCC 43300, *Staphylococcus aureus* OXA S ATCC 25923, *Staphylococcus aureus* ATCC 33862, *Candida albicans* and *Aspergillus niger* ATCC 106404 were kindly provided by the university hospital Mustapha Pasha of Algiers (Algeria). Prior to the experiment the strains were maintained by subculture in the specific media; the inoculums suspensions were obtained by taking five colonies from 24-hour cultures. The colonies were suspended in 5 ml of sterile saline (0.85% NaCl) and shaken for 15 seconds. The density was adjusted to the turbidity of a 0.5 McFarland Standard (equivalent to $1-5 \times 10^6$ cfu/ml) using sterile saline.

- *Minimum Inhibitory Concentration Measurement (MIC)*

The Minimum Inhibitory Concentration (MIC) of Cade oil has to be determined by using the incorporation method; concentrations of diluted Cade oil in the absolute ethanol (1:10, v/v) between 0.05% and 0.1% (vol/vol) were added into Mueller Hinton agar media to test their efficiency against bacteria. For *Candida albicans*, and *A.niger* concentrations of diluted Cade essential oil between 0.1% and 0.4% were incorporated into Sabouraud agar media. The final volume of essential oil and media in each plate (60 mm) was 5mL. Then standard inoculums of 0.5 McFarland of each microbial strains was inoculated and the plates were incubated at 37 °C for 24 h for bacteria and at 35 °C for 48 h for *C. albicans* and for 5days for *A.niger*. While the absolute ethanol was used as a control. The minimum inhibitory concentration (MIC) was determined by finding the plates with the lowest concentration of the cade essential oil on which the strain would not grow. Tests were repeated in triplicate. All MIC values are expressed in percentage (vol/vol).

C. Antioxidant activity

- *Free radical scavenging activity (DPPH test)*

The principle of the assay is the reduction of the violet 2,2-diphenyl- 1-picrylhydrazil (DPPH) radical in the reaction with "scavengers" of free radicals to the yellow colored diphenylpicrylhydrazil. This change of color represents the measure of highness of "scavengers" and is determined by the spectrophotometry. Lowering the absorption of solution of DPPH is in relation to the hydrogen donor activity of the examined compound and is measured at 517 nm on the spectrophotometer [10].

Antioxidant scavenging activity was studied using 1,1-diphenyl- 2-picrylhydrazyl free radical (DPPH) as described by Blois[11] with some modifications; 1.5 mL of various dilutions of the Cade oil were mixed with 1.5 mL of a 0.2mM ethanolic DPPH solution. After an incubation period of 30 min at 25 C°, the absorbance at 517 nm, the wavelength of maximum absorbance of DPPH, were recorded as a (sample). A blank experiment was also carried out applying the same procedure to a solution without the test material and the absorbance was recorded as A (blank). The free radical-scavenging activity of each solution was then calculated as percent inhibition according to the following equation:

$$\% \text{ inhibition} = 100 (A (\text{blank}) - A (\text{sample}) / A (\text{blank}))$$

The antioxidant activity of Cade essential oil was expressed as IC50, defined as the concentration of the test material required to cause a 50% decrease in initial DPPH concentration. Ascorbic acid and Gallic acid were used as a standard. All measurements were performed in triplicate.

- *Ferric Reduction Antioxydant Power (FRAP Assay)*

The FRAP assay is one of the most frequently used analytical strategies for antioxidant activity. The Fe^{3+} reducing power of Cade essential oil was determined by the method of Yen and Duh[12] with slight modifications. 2.5 mL of the Cade oil at various concentrations (0.0625, 0.125, 0.25, 0.5 and 1 $\mu\text{l/ml}$) was mixed with phosphate buffer (2.5 mL, 0.2 M, pH 6.6) and 1% potassium ferricyanide (2.5 mL). The mixtures were

incubated for 20 min at 50 °C. After incubation, 10% trichloroacetic acid (2.5 mL) was added to the mixtures, followed by centrifugation at 3000 rpm for 10 min. The upper layer (1 mL) was mixed with distilled water (1 mL) and 0.1% ferric chloride (0.5 mL). The reducing potential of Cade oil and standards (gallic acid and ascorbic acid) is expressed by the values of the effective concentrations 50% (EC50) that correspond to the concentration of sample needed to give an absorbance equal to 0.5 at 700 nm.

III. Result and Discussion

A. Result of the antimicrobial activity

Plants are a good source of various natural biomolecules involved in their different biological activities [13]. The results of the antimicrobial activity of our sturdy showed that the Cade oil was active against all the tested microorganisms (Table1).

TABLE 1. Antimicrobial activity of Cade essential oil:

| Microbial strain | MIC value |
|---|-----------|
| <i>Staphylococcus aureus</i> OXA R ATCC 43300 | 0.1% |
| <i>Staphylococcus aureus</i> OXA S ATCC 25923 | 0.05% |
| <i>Staphylococcus aureus</i> ATCC 33862 | 0.05% |
| <i>Bacillus cereus</i> ATCC 10876 | 0.2% |
| <i>Escherichia coli</i> ATCC 25922 | 0.6% |
| <i>Pseudomonas aeruginosa</i> ATCC 27853 | 0.4% |
| <i>Aspergillus niger</i> ATCC 106 404 | 0.2% |
| <i>Candida albicans</i> | 0.3% |

The results of the antimicrobial effect revealed that the Cade oil possess an antibacterial and antifungal effect against all the tested strains, the activity of the essential oil varies with its concentration and the microbial strain; *Staphylococcus aureus* is the most sensitive species with an MIC value of 0.05% and *Escherichia coli* is the species the most resistance with an MIC value of 0.6%. These findings confirm what has been reported by others authors Angioni et al [14] and Medini et al [15] they showed that *E. coli* has a resistance to essential oil of *J. oxycedrus* ssp. *oxycedrus* leaves of Sardinia and Tunisia. While *Staphylococcus aureus* was the most sensitive microorganism. This results showed that the Gram-negative bacteria are more resistant than the Gram-positive bacteria. It has been showned that Gram-positive bacteria are more sensitive than Gram-negative as was showned by Bouzouita et al [16], Ait Ouazzou et al [17] and Ramdhani et al [18].

These differences in the susceptibility of the tested microorganisms to the essential oil could be attributed to the variation in the rate of the essential oil constituents penetration through the cell wall and cell membrane structures. The ability of the essential oil to disrupt the permeability barrier of cell membrane structures and the accompanying loss of chemiosmotic control are the most likely reasons for its lethal action [19].

Better effectiveness of essential oils against Gram-positive bacteria may be due to volatile action of essential oil and due to absence of lipo-polysaccharide layer in Gram positive bacteria that might function as an effective barrier against any incoming bio-molecule [20].

The lower susceptibility of Gram-negative bacteria to the essential oil may be explained in terms of diffusion limitations of essential compounds through their external membrane caused by the presence of a hydrophilic barrier. Although this barrier is not totally impermeable, it hinders the transport of macromolecules and hydrophobic components [21].

In addition, the resistance in the Gram-negative bacteria may be related to the possible resistance genes on plasmids that may inactivate essential oil components with antimicrobial potential [22].

The inhibitory action of the Cade oil could be attributed to the occurrence of high proportions of monoterpenes and sesquiterpenes in the oil [23]. The essential oils containing terpenes are also reported to possess antimicrobial activity [24], which are consistent with our present study. This activity could, in part, be associated with their major constituents such as α - pinene, β -phellandrene, α -Terpinyl acetate and cedrol [25]. These components have been reported to display antimicrobial effects. In addition, the components in lower amount may also contribute to antimicrobial activity of the essential oils, involving probably some type of synergism with other active compounds [26]. Essential oils of many *Juniperus* species were known to exhibit antimicrobial activity against several microorganisms.

Ennajar et al [19] found in their study that the essential oils of leaves and berries of *Juniperus phoenicea* showed reasonable *in vitro* antimicrobial activity against all the tested microorganisms including Gram-positive

bacteria (*Bacillus subtilis* ATCC 6633, *Staphylococcus aureus* CIP7625, *Listeria monocytogenes* Scott A 724) and Gram-negative bacteria (*Pseudomonas aeruginosa* CIPA22, *Escherichia coli* ATCC10536, *Klebsiella pneumoniae* CIP8291), yeast (*Saccharomyces cerevisiae* ATCC 4226 A), and fungi (*Mucor ramamnianus* ATCC 9314, *Aspergillus westerdijkiae*). The leaves essential oil has an antimicrobial activity greater than that of berries (except *M. ramamnianus*) that may be due to the wealth of leaves essential oil by oxygenated compounds that are totally absent in the berries essential oil. In addition, the amount of sesquiterpenes in the leaves essential oil was higher than in berries essential oil.

The *Juniperus excelsa* essential oil showed a strong antimicrobial activity against the anaerobic bacterium *Clostridium perfringens*, while exhibiting moderate activity against *Staphylococcus aureus*, *Staphylococcus pyogenes*, and *Candida albicans* [27].

Ehsani et al [28] identified the chemical composition of the essential oils of *J. excelsa* and *J. horizontalis* leaves and fruits and evaluated their antibacterial activity against thirteen bacterial species (*Bacillus anthracis*, *Bacillus cereus*, *Bacillus subtilis*, *S. aureus*, *Staphylococcus epidermidis*, *Citrobacter freundii*, *Escherichia coli*, *Listeria monocytogenes*, *Pseudomonas aeruginosa*, *Klebsiella pneumoniae*, *Serratia marcescens*, *Enterobacter aerogenes*, and *Shigella dysenteriae*). The result of this study indicated that Juniper essential oils showed more antibacterial activities against Gram-positive as compared to Gram-negative bacteria species. The antibacterial activity of essential oils may be related to presence of α -pinene, limonene, and sabinene which are known to have antibacterial properties.

Stassi et al [29] have tested the antimicrobial activity of essential oils of 4 *Juniperus* species (*Juniperus drupacea* Labill. ; *Juniperus oxycedrus* L. subsp. *macrocarpa* (Sm.) Ball; *Juniperus oxycedrus* L. subsp. *oxycedrus*; *Juniperus phoenicea* L. ; Cupressaceae;) against five Gram-positive bacteria (*Bacillus cereus* ATCC:11778, *Bacillus subtilis* ATCC: 6633, *Micrococcus luteus* ATCC: 9341, *Staphylococcus aureus* ATCC: 6538 *Staphylococcus epidermidis* ATCC: 12228) and two Gram-negative bacteria (*Escherichia coli* ATCC: 10536, *Pseudomonas aeruginosa* ATCC: 9027). They approved that essential oils of the berries generally appear more active than essential oils of the leaves. Essential oils of the berries inhibit the growth of *E. coli*, *P. aeruginosa*, and *S. aureus*, while essential oils of the leaves do not.

In a study done by Sela et al [30] the chemical composition and antimicrobial activity of essential oil isolated from berries from 2 different samples of *Juniperus oxycedrus* L. (Cupressaceae), growing wild in Republic of Macedonia was investigated. The major components of the essential oil were α -pinene (22.54- 27.12%), myrcene (11.26- 15.13%) and limonene (2.78-18.06%). In this study the antimicrobial screening of the *J. oxycedrus* essential oils was evaluated against 16 bacterial isolates of Gram positive and Gram negative bacteria and one strain of *Candida albicans*. The most sensitive bacteria was *Haemophilus influenzae* (MIC = 125 ml/ml). The essential oils showed moderate antimicrobial activity against *Streptococcus pneumoniae*, *Staphylococcus aureus*, *Streptococcus agalactiae*, *Streptococcus pyogenes*, *Corynebacterium* spp., *Escherichia coli* and *Campylobacter jejuni* (MIC > 500 ml/ml) and no activity against *Candida albicans*, *Staphylococcus epidermidis*, *Acinetobacter* spp., *Salmonella enteritidis*, *Shigella flexneri*, *Klebsiella pneumoniae*, *Pseudomonas aeruginosa*, *Enterococcus* and *Proteus mirabilis*.

Medini et al [15] studied the chemical composition and the antibacterial activity of the essential oils of two Tunisian subspecies of *Juniperus oxycedrus* leaves (*Juniperus oxycedrus* ssp. *Oxycedrus* and *Juniperus oxycedrus* ssp. *Macrocarpa*) against the following bacterial strains: *Salmonella typhimurium*, *Salmonella enteritidis*, *Staphylococcus aureus* and *Escherichia coli*. The result of this study revealed that α -pinene, sylvestrene, p-cymene, and 13-epi-manoyl oxide were the principal components of the essential oils. The study of the antibacterial activity showed that *Escherichia coli* was found to be extremely resistant (zone diameter 0 mm) to all the tested oils, while *Staphylococcus aureus* was the most sensitive strain (zone diameter 13.5 mm and MIC ranged from 600 to 650 μ g/mL).

In Egyptian study done by El-Sawi et al [31] they found that essential oils of Leaves and Berries of *Juniperus Phoenicea* showed major activity against most of the tested strains including gram positive bacteria like *Enterobacter cloacae* and *Staphylococcus aureus*, and gram negative bacteria like *Escherichia coli*, *Salmonella*, *Pseudomonas syringae* etc. Both oils showed very high cytotoxic activities against all tested cell line.

In study done by Moein et al [32] the essential oil of leaves of *Juniperus excelsa* was analyzed by gas chromatography/mass spectrometry (GC/MS) and studied for antimicrobial and antioxidant activities. The results indicated α -pinene (67.71%) as the major compound and α -cedral (11.5%), δ^3 -carene (5.19%) and limonene (4.41%) in moderate amounts. The Antimicrobial tests showed that all the Gram positive bacteria (*Staphylococcus aureus* PTCC 1112, *Staphylococcus epidermidis* PTCC 1114, *Bacillus subtilis* PTCC 1023, *Enterococcus faecalis* ATCC 8043), and Gram negative bacteria (*Escherichia coli* PTCC 1338, *Shigella sonnei* PTCC 1235, *Proteus vulgaris* PTCC 1312, *Pseudomonas aeruginosa* PTCC 1047, *Salmonella typhi* PTCC1609), yeasts (*Candida albicans* ATCC 14053, *Candida kefyr* ATCC 3826) and fungi (*Aspergillus niger* PLM 1140,

Aspergillus fumigatus PLM 712) were susceptible to essential oil. The oil showed radical scavenging and antioxidant effects.

In a study done by Karaman et al [4] Aqueous and methanol extracts of the leaves of *Juniperus oxycedrus* were investigated for their *in vitro* antimicrobial properties. The results showed that the methanol extract has inhibition effect on the growth of 11 of 23 yeast (*C. albicans*) isolates and 57 of 178 strains in 24 bacterial species which were *Acinetobacter calcoaceticus*, *Bacillus amyloliquefaciens*, *Bacillus atrophaeus*, *Bacillus cereus*, *Bacillus circulans*, *Bacillus lentimorbus*, *Bacillus licheniformis*, *Bacillus macerans*, *Bacillus megaterium*, *Bacillus pumilus*, *Bacillus sphaericus*, *Bacillus substilis*, *Brevundimonas diminuta*, *Brucella abortus*, *Enterobacter agglomerans*, *Enterobacter pyrinus*, *Escherichia coli*, *Micrococcus luteus*, *Pseudomonas aeruginosa*, *Pseudomonas putida*, *Pseudomonassyringae*, *Staphylococcus aureus*, *Staphylococcus epidermidis*, and *Xanthomonas campestris*.

A study done by Amri et al [33] they found that the essential oil isolated from the leaves of *Juniperus oxycedrus* has a significantly antifungal activity and inhibited the growth of nine plant pathogenic fungi *F. equisiti*, *F. culmorum*, *F. oxysporum*, *F. solani*, *F. verticillioides*, *F. nygamai*, *Botrytis cinerea*, *Microdochium nivale var nivale*, *Alternaria sp*. This property is attributed to its presence of chemical constituents tested by GC-MS and its 42 compounds that represent 96.73% of total oil, α -pinene (39.63%), manoyl oxide (12.34), Z-caryophyllene (4.1%) and extensively high amounts of monoterpenes hydrocarbons and sesquiterpenes. The existence of these strong properties makes the oil prove best in its antifungal activities. With its antifungal effects, Cade oil fights against the growth of fungus and checks various fungal infections like ringworm, athlete's foot, dandruff etc.

Clark et al [34] explained that methanol extracts from *Juniperus virginiana* heartwood and needles exhibited antifungal and antibacterial activity.

Ates et al [35] reported that methanol extract from *juniperus foetidissima* sapdwood and heartwood has antifungal activity against *Pleurotus ostreatus*.

Bachir Raho et al [36] found in their sturdy that *Juniperus oxycedrus* essential oil was active against *Staphylococcus aureus*, *Streptococcus sp*, *Bacillus sp*, *Escherichia coli*, *Pseudomonas aeruginosa*, *Klebsiella pneumonia* and *Candida albicans*.

B. Results of the antioxidant activity

The antioxidant activity of the essential oils is another biological property of great interest because there is a strong need for effective antioxidants from natural sources as alternatives to synthetic food additives in order to prevent deterioration of foods, drugs and cosmetics. Moreover, essential oils being also able of scavenging free radicals may play an important role in some diseases prevention such as brain dysfunction, cancer, heart disease and immune system decline. Increasing evidence has suggested that these diseases may result from cellular damage caused by free radicals [37]. The result of the antioxidant activity of the Cade oil evaluated by the DPPH test is showed in Table 2.

TABLE 2: Result of Free radical scavenging activity (DPPH test)

| Substance | Cade oil | Ascorbic acid | Gallic Acid |
|---------------------------|------------------|------------------|-------------------|
| CI50 ($\mu\text{g/ml}$) | 0.06 \pm 0.003 | 7,24 \pm 0,209 | 04,26 \pm 0,185 |

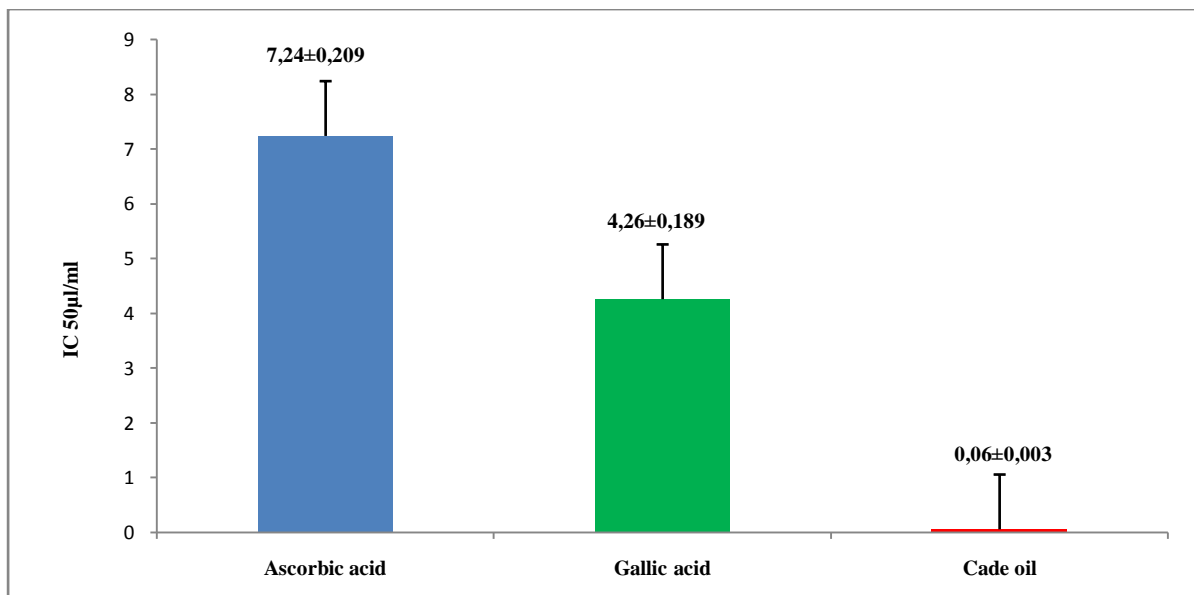


Fig 1. Free radical-scavenging capacities of Cade oil, Ascorbic acid and Gallic acid measured in DPPH assay

The results of DPPH test showed that Cade oil has a strong antioxidant activity with IC₅₀ values of 0.063 ± 0.0035 µl / ml. This result is higher than the standards antioxidant, ascorbic acid, and Gallic acid, which exhibit IC₅₀ of the order of 7.24 ± 0.209 µg / ml and 04.26 ± 0.185 µg / ml respectively.

The results of the reducing power of the Cade oil, Gallic acid and ascorbic acid expressed by EC₅₀ values are shown in Table 3.

TABLE 3: Result of FRAP essay of the Cade essential oil:

| Substance | Cade oil | Ascorbic acid | Gallic Acid |
|--------------|-------------|---------------|---------------|
| CE50 (µg/ml) | 0.15 ± 0.02 | 50 ± 0.065 | 24,72 ± 0.025 |

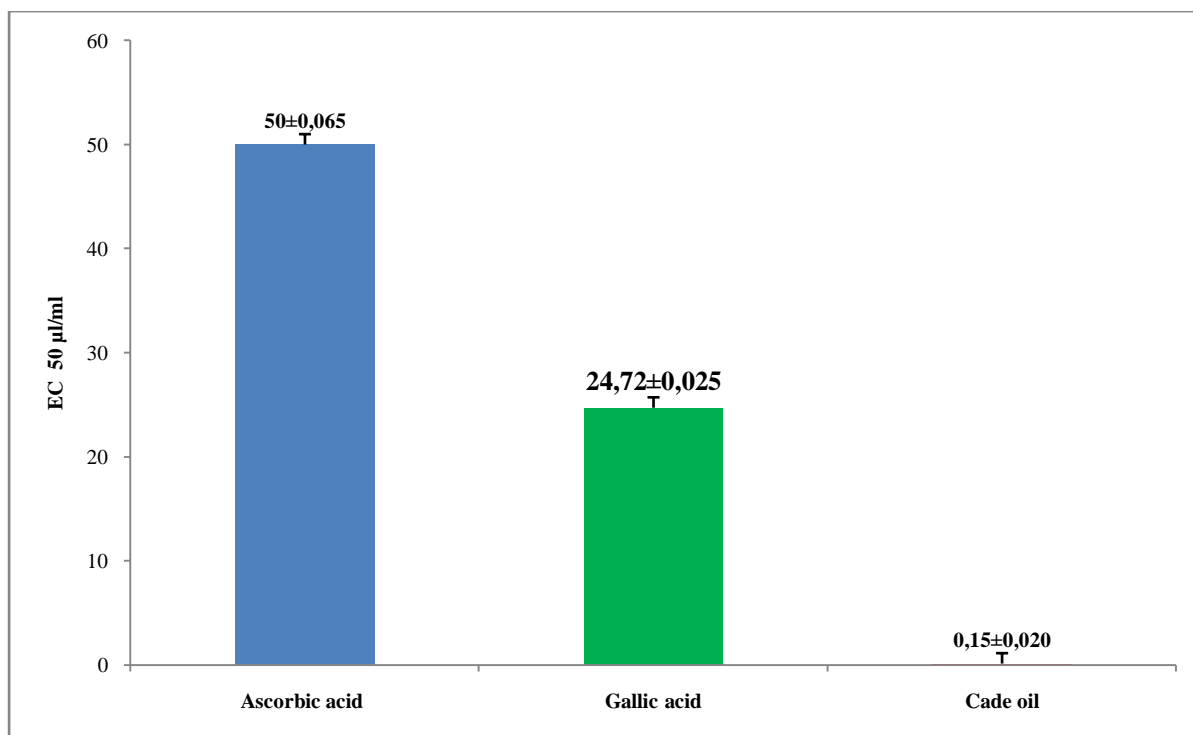


Fig 2. Reductive potential of Cade oil, Ascorbic acid and Gallic acid

The antioxidant activity of Cade oil evaluated by reducing potential test revealed that this oil has an important antioxidant activity with EC₅₀ values of $0.15 \pm 0.020 \mu\text{l} / \text{ml}$. The reducing power of the Cade oil is much higher than that of Gallic acid (EC₅₀ = $24.72 \pm 0.025 \mu\text{g} / \text{ml}$) and of ascorbic acid (CE₅₀ = $50 \pm 0.065 \mu\text{g} / \text{ml}$). The antioxidant measurement by DPPH and FRAP methods showed that Cade essential oil exhibited an important antioxidant activity higher than that of ascorbic acid and gallic acid. The Antioxidant activities of essential oils from aromatic plants are mainly attributed to the active compounds present in them. This can be due to the high percentage of main constituents, but also to the presence of other constituents in small quantities or to synergy among them [38]. Anti-radical activity depends on the oil components, *i.e.*, their chemical nature and concentration. Regardless of the differences in the composition of juniper essential oils, they are dominated by terpene hydrocarbons. A number of studies have shown that the monoterpene components also contained in juniper essential oil enhance, through their antioxidant activity, the oxidative stress resistance of living organisms [39]. There have been diverse reports on antioxidant activity of a number of *Juniperus* species.

Lim et al [40] reported that the methanol extracts of heartwood of *J. chinensis* showed strong antioxidant activity, determined by measuring the radical scavenging effect on DPPH.

In a study on antioxidant activity of the Iranian conifers done by Emami et al [41] the methanol extracts of the fruits and leaves from *J. communis* ssp. *hemisphaerica*, *J. excelsa* ssp. *exselca*, *J. excelsa* ssp. *polycarpus*, *Juniperus oblonga*, *J. foetidissima*, and *J. sabina* were examined using two different tests of the ferric thiocyanate method and thiobarbituric acid and most of them showed a potent antioxidant effect in these tests, which is in accordance with our data high DPPH scavenging. Different extracts of leaves, ripe fruits, and unripe fruits of *Juniperus* species, including *J. oxycedrus*, were studied for the anticholinesterase and antioxidant activity. They all showed good antioxidant activity, but the leaf extracts usually had higher antioxidant activity [42].

In study done by Loizzo et al [43] *J. oxycedrus* ssp. *oxycedrus* berry and wood essential oils were tentatively identified by GC and GC/MS. Fifty compounds were identified in the berry oil and 23 compounds were identified in the wood oil. The *J. oxycedrus* ssp. *oxycedrus* berry oil was characterized by high contents of α -pinene (27.4%) and β -myrcene (18.9%). Other important compounds were α -phellandrene (7.1%), limonene (6.7%), epibicyclo sesquiphellandrene (2.3%) and δ -cadinene (2.2%) while, in the wood oil, δ -cadinene (14.5%) is a major main component, together with *cis* thujopsene (9.2%) and amurolene (4.9%). *In vitro* evaluation of antioxidant activity by the DPPH method showed a significant activity for both oils with IC₅₀ values of $1.45 \mu\text{l}/\text{ml}$ for wood and $7.42 \mu\text{l}/\text{ml}$ for berries.

In a study done by Saab et al [44] the chemical composition and antiproliferative activity of wood and seeds essential oils of *J. oxycedrus*, grown wild in Lebanon, were evaluated in order to investigate whether these products could be used as sources of functional compounds. The result of this study showed that the most

abundant components of the seeds essential oils were α -pinene, β -myrcene, limonene and δ -cadinene, while wood oil components included δ -cadinene, *cis*-thujopsene, τ -muurolol, widdrol, *epi*-cubenol, β -caryophyllene and α -calacorene. Both wood and seeds essential oils inhibited the proliferation of K562 cell line with IC₅₀ values of 39.8±2.7 and 147.7±3.6 μ g/mL, respectively. The *J. oxycedrus* wood oil showed erythroid differentiation of 16.0±2.0% at a concentration of 5 μ g/mL, while the seeds essential oil showed erythroid differentiation of 25.0 ± 2.8% at a concentration of 50 μ g/mL.

Previous work has attributed antioxidant activity and acetylcholinesterase inhibitory activity to extracts of some *Juniperus* sp. These properties along with their multiple aforementioned bioactivities make *Juniperus* sp. interesting plants in the search for new natural products to treat neurodegenerative diseases.

Tavares et al [45] found in their study that phenolic-enriched fractions (PEFs) from four wild *Juniperus* sp. found in Portugal (*Juniperus navicularis*, *Juniperus oxycedrus badia*, *Juniperus phoenicea* and *Juniperus turbinata*) exhibited acetylcholinesterase (AChE) inhibitory activity and also displayed effective intracellular radical scavenging properties in neurons submitted to oxidative injury. These properties made them good candidates for testing in a neurodegeneration cell model. Pre-incubation with *J. oxycedrus badia* PEF for 24 h protected neurons from injury in the neurodegeneration cell model.

Topcu et al [46] showed that diterpenes and sesquiterpenes extracted from the berries of *J. excelsa* subsp. *excelsa* had cytotoxic activity against a panel of cell lines [human colon cancer cell line (LNCaP), KB-V (+VLB) and KB-V (- VLB)] and *Mycobacterium tuberculosis*.

Sadeghi-aliabadi et al [47] found that hydroalcoholic extracts of the terminal branchlets and berries of *J. excelsa* subsp. *Polycarpus* and *J. excelsa* subsp. *excelsa* showed an inhibitory effect against Hela cells and KB cells, the extracts were cytotoxic against this cell line.

IV. Conclusion

The results of our study may suggest that the Cade oil possess natural compounds with antimicrobial and antioxidant properties which can be used as antimicrobial agents in new drugs for therapy of infectious diseases. This oil may be used also as alternative to synthetic food additives in order to prevent deterioration of foods, drugs and cosmetics.

ACKNOWLEDGEMENTS

The authors acknowledge the funding of this study by Laboratory of Research on Local Animal Products at Ibn Khaldoun University, Algeria.

References

- [1] H. Mehrgana, F. Mojab, S. Pakdaman and M. Poursaeed, Antibacterial activity of *thymus pubescens* methanolic extract. Iran J Pharm Res, Vol.7, pp.291-295, May 2008.
- [2] A. Zeraib, M.Ramdani, L. Boudjedjou, P. Chalard, G. Figuredo, Chemical composition and antibacterial activity of *Juniperus thurifera* L. essential oils. J. BioSci. Biotech, Vol. 3, pp.147-154, June 2014.
- [3] J. Bellakhder, La Pharmacopée Marocaine traditionnelle. Paris: Ibis Press, 1997, p272.
- [4] I. Karaman, F. Sahin, M. Güllüce, HÖ gütcü, M. Sengül, A. Adıgüzel.. Antimicrobial activity of aqueous and methanol extracts of *Juniperus oxycedrus* L. J Ethnopharmacol, Vol. 85, pp.231–235, April 2003.
- [5] SP, Mun and L, prewitt, Antifungal activity of organic extract from *Juniperus virginiana* Heartwood against wood decay fungi. Forest prod j , Vol.61, pp.443-449, October 2011.
- [6] J.Karchesy.. The Literature of Juniper utilization for oils and specialty products: A report to the western juniper steering committee. Department of Forest Products Oregon State University Corvallis, Oregon 97331. 1998.
- [7] D. Lamnauer, A Guide to Medicinal Plants in North Africa; IUCN Centre for Mediterranean Cooperation Malaga, pp.157-158, 2005.
- [8] K. Bouhlal, JM. Meynadier, JL. Peyron, L. Peyron, JP Marion, G. Bonetti, J. Meynadier, Le cade en dermatology. Parfums, Cosmétiques et Aromes, Vol. 83, pp.73–82, 1988.

- [9] A. Leung and S. Foster, Encyclopedia of Common Natural Ingredients. Wiley, New York, p. 109, 1996.
- [10] D. Stanisavljević, S. Đorđević, M. Milenković, M. Lazić, D. Veličković, N. Randelović and B. Zlatković, Antimicrobial and Antioxidant Activity of the Essential Oils Obtained from *Mentha longifolia* L. Hudson, Dried by Three Different Techniques. Rec. Nat. Prod, Vol.8, pp. 61-65, September 2014.
- [11] MS. Blois, Antioxidant determinations by the use of a stable free radical. *Nature*. Vol.181, pp.1199–1200, 1958.
- [12] GC. Yen and PD. Duh, Antioxidative properties of methanolic extracts from peanut hulls. J Am Oil Chem Soc.Vol. 70, pp. 383–386, April 1993.
- [13] KG. Kiran, RD. Sri Rami, SNT. Yagnika and SJ. Annie, Exploitation of Aqueous Plant Extracts for Reduction of Fungal Growth and Detoxification of Aflatoxins. *KMITL Science and Tech J*, Vol.10, pp.52-62, 2010.
- [14] A. Angioni, M. Barra, T. Russo, V. Coroneo, S. Dessí. and Cabras .P, Chemical composition of the essential oils of *Juniperus* from ripe and unripe berries and leaves and their antimicrobial activity. J Agric Food Chem, Vol.51, pp.373–374, 2003.
- [15] H.Medini, B. Manongiu, A. Neffati, L. Chekir-Ghedira, F. Harzalla-Skhiri, and ML Khouja,. Chemical and Antibacterial Polymorphism of *Juniperus oxycedrus* ssp. *oxycedrus* and *Juniperus oxycedrus* ssp. *macrocarpa* (Cupressaceae) Leaf Essential Oils from Tunisia. J Agric Sci .Vol.1, pp.166-173,September 2013.
- [16] N. Bouzouita, F. Kachouri, M. Ben Halima, MM. Chaabouni, Composition chimique et activité antioxydante, antimicrobienne et insecticide de l'huile essentielle de *Juniperus phoenicea*. Société Chimique de Tunisie.Vol.10, pp. 119–125, 2008.
- [17] A. Ait Ouazzou, S. Loran, A. Arakrak, A. Laglaoui, C. Rota, A. Herrera, R. Pagan, P. Conchello, Evaluation of the chemical composition and antimicrobial activity of *Mentha pulegium*, *Juniperus phoenicea*, and *Cyperus longus* essential oils from Morocco, food res int vol. 45, pp. 313–319, 2012.
- [18] Ramdani M, Lograda T, Silini H, Zeraib A, Chalard P, Figueredo G, Bouchaala M and Zerrar S. Antibacterial Activity of Essential oils of *Juniperus phoenicea* from Eastern Algeria. Food Res Int, Vol. 3, pp. 022-028, November 2013.
- [19] M. Ennajar, J. Bouajila, A. Lebrihi, F. Mathieu, M. Abderraba, A. Raies, M. Romdhane, Chemical Composition and Antimicrobial and Antioxidant Activities of Essential Oils and Various Extracts of *Juniperus phoenicea* L.(Cupressacees). J Food Sci, Vol. 74 pp, 364-371. September 2009.
- [20] PJ. Delaquis, K. Stanich, B. Girard, and G. Mazza, Antimicrobial activity of individual and mixed fractions of dill, cilantro, coriander and eucalyptus essential oils. Int J Food Microbiol. Vol. 74,pp. 101-109. Mars 2002.
- [21] M K. Pierozan, GF. Pauletti, L.Rota, ACAd Santos, A. Lerin, M. Di luccio, A J. Mossi, L. Atti-serafini, RL. Cansian, J. Vladimiroliveira,Chemical characterization and antimicrobial activity of essential oils of *salvia* L. species. Ciênc. Tecnol. Aliment, Vol.29, pp. 764-770. 2009.
- [22] LA. Shelef, OA. Naglik, DW. Bogen, Sensitivity of some common food-borne bacteria to the spices sage, rosemary and all spice. J. Food Sci, Vol.45, pp.1042-1044, July 1980.
- [23] A. Cakir, Kordali .S, H. Zengin, S. Izumi, Hirata.T, Composition and antifungal activity of essential oils isolated from *Hypericum hyssopifolium* and *Hypericum heterophyllum*. Flavour Frag. J, Vol.19, pp.62–68, February 2004.

- [24] HJD. Dorman and SG. Deans . Antimicrobial agents from plants: Antibacterial activity of plant volatile oils. J Appl Microbiol, Vol.88, pp. 308-316, February 2000.
- [25] K. Mazari, N. Bendimerad, C. Bekhechi and X.Fernandez, Chemical composition and antimicrobial activity of essential oils isolated from Algerian *Juniperus phoenicea* L. and *Cupressus sempervirens* L. J Med Plant Res, Vol.4, pp. 959-964, May 2010.
- [26] M. Marino, C. Bersani, G. Comi, Impedance measurements to study the antimicrobial activity of essential oils from Lamiaceae and Compositae. Int J Food Microbiol, Vol.67, pp. 187-195, August 2001.
- [27] M. Unlu, G. Varder-Unlu, N. Vural, E. Donmez, O. Cakmak, Composition and antimicrobial activity of *Juniperus excelsa* essential oil. Chem of Natural Compounds. Vol.44, pp. 129-131, 2008.
- [28] E. Ehsani, K. Akbari, M. Teimouri and A. Khadem.. Chemical composition and antibacterial activity of two *Juniperus* species essential oils. Afr. J. Microbiol. Res, Vol. 6, pp.6704-6710, 2012.
- [29] V. Stassi, E. Verykokidou, A. Loukis, C. Harvala, S. Philianos, The antimicrobial activity of the essential oils of four *Juniperus* species growing wild in Greece. Flavour Frag. J Vol.11, pp.71- 4, 1996.
- [30] F. Sela, M. Karapandzova, G. Stefkov, I. Cvetkovikj, E.Trajkovska-Dokikj, A. Kaftan dzieva, S..Kulevanova Chemical composition and antimicrobial activity of berry essential oil of *Juniperus oxycedrus* L. (Cupressaceae) grown wild in Republic of Macedonia. *Macedonian*, Chem. Pharm. Bull, Vol.59, pp. 41 – 48. June 2013.
- [31] S A. El-Sawi , H M. Motawae , AM. Ali, Chemical Composition, Cytotoxic Activity and Antimicrobial Activity of Essential Oils of Leaves and Berries of *Juniperus Phoenicea* L. Grown in Egypt. Afr J Tradit Complement Altern Med ,Vol.4,pp.417–426, June 2007.
- [32] MR. Moein, Y. Ghasemi, S. Moein, M, Nejati, Analysis of antimicrobial, antifungal and antioxidant activities of *Juniperus excelsa* M. B subsp. *Polycarpus* (K. Koch) Takhtajan essential oil. Pharmacognosy Res, Vol. 2, pp.128–131, May-June 2010.
- [33] I. Amri, L. Hamrouni, M. Gargouri, M. Hanana, B.Jamoussi, Chemical composition and antifungal activity of essential oils isolated from *juniperus oxycedrus*. Int J Appl Biol Pharm, Vol. 4, pp. 227-233, February 2013.
- [34] AM.Clark, JD.Mcchensey, RP. Adam, Antimicrobial properties of heartwood, bark/sapwood and leaves of juniperus specie. Phytother Res, Vol.4, pp.15-19. February 1990.
- [35] S. Ates, M. Gür, OE. özkan, M. AkÇa, Ç. Olgan, A. Guder, Chemical contents and antifungal activity of some durable wood extractives Vs *Pleurotus ostreatus*. Bioresource Vol.10, pp. 2433-2443, 2015.
- [36] G. Bachir Raho, M. Otsmane, F. Sebaa, Inhibitory effects of *Juniperus oxycedrus* essential oils against some pathogens, Int J Microbiol Biotechnol, Vol.2, pp. 29-33, February 2017.
- [37] MG. Miguel, Antioxidant and Anti-Inflammatory Activities of Essential Oils: A Short Review. Molecules. Vol. 15, pp.9252-9287, December 2010.
- [38] Politeo O, Juki M, and Milo M, Chemical Composition and Antioxidant Activity of Essential Oils of Twelve Spice Plants. Croat. Chem. Acta. Vol.79, pp. 545-552, March 2006.
- [39] M. Höferl , I. Stoilova , E. Schmidt , J. Wanner, L. Jirovetz , D. Trifonova, L. Krastev , A. Krastanov, Chemical Composition and Antioxidant Properties of Juniper Berry (*Juniperus communis* L.) Essential Oil. Action of the Essential Oil on the Antioxidant Protection of *Saccharomyces cerevisiae* Model Organism. Antioxidants , Vol.3, pp. 81-98, February 2014.
- [40] JP. Lim, YC. Song, JW. Kim, CH. Ku, JS. Eun, KH, Leem, DK. Kim,. Freeradical scavengers from the heartwood of *Juniperus chinensis*. Arch pharm res, Vol.25, pp.449–452, 2002.

- [41] SA. Emami, J. Asili, Z. Mohagheghi, MK. Hassanzadeh, Antioxidant activity of leaves and fruits of Iranian conifers. *Evid Based Complementary Altern Med*, Vol.4, pp.313–319. Mars 2007.
- [42] N. Orhan, IE. Orhan, F. Ergun, Insights into cholinesterase inhibitory and antioxidant activities of five *Juniperus* species, *Food Chem Toxicol*, Vol.49, pp. 2305–2312, September 2011.
- [43] M R. Loizzo, R. Tundis, F. Conforti, A M. Saab, G A. Statti, F. Menichini, Comparative chemical composition, antioxidant and hypoglycaemic activities of *Juniperus oxycedrus* ssp. *oxycedrus* L. berry and wood oils from Lebanon. *Food Chem*, Vol.105, pp. 572–578, April 2007.
- [44] AM. Saab, H. Gali-Muhtasib, S. Maietti, A. Grandini, D. Rossi, I. Lampronti, E. Gallerani, E. Fabbri, R. Gambari, Comparative Antiproliferative activities of wood and seeds essential oils of *Juniperus Oxycedrus* L. against K562 human chronic myelogenous leukemia cells. *J essent oil res*, Vol. 26, pp.301-307, December 2014.
- [45] L. Tavares, G J. McDougall, S. Fortalezas, D. Stewart, R B. Ferreira, CN. Santos, The neuroprotective potential of phenolic-enriched fractions from four *Juniperus* species found in Portugal. *Food Chem*, Vol.135, pp. 562–570, November 2012.
- [46] Topcu G, Erenler R, Cakmak O, Johansson CB, Celik C, Chai HB, pezzuto JM, Diterpenes from the berries of *Juniperus excelsa*. *Phytochemistry*. Vol.50, pp.1195-1199, April 1999.
- [47] H. Sadeghi-aliabadi, A. Emami, B. Sadeghi, A. Jafarian, *In Vitro* Cytotoxicity of Two Subspecies of *Juniperus excelsa* on Cancer Cells. *Iran J Basic Med Sci*, Vol.11 pp. 250-253, October 2009.

Combining of Cryptography and Steganography for Improving of Security

Muharrem Tuncay Gençoğlu

Department of Computer Technology, Firat University
Elazig, TURKEY

Sarhad Baez Hasan

Department of Software Engineering, Firat University
Elazig, TURKEY

ABSTRACT

To hide hidden data in digital images, a variety of techniques are available, some of which are more complex than others. Public key cryptography is very useful for applications, and the technique used depends on the requirements for encryption and encryption data. Hiding is a kind of hiding method in which the host image is exactly retrievable. Presence lossless makes this technique suitable for medical and military applications. The image pixels are replaced with additional data into new values to embed several data pixels by S-block at multiple layers. From the original image, the embedded data can be extracted and the original image can be recovered from the decrypted image directly. Embedded data can be extracted directly from the encrypted domain. The decryption of the original plaintext image doesn't affect the data embedding operation. With the combined technique, before decryption, a receiver may extract a part of embedded data, and recover the original plaintext image after decryption. A slight distortion is introduced due to the compatibility between the lossless and reversible schemes. The data embedding operations can be performed in the two manners simultaneously performed in an encrypted image and decrypted image. In this thesis, the design of Caesar cipher and Vigenere cipher is presented. Block 4 provides good encryption properties and software productivity. The proposed technique for the design of the S-box chain chaos provides a very secure level. The result of the implementation shows that the proposed method is suitable for lightweight cryptography due to the use of low resources using the C # .Net implementation tool.

Keywords—Image encryption, Lossless data hiding, data hiding, Public key encryption, Caesar cipher etc.

I. INTRODUCTION

These days security is the most basic factor in any correspondence framework. Issues in such security frameworks are trustworthy in protection's verification and non-disavowal; such issues should be dealt with deliberately. The security objectives are specific: classification of the accessibility and honesty that can be debilitated by security assaults. Hence, to ensure the first data from such assaults the information concealing procedures are actualized. Reversible Data Hiding (RDH) systems are connected to steganography and cryptography capacities for the purpose of looking after security and verification [3]. Encryption and information covering up are two methods of information security. Concealing procedures insert unique information which we wouldn't prefer to reveal into cover media by presenting satisfactory slight adjustments while encryption strategies convert plaintext information into mixed up frame i.e. ciphertext. It is valuable to insert the information into an advanced media to convey the mystery messages. The proprietor can alter the first content of the utilizing media pictures, so that the implanted information is hidden. [1] Encryption gives classification for pictures and videos; it is also a successful system which changes over the first and mystery information to an immense one.

II. GENERAL REVIEW OF CRYPTOGRAPHY AND STEGANOGRAPHY

Many researchers believe that security is considered as the most critical factor in any communication systems. Issues in such security systems are integrity, privacy, authentication and non-repudiation; it should be handled carefully. Here the security goals are namely: confidentiality, availability and integrity that can be threatened by security attacks. Thus, to protect the original information from such attacks the data hiding techniques are implemented. Boghdad et al [1] believed that the information on the images has brought a lot of enthusiasm with the use of systems of impotence or immobilization. Despite the fact that miserable systems can create widespread concealment, a high-resolution image cannot be recovered. The number of applications needs to restore the correct image of the host; for example, medications can be installed quietly without knowing the medication picture. Using the hidden methods of unparalleled information, the restriction is limited because the host image should be preserved. In this paper, a pressure-free installation system is proposed. In this way, image histograms detect that they detect the limitations of installing different photos. The Maxima and Minima histograms are used in placing limited estimates. The proposed system provides a hidden border that can match up to half the size of the host image for wide-area images (similarly).

Tian [2] investigated on a case study to enter the layout installation methods in a distinctive image. They have not come up with a separate image for another image that has been placed on another layer unless the current image has any contrast enhancements. The burden of these procedures is that the image quality may be very corrupt, even before it installs the next layer, considering the fact that placing the last layer uses any expandable contrast, including ones they are very intense. Based on the total number of Haar waveforms, we propose that we install another DE calculation, which uses the flat as the vertical contrast images to cover the information. We present a tracking and dynamic distinction section now. The system even shoots low-contrast photos in two different images and dramatically avoids the situation, with the largest contrast in the primary contrast image being used, while there's almost no option for low contrast adjustment. There is no second image.

GENÇOĞLU (2017) [31] shows the linking cryptography with steganography, a diverse cryptographic way is introduced by using power sequence convert, codes of ASCII and science of steganography. In this perspective, he created a new algorithm for cryptology, he adapted extended Laplace alert of the exponential duty for encrypting the basic text and he used codes of ASCII for sustaining the privacy of the hypertext Alert. Chipertext has fixed by steganography technique in another main text to cover the being of chipertext. For encryption, he displayed the equivalent converse of power sequence alert.

For the purpose of maintaining the security and authentication, Reversible Data Hiding (RDH) techniques are related to steganography and cryptography function. Encryption and data hiding are two techniques of data protection. Data hiding techniques embed original data which we don't want to disclose into cover media by introducing slight acceptable modifications; while encryption techniques convert plaintext data into unreadable form i.e. ciphertext. It is beneficial to embed the data into digital media to communicate the secret messages. The owner can modify the original content of the media using images so that the embedded data is hidden. Encryption provides confidentiality for images and video as well as it is an effective technique which converts the original and secret data to incomprehensible one.

III. TAXONOMY & ARCHITECTURE

A. Reversible Data Hiding

Reversible or lossless information concealing systems shroud information in a host motion (for instance, a picture) and permit extraction of the first host flag and furthermore the installed message. There are two imperative necessities for reversible information concealing systems: the inserting limit ought to be substantial, and bending ought to be low. These two necessities are fighting each other.

When all is said to be doing your work, a higher level of implanting will cause a high level of twisting. An enhanced strategy inserts a similar limit with bring down twisting or the other way around.

Tian's distinction extension system already had the most elevated installing limit and the least contortion in picture quality. His strategy separates the picture into sets of pixels and uses each genuine match for concealing one piece of data. Along these lines, his implanting limit is best case scenario 0.5 b/pixel. The joined utilization of the rhombus expectation conspires, arranging, histogram move technique, and, subsequently, little size of area delineate generally better outcomes looked at than existing plans.

Information covering up, frequently alluded to as computerized watermarking, has as of late been proposed as a promising strategy for data affirmation. Inferable from information stowing away, notwithstanding, some perpetual twisting may happen and subsequently the first cover medium will be unable to be turned around precisely even after the concealed information have been separated out. Following the arrangement of information pressure calculations, this kind of information concealing calculations can be alluded to as lossy information covering up. It very well may be demonstrated that the greater part of the information concealing calculations announced in the writing are lossy. Here, let us inspect three noteworthy classes of information concealing calculation. With the most prevalently used spread-range watermarking systems, either in DCT space or square 8x8 DCT areas, round off blunder as well as truncation mistake may occur amid information implanting. Therefore, there is no real way to invert the stego media back to the first without mutilation. For the slightest noteworthy piece plane (LSB) inserting techniques, the bits in the LSB are substituted by the information to be implanted and the bit-substitution isn't retained. Thus, the LSB strategy isn't reversible. With the third gathering of much of the time utilized watermarking procedures, called quantization file tweak (QIM), quantization blunder renders lossy information covering up.

In applications, for example, in law implementation, medicinal picture frameworks, it is wanted to have the capacity to turn around the stego-media back to the first cover media for legitimate thought. In remote detecting and military imaging, high precision is required. In some logical research, test information is costly to accomplish. Under these conditions, the reversibility of the first media is wanted. The information concealing plans fulfilling this prerequisite can be alluded to as lossless. The terms of reversible, or invertible are additionally utilized much of the time. These procedures, similar to their lossy partners, embed data bits by altering the host flag, along these lines prompting an inserting bending. All things considered, they likewise empower the evacuation of such twists and the correct lossless-reclamation of the first host motion after extraction of installed data.

One of the main elements of this algorithm is that it is based on a piecewise theory. In other words, in each region, the central vector orientation of the center is determined by all the pixels in that area. As a result, the algorithm is a certain amount of compression of the image. Another key element of this algorithm is that it uses the plugin modulo-256 to prevent overflow and the following flow, so it has reversibility. As a result, however, as mentioned, this algorithm suffers from salt and pepper noise. In the stoical medical image, the intense noise of salt and pepper is clear. PSNR The stego image is less than 10dB compared to the original image, while 476 bits of information are embedded in this 512x512 image. Not only for medical imaging, salt noise and pepper may also be intense for color images. We applied this algorithm to eight JPEG2000 color test images. There are four of eight pictures that suffer from intense salt and peppery noise, while four others experience less intense pepper noise. PSNR can be as low as less than 20 dB when there is intense noise when 1412 bits of information are embedded in a color image of 1536x1920x24. From the above, it can be concluded that all the hidden algorithms of reversible data are based on the incremental modulo-256 to prevent overflow and downstream flow, and cannot be applied to many real applications, and from this, it should be avoided.

B. Flexible data technique with room reservation before encryption

In the previous method, the data embedded can be available without any error after the decryption of the encoded data. But the cover that is the image which contains the data cannot be effectively rebuilt. That is the major drawback of the framework mentioned previously.

a. Generation of Encrypted Image

To create a coded image, the initial stage can be divided into three stages: image packaging, auto-reversal installation after photo encryption. To the beginning, the stage of the image step divides the first image into two parts An and B. At that moment, LSBs come from A inversely to B using Rambo justification calculations, with the goal that LSBs use A to retrieve messages.

b. Image Partition

The supervisor is here to save the room before encoding a standard RDH system, so the packaging goal is to create a normal B region in which the Rambo computing method can perform better. To do that, without loss of consensus, accept the first picture C is a dim scale picture with its size $M \times N$, it is isolated into two equivalent measured pictures. In this, the B part has the smoother region to apply the RDH procedure. The LSBs of the pixels of A where the information is stowing away is put away.

c. Self-Reversible Embedding

The objective of self-reversible inserting is to implant the LSB-planes of an into B by utilizing the basis rhombus calculation.

d. Image Encryption

In the wake of revamping self-inserted picture and saving rooms, the encryption is finished with the assistance of encryption key. It is an 8-bit key. In this, the encryption is finished by XORing the picture with the key. At last, we insert 10 bits data into LSBs of initial 10 pixels in encoded rendition of A to tell the information hider the number of lines and the number of bit-planes he can implant data into. After picture encryption, the information hider or an outsider can't get to the substance of unique picture without the encryption key, consequently, the security of the substance proprietor is ensured.

e. Data Hiding In Encrypted Image

Once the information hider secures the scrambled picture, he can implant a few information into it, despite the fact that he doesn't gain admittance to the first picture, The inserting procedure begins with finding pixels in which the information can implant in the scrambled adaptation of picture. Since the information hider has the areas where the information can be installed it is easy for the information hider to peruse bits data in LSBs of encoded pixels. Subsequent to knowing what number of bit-planes and lines of pixels he can alter, the information hider just receives LSB substitution to substitute the accessible piece planes with extra information. At long last, the information hider encodes as indicated by the information concealing key to defining scrambled pictures containing information.

f. Data Extraction and Image Recovery

Since information extraction is totally free from picture decoding, the request of them infers two diverse down to earth applications. To oversee and refresh individual data of pictures which are encoded for ensuring customers' security, a sub-par database supervisor may just gain admittance to the information concealing key and need to control information in the scrambled space. The request for information extraction before picture decoding ensures the practicality of our work for this situation. At the point when the database administrator gets the information concealing key, he can decode the LSB-planes of An and remove the extra information by straightforwardly perusing the unscrambled adaptation. While asking for refreshed data of scrambled pictures, the database administrator, at that point, refreshes data through LSB substitution and encodes refreshed data as indicated by the information concealing key once more. As the entire procedure is totally worked on the scrambled area, it maintains a strategic distance from the spillage of unique substance.

C. Data Hiding and Image Encryption

The procedure of information covering up and picture encryption in this technique is completed in four stages. Be that as it may, before the procedure starts, the sender's sign into the application utilizing a substantial client id and a secret phrase. This GUI is given to guarantee a higher level of security even before the genuine procedure starts. Therefore, with such high security there stays just a little line for an interloper to sniff into the exchange. The procedure of real information covering up and encoding the pictures alongside inserting them with information is as per the following. In the initial step, the picture chosen by the sender is partitioned into three shades. These shades are disintegrated so that we get decayed picture segments as Red, Green and Blue. These decayed pictures frame RGB plane for every one of the segments, in this manner bringing about the principal plane being the red plane, the second the green plane and the third the blue plane. So the determination is that a shading picture is shaped by stacking the three planes together, similar to a sandwich. The second step is saving room before encryption for the information. The principal stage can be isolated into two stages: the picture parceling and self-reversible implanting. At first, the picture parcel step isolates the blue plane of the first picture picked by the sender, into two sections say A and B; at that point, the LSBs of A are reversibly installed into B with a standard RDH calculation utilizing addition so LSBs of A can be utilized for obliging messages. Presently, the last stage is known as picture encryption. Here at this stage, we utilize Algorithm Encryption Standard (AES Algorithm) to encode the picture for secure exchange over the system. It encodes the first picture pixel esteems with encryption key esteem. We utilize an open key encryption technique to create the keys. The last stage is concealing the information in scrambled pictures. Subsequently in the wake of having what number of bit-planes and the lines of the pixels the information hider or sender can adjust, the information hider consequently basically utilizes a side-coordinate forecast technique or just a LSB substitution way to deal with swap the accessible piece planes with extra information that he expects to send safely without making it defenseless against dangers. In the side-coordinate forecast approach, the histogram is made by misusing the distinction in every one of the qualities among pixels and their prescient qualities. All prescient mistake esteems are changed into histograms to make higher pinnacle esteems. In the extraction and turning around the process, the side-coordinate forecast is connected to the stego-picture, and the made histogram is handled for extraction and switching. At long last, the information hider sets a name following 'n' to bring up the end position of the installing procedure and further encodes 'n' as per the information concealing key to figure the stamped scrambled picture.

D. Pre-Process for Complete Recovery

In the previously mentioned calculation, it is necessitated that all pixels checked in are inside. In the event that there is any bouncing pixel esteem (0 or 255), flood or sub-current will be caused by histogram moving. To maintain a strategic distance from it, the histogram should be pre-handled preceding the histogram adjustment activities. In particular, the pixel estimations of 0 and 255 are adjusted to 1 and 254, separately. Hence, no flood or undercurrent will be caused in light of the fact that the conceivable difference in every pixel esteem is to retain the pre-prepared pixels, an area outline indistinguishable size from the first picture is produced by allocating 1 to the area of an altered pixel, and 0 to that of an unaltered one (counting the 16 prohibited pixels).

E. Contrast Enhancement

Every one of the two tops in the histogram is part into two contiguous canisters with comparable or same statures in light of the fact that the quantities of 1s in the message bits are required to be relatively equivalent. To build the concealing rate, the most noteworthy two containers in the adjusted histogram are additionally been part by applying Eq. (1) to all pixels checked in the histogram. A similar procedure can be rehashed by part every one of the two crests into two contiguous canisters with comparable statures to accomplish the histogram evening out impact.

F. Data Hiding For JPEG Images

This paper proposes a lossless information concealing method for JPEG pictures in light of histogram sets. It inserts information into the JPEG quantised 8x8 square DCT coefficients and can accomplish great execution as far as PSNR versus payload through controlling histogram sets with ideal limit and ideal district of the JPEG DCT coefficients. It can acquire higher payload than the earlier expressions. What's more, the expansion of JPEG document measure after information inserting stays unnoticeable. These have been confirmed by our broad tests.

G. Digital Image Water Marking

Watermarking, which have a place with the data concealing field, has seen a considerable measure of research intrigue as of late. There is a great deal of work starting to be directed in various branches in this field. Steganography is utilized for mystery correspondence, though watermarking is utilized for content assurance, copyright administration, content verification and alter recognition. In this paper, we present a definite review of existing and recently proposed steganographic and watermarking procedures. We group the systems in light of various areas in which information is installed.

H. Digital Image Steganography

In basic terms, steganography can be characterized as the workmanship and study of undetectable correspondence. This is refined through concealing data in other data, subsequently concealing the presence of the imported data. In spite of the fact that the idea of steganography and cryptography are the same, steganography contrasts from cryptography. Cryptography centers around keeping the substance of a message mystery, steganography centers around keeping the presence of a message mystery. Steganography and cryptography are both approaches to shield data from undesirable gatherings however neither innovation alone is impeccable and can be endangered. Once the nearness of concealed data is uncovered or even suspected, the reason for steganography is halfway vanquished. The quality of steganography would thus be able to be intensified by joining it with cryptography.

IV. PKC (PUBLIC-KEY CRYPTOGRAPHY)

Whitfield Diffie, Martin Hellman and Ralph Merkle presented an altogether extraordinary kind of figure in 1976. In these cryptographic frameworks, encryption and decoding utilize two distinctive keys i.e. one is an open key, known to everybody and other is a private key which is just known to the beneficiary of the message. At the point when sender A needs to communicate something specific safely to beneficiary B, he utilizes the general population key of B to encode the message. Beneficiary B at that point utilizes her private key to unscramble the message. Uneven calculations are prevalent for traditional information encryption as well as for application, for example, computerized marks and key foundation.

A. Least Significant Bit Based Steganography

It is the most popularly and commonly used approach for data hiding scheme where data is hidden in the least important part of the image. It is the simplest steganographic method where secret information is hidden in a subset of the LSB plane of the image. This method is the easiest and simplest and yet very effective way of hiding information in an image. In this method, the LSB of each pixel value in the cover image is used to hide the MSB of another image. It is assumed that LSB of the image is the non-important value which does not impact the appearance of the image. There are various steganographic tools available like S-Tools 4, Steganos and StegoDos, which implement LSB replacement in the spatial domain. This approach works by substituting duplicate values of the image with secret information. The embedding process involves a cover image in which substitution is done to hide information. This method works with a grid of pixels (raster image) which are used without compression (*.gif, *.bmp). *.GIF, *.BMP are more preferred file formats as they involve lossless compression. Along with *.gif, *.bmp, other image formats are used as cover images. Lossless compression is used because it maximises the embedding capacity of the image. Using the least

significant bit technique to hide the data, both invisibility and reasonably high storage payload is achieved

B. Proposed Chaotic Image Encryption Algorithm

The calculation that can be utilized to create n-bit x nbit S-boxes essentially works by changing over the yields of disordered frameworks into whole numbers somewhere in the range of 0 and 2n. The calculation's task is given underneath: Algorithm

Step1: System directions are gotten by explaining the partial disorganized Lorenz framework with chose introductory conditions and confused parameter esteems utilizing.

Step2: Select four parameters, base-ten esteem meant by these digits is changed over into whole numbers somewhere in the range of 0 and 2n by taking the modulus of this number at mod (2n).

Step3: S-Box is produced utilizing the codes relating to yields with the code comparing to the littlest yield being the main cell of the S-Box.

Step4: The got number is added to the table on the off chance that it isn't now present; generally the procedure returns to Step 1 to produce another whole number esteem.

Step5: The procedure goes ahead until the point that all cell esteems are filled.

Step6: After the S-Box is produced; we have applied the relative change to every component of our riotous S-boxes components $xT = [x_0, x_1, x_2, \dots, x_7] T$, i.e.;

$$\begin{bmatrix} y_0 \\ y_1 \\ y_2 \\ y_3 \\ y_4 \\ y_5 \\ y_6 \\ y_7 \end{bmatrix} = \begin{bmatrix} 1 & 0 & 0 & 0 & 1 & 1 & 1 & 1 \\ 1 & 1 & 0 & 0 & 0 & 1 & 1 & 1 \\ 1 & 1 & 1 & 0 & 0 & 0 & 1 & 1 \\ 1 & 1 & 1 & 1 & 0 & 0 & 0 & 1 \\ 1 & 1 & 1 & 1 & 1 & 0 & 0 & 0 \\ 0 & 1 & 1 & 1 & 1 & 1 & 0 & 0 \\ 0 & 0 & 1 & 1 & 1 & 1 & 1 & 0 \\ 0 & 0 & 0 & 1 & 1 & 1 & 1 & 1 \end{bmatrix} \begin{bmatrix} x_0 \\ x_1 \\ x_2 \\ x_3 \\ x_4 \\ x_5 \\ x_6 \\ x_7 \end{bmatrix} \oplus \begin{bmatrix} 1 \\ 1 \\ 0 \\ 0 \\ 0 \\ 1 \\ 1 \\ 0 \end{bmatrix}$$

(1)

Step7: We have connected S-box change on the got S-encloses Step 6 for picture encryption.

CONCLUSION

In the lossless program, the installed information can be specifically separated from the encoded space; the task of placing information on the encryption does not affect the first plain text file. In the reversible layout, additional information can be removed from plain text space, and although the slight bending in the decoding image is provided, the first simple image can be restored without any fault. Given the similarity of the two programs, the tasks of inserting data from irreversible and irreversible programs can be done while encoded in the image. Along these lines, the receiver may separate a piece of information entered in the coding area and focus on another piece of information installed and reconstruct the first simple text file in plain text space. A safe encryption and Caesar figure implanting plan in view of change dissemination engineering has been proposed. Additionally, by utilizing the novel proposed strategy for installing the information, the extent of the net payload can be expanded adequately. That is, we can shroud enough information into the encoded picture and furthermore look at the execution of the current strategy and proposed technique pictures regarding parameters like PSNR esteems information limit, size of the cover picture and so on. In our plan, both the pixel level and bit level stage are supplanted by square change and the S-square guide is utilized to process each square in such a route in this way, to the point that its key space can be moved forward. It includes pseudorandom number age in light of various keys and utilizes coordination's maps for dissemination. Reproduction results demonstrate that acceptable security execution is accomplished in just a single encryption round itself. The proposed conspire is checked by the

security examination on its key affectability, arbitrariness test, factual and differential properties and is reasonable for continuous application.

ACKNOWLEDGMENTS

Before going into details, I would like to give my gratitude to Almighty Allah for granting me the ability to finish this report that will hopefully lead to me going on to do a Master's degree. In addition, I want to honour my supervisor Assist. Prof. Dr. Muharrem Tuncay GENÇOĞLU for his warm support and guidance whilst working on this project. This will be my first step towards a Master's degree and is the beginning of a project and ideas that have been piled up in my mind for years. I highly regard this field to work in and it marks my professional career. Moreover, I appreciate my previous instructors who made me consider a new and different field. This paper is going to mark my knowledge about a new invention of information security by displaying, making and solving some principles of the field and adding one more branch to the tree of the computer world.

REFERENCE

- [1] N. A. Saleh, H. N. Boghdad, S. I. Shaheen, A. M. Darwish, "High Capacity Lossless Data Embedding Technique for Palette Images Based on Histogram Analysis," *Digital Signal Processing*, 20, pp. 1629–1636, 2010.
- [2] J. Tian, "Reversible Data Embedding Using a Difference Expansion," *IEEE Trans. on Circuits and Systems for Video Technology*, 13(8), pp. 890–896, 2003.
- [3] Z. Ni, Y.-Q. Shi, N. Ansari, and W. Su, "Reversible Data Hiding," *IEEE Trans. on Circuits and Systems for Video Technology*, 16(3), pp. 354–362, 2006.
- [4] M. U. Celik, G. Sharma, A. M. Tekalp, and E. Saber, "Lossless Generalized-LSB Data Embedding," *IEEE Trans. on Image Processing*, 14(2), pp. 253–266, 2005.
- [5] X. Hu, W. Zhang, X. Li, and N. Yu, "Minimum Rate Prediction and Optimized Histograms Modification for Reversible Data Hiding," *IEEE Trans. on Information Forensics and Security*, 10(3), pp. 653–664, 2015.
- [6] Kede Ma, Wei. Zhang, Xianfeng Zhao, "Reversible Data Hiding in Encrypted Images by reserving Room before encryption", *IEEE Trans. On information forensics and security*, vol,8 No.3, March 2013.
- [7] W. Zhang, B. Chen, and N. Yu, "Improving various reversible data hiding schemes via optimal codes for binary covers" vol. 21, no. 6, pp. 2991–3003, June. 2012.
- [8] X. L. Li, B. Yang, and T. Y. Zeng, "Efficient reversible watermarking based error expansion and pixel selection," *IEEE Trans. Image Process.*, vol. 20, no. 12, pp. 3524–3533, December.2011.
- [9] L. Luo et al., "Reversible image watermarking using interpolation," *IEEE Trans. Inf. Forensics Security*, vol. 5, no. 1, pp. 187–G. Xuan, J. Chen, J. Zhu, Y.Q. Shi, Z. Ni, and W. Su, "Lossless Data hiding.
- [10] I.-J. Lai and W.-H. Tsai, "Secret-fragment-visible mosaic image—a new computer art and its application to information hiding," *IEEE Trans. Information Forensics and Security*, vol. 6, no. 3, pp. 936–945, 2011.
- [11] K. Ma, W. Zhang, X. Zhao, N. Yu, F. Li, "Reversible data hiding in encrypted images by reserving room before encryption," *IEEE Trans. on Information Forensics and Security*, vol. 8, no. 3, pp. 553–562, Mar. 2013.
- [12] Xinpeng Zhang, Jing Long, Zichi Wang, and Hang Cheng, "Lossless and Reversible Data Hiding in Encrypted Images with Public Key Cryptography," *IEEE Trans. on Circuits and Systems for Video Technology*, 2015.
- [13] J. Zhou, W. Sun, L. Dong, et al., "Secure reversible image data hiding over encrypted domain via key modulation," *IEEE Trans. on Circuits and Systems for Video Technology*, vol. 26, no. 3, pp. 441–452, Mar. 2016.
- [14] Z. Qian, and X. Zhang, "Reversible data hiding in encrypted image with distributed source encoding," *IEEE Trans. on Circuits and Systems for Video Technology*, vol. 26, no. 4, pp. 636–646, Apr. 2016.

- [15] X. Cao, L. Du, X. Wei, et al., "High capacity reversible data hiding in encrypted images by patch-level sparse representation," *IEEE Trans. On Cybernetics*, vol. 46, no. 5, pp. 1132-1143, May. 2016.
- [16] W. Hong, T. Chen, H. Wu, "An improved reversible data hiding in encrypted images using side match," *IEEE Signal Processing Letters*, vol. 19, no. 4, pp. 199-202, Apr. 2012.
- [17] Alka Dileep, K.Anusudha, Muhammed Asad P. T., " An Efficient Reversible Data Hiding Technique in Encrypted Images Based on Chaotic Map," *IEEE International Conference on Control Instrumentation, Communication and Computational Technologies*, 2015.
- [18]. Rintu Jose, Gincy Abraham "A Separable Reversible Data Hiding in Encrypted Image with Improved Performance" *IEEE International Conference on Microelectronics, Communication and Renewable Energy (ICMiCR-2013)*, DOI:10.1109/AICERA-ICMiCR.2013.6576038, Pages:1-5
- [19]. Zhenxing Qian, Xinpeng Zhang, Guorui Feng "Reversible Data Hiding in Encrypted Images Based on Progressive Recovery" *IEEE Signal Processing Letters*, DOI:10.1109/LSP.2016.2585580, Volume: 23, Issue: 11, Nov. 2016, Pages:1672-1676
- [20]. Shuang Yi, Yicong Zhou "An Improved Reversible Data Hiding In Encrypted Images" *Signal and Information Processing (ChinaSIP)*, 2015 *IEEE China Summit and International Conference on*, DOI:10.1109/ChinaSIP.2015.7230396, Pages:225-229
- [21]. Zhaoxia Yin, Andrew Abel, Xinpeng Zhan, Bin Luo "Reversible Data Hiding In Encrypted Image Based On Block Histogram Shifting" *Acoustics, Speech and Signal Processing (ICASSP)*, 2016 *IEEE International Conference on*, DOI: 10.1109/ICASSP.2016.7472053, Pages:2129-2133
- [22]. Xinpeng Zhang, Jing Long, Zichi Wang, and Hang Cheng "Lossless and Reversible Data Hiding in Encrypted Images with Public Key Cryptography" *IEEE Transactions on Circuits and Systems for Video Technology*, DOI:10.1109/TCSVT.2015.2433194, Volume: 26, Issue: 9, Sept. 2016, Pages:1622-1631
- [23] X. Hu, W. Zhang, X. Li, N. Yu, "Minimum rate prediction and optimized histograms modification for reversible data hiding," *IEEE Trans. On Information Forensics and Security*, vol. 10, no. 3, 653-664, Mar. 2015.
- [24] W. Zhang, X. Hu, N. Yu, "Optimal transition probability of reversible data hiding for general distortion metrics and its applications," *IEEE Trans. on Image Processing*, vol. 24, no. 1, pp. 294-304, Jan. 2015.
- [25] Ioan-Catalin Dragoi, Dinu Coltuc, "Local-prediction-based difference expansion reversible watermarking," *IEEE Trans. on Image Processing*, vol. 23, no. 4, pp. 1779-1790, Apr. 2014.
- [26] W. Zhang, K. Ma and N. Yu, "Reversibility improved data hiding in encrypted images," *Signal Processing*, vol. 94, pp. 118-127, Jan. 2014.
- [27] Wu J, Zhang R et al. Reliable Detection of BPCS Steganography [J]. *Journal of Beijing University of Posts and Telecommunications*, 2009, 32(4): 113-121
- [28] ZHANG H L, ZHANG X Y. A secure BPCS steganography against statistical analysis[C]. *8th International Conference on Signal Processing*. 2006: 990-992.
- [29] Arti Yadav, Minaxi Doorwar "Novel Framework for Improving Embedding Capacity of the System using Reversible Data Hiding Technique" July 2015
- [30] Veena S. Nair , Dhanya K. Sudhish " Lossless and Reversible data hiding in Encrypted Images" Feb 2017.
- [31] GENÇOĞLU, M. T. (2017). Combining Cryptography with Steganography. *Second International Conference on Computational Mathematics and Engineering Sciences(CMES)* (p. 16). Istanbul: CMES2017.
- [32] GENÇOĞLU, M. T. (2017). Programming Encryption Algorithms with Steganography. *International Conference on Engineering Technology and Innovation (ICETI)*. Sarajevo: ICETI 2017.
- [33] Shweta Patil Student, Electronics Amrutvahini college of engineering, Sangamner Maharashtra, India, "Data Hiding Techniques: A Review" *International Journal of Computer Applications* (0975 – 8887) Volume 122 – No.17, July 2015.

Physico-Chemical Analysis of River Benue within Makurdi Reach for Irrigational Use

Aho M.I¹, Ajayi, S.D², Lagasi, J.E.³

^{1,2}Civil Engineering Department, University of Agriculture Makurdi, Nigeria.

³Department of Civil Engineering, Federal Polytechnic, Bauchi.

ABSTRACT

River Benue is one of the largest rivers in Nigeria, second only after River Niger. The reach of the River within Makurdi metropolis is inhabited by farmers, who depend largely on the availability of the water resource for agricultural and irrigational purposes. The sustained human activities within the reach of the River all year round, necessitated the investigation into the physico-chemical status as well as some selected cations, anions, nutrient load and heavy metals for comparison with FAO and WHO permissible limits. One hundred and ten samples (110), collected at ten (10) different locations within the study area were analyzed between December, 2015 to October, 2016. Heavy metals such as cadmium, manganese and lead were undetectable in the study area, except iron and zinc which were found in traces between 0.018 – 0.038 and 0.014 – 0.035mg/L in the dry and rainy seasons respectively. Sodium Adsorption Ratio (SAR), Residual sodium bi carbonate (RSBC) and Permeability Index (PI) were adopted in the assessment of the water quality for irrigation. The SAR and Electrical Conductivity (EC) values ranged from 0.0896 – 0.503epm and 0.163 – 0.281ds/m in the dry and rainy seasons respectively. Following Wilcox classification, the water quality within the reach of River Benue is observed to be of low sodium content, moderate pH, without sodicity challenge for irrigation.

Keywords: Physico-chemical Parameters, Sodium Adsorption Ratio, Water Quality, Irrigation, River Benue.

I. INTRODUCTION

Water is the most vital element among the natural resources, and is crucial for the survival of all living organisms', plants and animals inclusive [1]. The economic burden of environmental degradation owing to water pollution is very huge in the Third world countries like Nigeria when it comes to restoring the quality of life and installing controls. The increasing urbanization and industrialization of Nigeria have negative implications on water quality [2]. The pollution from industrial and urban waste effluents and from agrochemicals in water bodies of Nigeria has reached alarming levels. The long-term effects of this water contamination by organic and inorganic substances, many of them are toxic, are incalculable. The marine and aquatic ecosystems are affected, and the chemicals that enter the food chain have public health implications

Irrigated agriculture is dependent on an adequate water supply of usable quality. Water quality concerns have often been neglected because good quality water supplies have been plentiful and readily available. This situation is now changing in many areas. Intensive use of nearly all good quality supplies means that new irrigation projects and old projects seeking new or supplemental supplies must rely on lower quality and less desirable sources. To avoid problems when using these poor quality water supplies, there must be sound planning to ensure that the quality of water available is put to the best use [3].

The quality of surface waters is very significant. Much attention has been drawn to it, that is why criteria and standards for its evaluation have existed since the late 1800's. Currently, there is much concern about the quality of natural water and about the presence of extremely small amount of potentially harmful substances in them, due to anthropogenic influences from urban, industrial as well as natural processes (changes in precipitation inputs, erosion, weathering of crustal materials). This has degraded surface water and has affected both domestic and irrigational activities making it unsuitable and unsafe [3].

Hence, water analysis is often carried out in areas where surface water are used frequently, and also areas where industries are known for discharging wastes (without adequate treatment measures). These wastes contain chemicals that can potentially affect nearby water sources contaminating these water bodies, making such sources to be unsuitable for irrigation, recreation and other purposes. Its effect when such water is used can be very severe for irrigation. It can go a long way in affecting the rapid growth of the crop producing smaller plants with fewer and smaller leaves, [4].

Therefore, proper awareness and enlightenment has to be given to users in such areas about the effect of such polluted waters. There are predefined criteria and standards as regards the suitability of water for irrigation and other purposes, this study will discuss important factors in assessing the suitability of River Benue for irrigation and other applications.

II. Materials and Methods

Study Area

The study area is Makurdi town; the administrative headquarter of Benue State. The city is one of the fastest growing urban areas in Nigeria. It lies between Latitude $7^{\circ} 44' 1.50''\text{N}$ and Longitude $8^{\circ} 31' 1.700''\text{E}$; and is located within the floodplain of the lower River Benue valley, (Figure 1). Due to the general low relief, sizeable portions of Makurdi is waterlogged and flooded during heavy rainstorms. It is drained principally by River Benue which divides it into Makurdi North and South with the banks connected by two bridges, adapted from [5]

The climate of the region is generally sub-tropical influenced by two air masses: the warm moist southwesterly air mass and the warm dry north- easterly air mass. The southwesterly air mass is a rain bearing wind that brings about rainfall from the months of April to October with an extended dry period of five months (November - March). Considering the rainfall, atmospheric temperature and evapotranspiration, sizeable portions of Makurdi is waterlogged and flooded during heavy rainstorms. The mean annual rainfall total is 1190 mm and ranges from 775-1792 mm. The mean monthly relative humidity varies from 43% in January to 81% in July-August period. Temperatures are generally high throughout the year, with February and March occurring as the hottest months. The dry northeasterly air mass blows over the region from November to April, thereby bringing about seasonal drought, [6].

Sample Collection

Ten (10) different study sites were selected with respect to concentrated dry season farming activities along the river course within Makurdi metropolis, Benue state as indicated in Fig 1, GPS technology was employed in the selection.

Water samples from River Benue were collected following standard procedure as described by [7]. Pre-cleaned one-litre plastic bottles were used to collect water samples for the physico-chemical analysis. Sample containers were labeled on the field using appropriate codes and water samples were temporarily stored in ice packed cooler and transported to the laboratory and stored in a refrigerator at about 4°C prior to analysis [7]. These samples were collected on a monthly basis consecutively for a period of eleven months (December 2015 to October 2016).

Sample Analysis

The physiochemical analyses of water samples were performed using standard analytical methods according to procedures outlined in the Standard Methods for the Examination of Water and Wastewater [7]. The instrument used chiefly was HACH Lange kits DR/2000 spectrophotometer as

described by [7]. The collected surface water samples were analyzed for pH, electrical conductivity, total dissolved solids, the cations such as nitrogen, calcium, magnesium, potassium, sodium; the anions such as, carbonate, bicarbonate, chloride, sulphate, phosphate and borate according to the standard methods and techniques [8]. The water quality determining indices, such as Sodium Adsorption Ratio (SAR), Residual Sodium Bicarbonate (RSBC), Soluble Sodium Percentage (SSP), Total Alkalinity (TA), Permeability Index (PI), were calculated by using the following recommended relationships.

$$SAR = \frac{Na^+}{\sqrt{\frac{Ca^{2+} + Mg^{2+}}{2}}} \quad - \quad (1)$$

$$RSBC = (Co_3 + HCo_3) - (Ca^{2+} + Mg^{2+}) \quad - \quad (2)$$

$$SSP = \frac{\text{Soluble Sodium Concentration}}{\text{Total Cation Concentration}} \times 100 \quad - \quad (3)$$

$$RSC = HCo_3 + (Ca + Mg) \quad - \quad (4)$$

$$\text{Total Alkalinity (TA)} = \frac{RSC}{RSBC} \quad - \quad (5)$$

$$\text{Permeability Index (PI)} = \frac{Na^+ + \sqrt{HCo_3} \times 100}{Ca^{2+} + Mg^{2+} + Na^+} \quad - \quad (6)$$

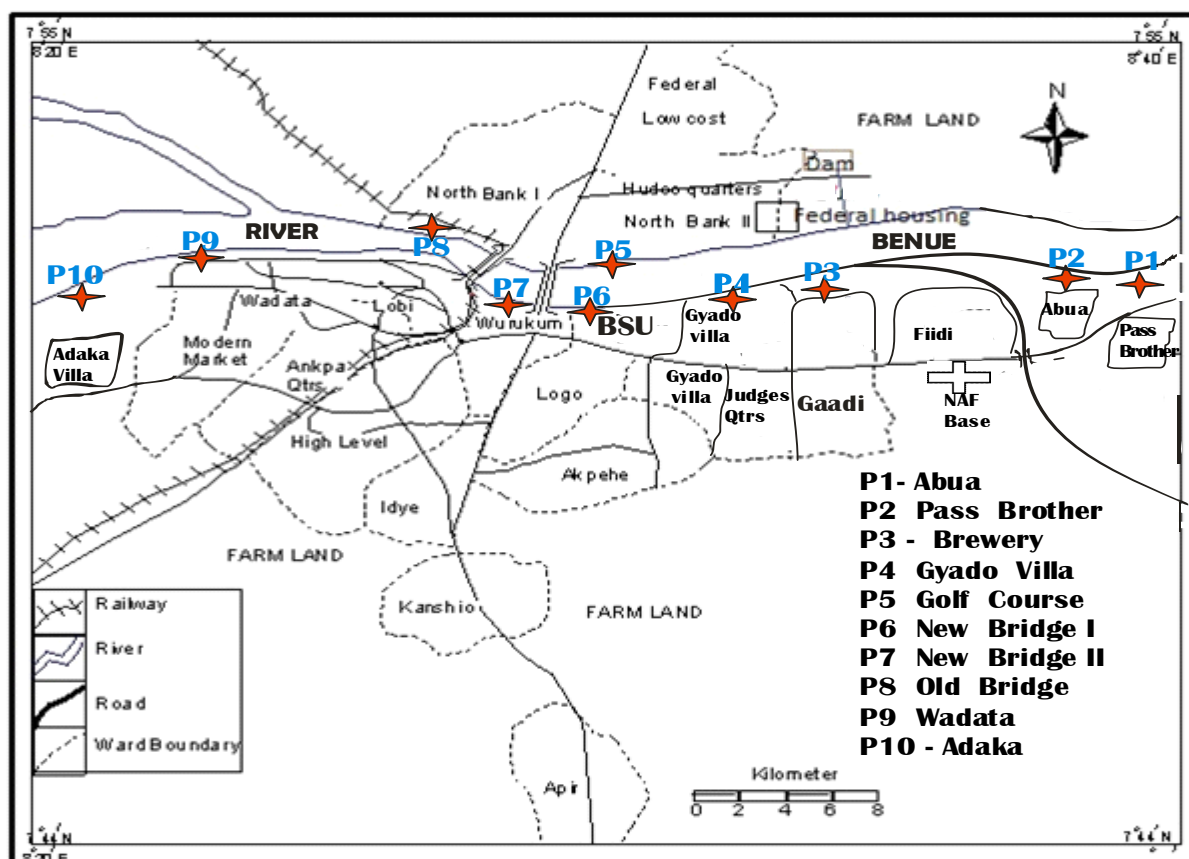


Figure 1: Water Sample Points Location of River Benue at Makurdi.

III. Results and Discussion

Temperature, pH and Electrical Conductivity (EC)

Temperature showed an upward trend from December to April, followed by downward trend from May onwards. The overall temperature range was 18.4^{0C} to 31.6^{0C} between January and April as seen in Table 2. The pH as seen in Table 2 is within permissible limits. The electrical conductivity values within the study area were below the maximum limit of 3.0ds/m as specified by FAO (2016).

Table 2: Summary of Mean values of physic-Chemical Characteristics of River Benue water measured in milligram per litre (mg/l)

| Date | Cl | SO ₄ | CO ₃ ²⁻ | HCO ₃ ⁻ | NO ₃ ⁻ | Na ⁺ | K ⁺ | Ca ²⁺ ₊ | Mg ²⁺ ₊ | Fe | Zn | EC | T | pH |
|---------|------|-----------------|-------------------------------|-------------------------------|------------------------------|-----------------|----------------|-------------------------------|-------------------------------|--------|--------|-------|-------|-------|
| Dec'15 | 2.48 | 2.52 | 1.46 | 2.59 | 2.39 | 5.01 | 2.64 | 42.60 | 23.30 | 0.030 | 0.033 | 0.220 | 18.60 | 7.30 |
| Jn'16 | 2.53 | 3.56 | 1.71 | 3.58 | 4.32 | 3.46 | 2.15 | 41.60 | 21.80 | 0.036 | 0.034 | 0.210 | 18.40 | 7.20 |
| Feb'16 | 2.58 | 3.57 | 1.95 | 4.58 | 5.22 | 1.91 | 1.97 | 40.70 | 20.30 | 0.038 | 0.035 | 0.121 | 23.20 | 7.10 |
| Mar'16 | 2.58 | 3.57 | 1.95 | 4.58 | 5.22 | 1.91 | 1.97 | 40.70 | 20.30 | 0.038 | 0.035 | 0.122 | 27.20 | 7.10 |
| Apr'16 | 2.55 | 3.57 | 1.95 | 4.58 | 5.22 | 1.91 | 1.97 | 40.70 | 20.30 | 0.038 | 0.035 | 0.142 | 31.60 | 7.12 |
| May'16 | 2.23 | 2.55 | 1.90 | 3.27 | 4.22 | 8.54 | 2.12 | 43.50 | 22.20 | 0.028 | 0.032 | 0.181 | 27.00 | 7.30 |
| Jun'16 | 1.87 | 2.45 | 1.82 | 2.80 | 3.35 | 11.12 | 2.42 | 44.93 | 23.30 | 0.025 | 0.029 | 0.220 | 24.60 | 7.40 |
| July'16 | 1.24 | 1.42 | 1.72 | 2.78 | 3.19 | 14.58 | 2.49 | 46.80 | 23.90 | 0.022 | 0.021 | 0.312 | 22.40 | 7.43 |
| Aug'16 | 0.31 | 0.28 | 1.26 | 2.71 | 1.83 | 22.60 | 3.49 | 50.50 | 24.10 | 0.014 | 0.018 | 0.325 | 22.20 | 7.64 |
| Sep'16 | 0.31 | 0.28 | 1.26 | 2.71 | 1.83 | 22.58 | 3.49 | 50.46 | 24.06 | 0.014 | 0.018 | 0.326 | 21.20 | 7.60 |
| Oct'16 | 0.31 | 0.28 | 1.26 | 2.71 | 1.83 | 22.60 | 3.49 | 50.50 | 24.10 | 0.014 | 0.018 | 0.322 | 20.80 | 7.60 |
| Mean | 1.73 | 2.19 | 1.66 | 2.94 | 3.51 | 10.57 | 2.56 | 44.82 | 22.52 | 0.027 | 0.028 | 0.216 | 23.38 | 7.34 |
| SD | 0.95 | 1.33 | 0.28 | 0.90 | 1.81 | 8.32 | 0.61 | 3.92 | 1.52 | 0.0095 | 0.0072 | 0.12 | 3.79 | 0.196 |

Source: Researchers' Field work.2015- 2016

Table 3: Summary of results from water quality analysis

| S/N o | Parameter | Unit | River Benue in the study Area | | Permissible limits for irrigation water | | Remarks |
|----------|------------|-------|----------------------------------|---------|--|------------|--------------|
| | | | Dry | Rainy | FAO (2016) | WHO (2016) | |
| 1 | Temp. | °C | 23.80 | 23.03 | <40.00 | <40.00 | Satisfactory |
| 2 | pH | - | 7.16 | 7.50 | 6.5 – 8.4 | 6.0 – 8.5 | Satisfactory |
| 3 | EC | dS/M | 0.163 | 0.281 | 0 – 30 | 0 – 3.0 | Satisfactory |
| 4 | TDS | Mg/L | 104.12 | 179.84 | 0 – 450 | 0 – 500 | Satisfactory |
| 5 | SAR | epm | 0.0896 | 0.503 | 0 – 15.00 | 0 – 15 | Satisfactory |
| 6 | SSP | % | 3.10 | 14.38 | 0 – 60 | 0 – 66 | Satisfactory |
| 7 | PI | % | 9.65 | 18.85 | - | - | - |
| 8 | SR | - | 0.0325 | 0.1709 | 0 – 1.00 | ≤1.0 | Satisfactory |
| 9 | RSC | Meq/L | -3.1482 | -4.2783 | ≤1.25 | ≤1.25 | Satisfactory |
| 10 | RSBC | Meq/L | -3.0881 | -4.277 | - | - | - |
| 11 | SCAR | Meq/L | 0.086 | 0.4781 | - | - | Satisfactory |
| 12 | Salt Index | Ppm | -36.72 | -29.09 | Negative value | - | Satisfactory |
| 13 | TA | Meq/L | 1.0195 | 1.0003 | 0 – 2.50 | ≤2.50 | Satisfactory |
| 14 | TH | Mg/L | 62.46 | 71.40 | 0 – 150 | 0 – 145 | Satisfactory |
| 15 | Sodicity | - | 1.042 | 1.052 | 0 – 10 | 0 – 10 | Satisfactory |
| 16 | Sulphate | Meq/L | 0.1065 | 0.0422 | 0 – 5 | 0 - 5 | Satisfactory |
| 17 | Chloride | Meq/L | 0.155 | 0.373 | 0 – 10 | 0 - 10 | Satisfactory |

Source: Researcher's field work 2015 – 2016.

Sodium Absorption Ratio (SAR)

The values of SAR of the collected water samples range from 0.0896epm in the dry season to 0.503epm in the rainy season, implying that the River has no Sodicity challenge. According to [9], all the water samples collected and analyzed fell under 'excellent' class of water for irrigation. As per salinity classification; all the water samples fell under 'low sodium' hazards (S_1) water which can be used for almost all crops. Irrigation water that has high sodium (Na^+) content can bring about a displacement of exchangeable cations Ca^{2+} and Mg^{2+} from the clay minerals of the soil, followed by the replacement of the cations by sodium. Sodium-saturated soil peptizes and loses their permeability, so that their fertility and suitability for cultivation decreases [10]. High SAR in any irrigation water implies hazard of sodium (Alkali) replacing Ca and Mg of the soil through cation exchange process, a situation eventually damaging to soil structure, namely permeability which ultimately affects the fertility status of the soil and reduction of crop yield [11].

Hardness and Total Alkalinity (TA)

Hardness of the river water fluctuated between 61.00 mg/L and 74.60 mg/L. The results indicates that, the water is soft, based on water hardness classification. The Total Alkalinity (TA) ranged between 1.0195 and 1.0003meq/L. Total Alkalinity in all the seasons at all the study sites were within low alkalinity limit as described by [11-12].

Cations

Calcium (Ca^{2+}), which is a major component of natural waters, comes mainly from the rocks, seepage, drainage, wastewater etc. Ca^{2+} in the samples under consideration varied from 40.70 mg/L to 50.50 mg/L. Magnesium (Mg^{2+}) is required as an essential nutrient for plants as well as for animals

and the concentration of 30 mg/L is recommended for drinking waters. The concentration of Mg^{2+} ions in the water samples under this study varied from 20.30 mg/L to 24.10 mg/L. In the study, Sodium (Na^+) concentration in water of River Benue ranged from 1.91– 5.01 mg/l in dry season and 8.54– 26.60 mg/l in rainy season. The highest average of Sodium concentration (22.60 mg/l) was found during the month of August in 2016 at rainy season. According to [12 – 15] Water Quality Standard, Sodium (Na^+) concentration was within permissible limit for irrigation in terms of salinity. When Sodium (Na^+) concentration in water reaches above 919.6 mg/l, water becomes saline and unsuitable for irrigation [3, 12].

Anions

In this study, the chloride contents were ranged from 0.31 mg/L to 2.58 mg/L. Chloride content was lower than the accepted limit of 250 mg/L at the sampling sites in the river. The levels downstream were slightly higher than those obtained upstream in all the seasons. Values indicate low seasonal variation of chlorides which show that there is little variation in domestic activities with change in the seasons. Overall, chloride concentration was within the acceptable limits. Sulphate (SO_4^{2-}) concentration in the river varied from 0.28 mg/L to 3.57 mg/L. The concentration of SO_4^{2-} was much lower in the Rainy season as compared to dry season. The maximum value was obtained in February while the minimum value was recorded in the month of August. The permissible limit of Sulphate is 20.00 mg/l for irrigation water [3]. It was observed that sulphate was present under acceptable limits. This shows that the percentage contributions of Sulphate from domestic as well as industrial activities are still minimal.

Bicarbonate concentration in water of River Benue ranged from 2.59– 4.58mg/l in dry season and 2.71– 3.27 mg/l in rainy season. The highest average of Bicarbonate (HCO_3^-) concentration (4.58 mg/l) was found at dry season during the month of February in 2016. The recommended limit of Bicarbonate (HCO_3^-) concentration in water is 50 –300 mg/l for fisheries [12, 18], and is 53.53 mg/l for irrigation water [3].

Heavy Metals

Nickel (Ni), Copper (Cu), Cadmium (Cd), Manganese (Mn) and Lead (Pb) were undetectable at both the sites in all the season therefore the river water is free from toxic metals. However, Iron (Fe) and Zinc (Zn) were found in traces. Zn values ranged between 0.014mg/L at the rainy season and 0.035 mg/L in dry season. The concentrations of Fe in the water ranged from 0.018 mg/L in the rainy season to 0.038 mg/L in the month of February 2016. Both season's values falls within the background level and the WHO limit of 0.3 mg/L [13].

Nutrient Loads

NO_3^- in river water promotes high primary productivity and excess of NO_3^- in surface water is taken as a warning for algal blooms. In this study, the NO_3^- levels were quite low, varying from 1.80 mg/L to 5.22 mg/L. The highest average (5.22 mg/l) of Nitrate (NO_3^-) concentration was found at dry season during the month of February in 2016.

IV. CONCLUSION

From the assessment of the physical and chemical parameters, as well as the quality determining indices of the River, it is safe to conclude that, the water quality is satisfactory for irrigational applications in the study area. However, regular monitoring and engineering evaluation of the water quality is recommended.

REFERENCES

- [1] K. Venkatesharaju, P. Ravikumar, R. Somashekar, and K. Prakash, Physico-chemical and Bacteriological Investigation on the river Cauvery of Kollegal Stretch in Karnataka, 2010 vol. 6.
- [2] Islam, F., Sharmin, R. and Junait, J. "A Detailed Pollution status and trends in water quality of the analysis on industrial pollution in Bangladesh," Workshop Discussion Paper. (1997)
- [3] Ayers, R. S, and Westcot, D. W. Water Quality for Agriculture. FAO, Irrigation and Drainage Paper No. 29, Rev. 1. FAO, Rome. (1985) 174 p.
- [4] Arora, K.R. *Irrigation, Water Power and Water Resources Engineering*. 4th Ed. A.K Jain for Standard Publishers Distributors, New Delhi. (2002).
- [5] Ocheri, M. I.; Mile, I. I. and Obeta, M.C. Seasonal variation of nitrate levels in hand dug wells in Makurdi metropolis, *Pakistan Journal of Nutrition*, (2010) 9: 539-542.
- [6] Ologunorisa, E. T. and Tersoo, T. The changing rainfall pattern and its implication for flood frequency in Makurdi, Northern Nigeria, *Journal of Applied Science and Environmental Management*, (2006) 10(3): 97-102
- [7] APHA (American Water Works Association) Standard methods for Examination of water and wastewater. 21st Edition. APHA-AWWA, Washington, DC, USA. (2005)
- [8] Jackson, M. *Soil Chemistry Analysis*. Prentice-Hall, Englewood Cliffs, USA. (1967). pp. 227-261.
- [9] Richards, L.A. *Diagnosis and improvement of saline alkali*. USDA Handbook 60, Washington DC (1954)160p
- [10] Matthes, G. *The Properties of Ground Water*, John Wiley and Sons, New York, USA. (1982) 397.
- [11] Gupta, I.C, Use of water in Agriculture. A study of arid and semi-arid zones of India, Revised ed. Oxford and IBH publishing Co., New Delhi (1990) 308.
- [12] FAO Simple Soil, Water and Plant Testing Technique for Soil Resource Management. Land and Water development Division, Food and Agriculture Organization, Rome, Italy. (2016)1-142
- [13] WHO (World Health Organization), *Guidelines for Drinking Water, WHO Criteria and Other Supporting Information*, World Health Organization: Geneva, (2016)
- [14] USEPA(United States Environmental Protection Agency), "Drinking Water Quality Standards," (2000)
- [15] Mezgebe, K.; Gebrekidan, A.; Hadera, A.; Weldegebriel, Y. "Assessment of Physico-Chemical Parameters of TsaedaAgam River in Mekelle City, Tigray, Ethiopia, *Bull. Chem. Soc. Ethiop.* (2015) 29(3): 377-385.